Binding Kinetics of Proteins at Immune-Cell Contacts

Chouliara, Manto

2022

Binding Kinetics of Proteins at Immune-Cell Contacts

MANTO CHOULIARA | DIVISION OF PHYSICAL CHEMISTRY | LUND UNIVERSITY

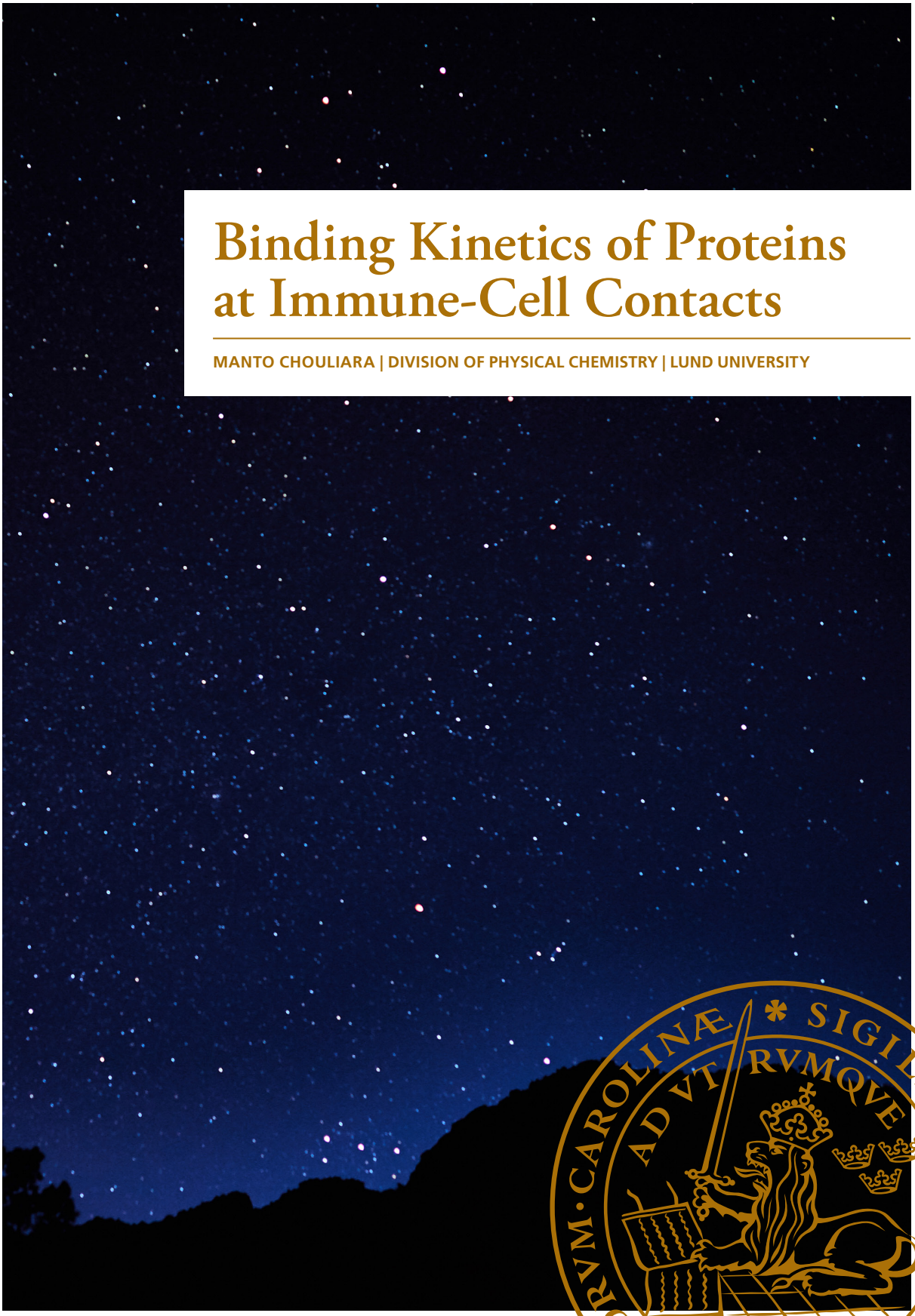

Binding Kinetics of Proteins at Immune-Cell Contacts

Binding Kinetics of Proteins at Immune-Cell Contacts

by

Manto Chouliara

LUND
UNIVERSITY

DOCTORAL DISSERTATION
by due permission of the Faculty of Science, Lund University, Sweden.
To be defended on the 28th of September, in lecture hall A at the Centre for Chemistry and Chemical Engineering at Lund University.

Faculty opponent
Dr. Kristina Ganzinger
Research institute AMOLF

Organization LUND UNIVERSITY Department of Chemistry Box 124 SE-221 00 LUND Sweden	**Document name** DOCTORAL DISSERTATION **Date of disputation** 2022-09-28
Author(s) Manto Chouliara	**Sponsoring organization**

Title and subtitle
Binding Kinetics of Proteins at Immune-Cell Contacts

Abstract

Protein-protein interactions are crucial in numerous cellular functions and biological processes that take place inside our body. It is therefore not surprising that these interactions also govern the response of our body´s defence mechanism, the so-called immune system, towards an infection. Understanding how proteins interact entails studying the binding affinity (strength) and the lifetime (duration) of the protein-protein interaction to better decompose how an immune response is initiated and how we can explore this knowledge to treat diseases. In this thesis, total internal fluorescence microscopy (TIRF) and single-molecule imaging were used to observe and characterize protein-functionalized supported lipid bilayers (SLBs) interacting with immune cells to obtain the binding kinetics of various protein-protein pairs.

In the first part of this thesis, the interaction between the rat CD2 (rCD2) adhesion protein and its ligand rat CD48T92A (rCD48T92A), a high-affinity mutant of the wild type rat CD48, was used to establish a new method of obtaining single-cell binding affinities of T cells interacting with SLBs using imidazole titrations. The results showed a relatively small spread in the rCD2-rCD48T92A binding affinity values despite the considerable spread of receptor densities within the cell population. The lifetime of the rCD2/rCD48T92A interaction was also investigated using single-molecule imaging and tracking displaying a similarly small lifetime spread within the cell population. Using both these methods, the single-cell binding affinity and lifetime of the cell population can be investigated and their spread can provide information concealed with population-average techniques.

The second part of the thesis focused on the CD4 co-receptor whose role in initiating an immune response is ambiguous. Even though the CD4 co-receptor increases the sensitivity of T cell signalling manyfold, it binds to its ligand, peptide major histocompatibility complex II (pMHCII), with the lowest binding affinity known to this day. The CD4-MHC II interaction is so weak that adhesion molecules are needed to ensure a successful CD4-MHC II contact formation. For this reason, the influence of an adhesion molecule, rat CD2, on the obtained binding kinetics of the human CD4 co-receptor was initially examined showing that the accumulation of CD4 was influenced when having a high concentration of bound CD2 inside the cell-SLB contacts. Later, the studies focused on the CD4-TCR-MHC II ternary complex where it was demonstrated that the presence of L3-12 TCR strongly supported the CD4-MHC II interaction by increasing the local density of MHC II inside the cell-SLB contacts. However, the presence of TCR did not seem to significantly influence the specific affinity for CD4 to MHC II. Lastly, CD4 binding studies showed that the co-receptor did not noticeably affect the TCR-MHC II binding at physiological levels of hCD4 in the SLB.

Key words
T cells, Binding Kinetics, Affinity, Lifetime, CD4, CD2, TIRF Microscopy, SLBs

Classification system and/or index terms (if any)

Supplementary bibliographical information		**Language** English
ISSN and key title		**ISBN** 978-91-7422-876-2
Recipient's notes	**Number of pages 166**	**Price**
	Security classification	

Binding Kinetics of Proteins at Immune-Cell Contacts

by

Manto Chouliara

Faculty of Science
Department of Chemistry
Division of Physical Chemistry

A doctoral thesis at a university in Sweden takes either the form of a single, cohesive research study (monograph) or a summary of research papers (compilation thesis), which the doctoral student has written alone or together with one or several other author(s).

In the latter case the thesis consists of two parts. An introductory text puts the research work into context and summarizes the main points of the papers. Then, the research publications themselves are reproduced, together with a description of the individual contributions of the authors. The research papers may either have been already published or are manuscripts at various stages (in press, submitted, or in draft).

Faculty of Science at Lund University
Department of Chemistry

ISBN (Print): 978-91-7422-876-2
ISBN (PDF): 978-91-7422-877-9

Printed in Sweden by Media-Tryck, Lund University
Lund 2022

The struggle itself toward the heights is enough to fill a man's heart.

One must imagine Sisyphus happy.

Albert Camus

Table of Contents

Acknowledgments

I would like to thank the following people without whom I would not have been able to complete this research.

First and foremost, I would like to thank my main supervisor **Peter Jönsson** for providing me with the necessary guidance and feedback throughout my PhD studies. Your support and optimism pushed me through the tough times and your ever-present enthusiasm was always a motive for me to try harder. I also want to thank my second supervisor, **Jonas Tegenfeldt**, for the constructive comments you provided me whenever we would talk about Physics and Biology. Also, I want to express my gratitude to all my closest colleagues for your valuable inputs and suggestions throughout my studies. I am particularly grateful for working with **Tommy**, **Marco**, **Alexandra**, **Patrick and Kasia**, thank you for all your helpful inputs, laughs and good memories we shared.

I wish you all the very best!

List of Publications

The work presented in this thesis is based on the following publications, which will be referred to by their roman numerals:

I **Single-Cell Measurements of Two-Dimensional Binding Affinity Across Cell Contacts**

Manto Chouliara, Victoria Junghans, Tommy Dam, Ana Mafalda Santos, Simon J. Davis, Peter Jönsson

Biophysical Journal, 120, 5032–5040, 2021.

II **Effects of a local auxiliary protein on the two-dimensional affinity of a TCR-peptide MHC interaction**

Victoria Junghans, Manto Chouliara, Ana Mafalda Santos, Deborah Hatherley, Jan Petersen, Tommy Dam, Lena M Svensson, Jamie Rossjohn, Simon J Davis, Peter Jönsson

Journal of Cell Science, 133(15), jcs245985, 2020.

III **Binding of CD4 to a TCR/pMHC II complex does not increase the affinity of CD4 to pMHC II**

Manto Chouliara, Tommy Dam, Victoria Junghans, Ana Mafalda Santos, Simon J Davis, Peter Jönsson

Manuscript

The publications are appended at the end of the thesis.

Authors Contribution

I Single-Cell Measurements of Two-Dimensional Binding Affinity Across Cell Contacts

MC planned the project together with PJ. MC conducted the experimental investigation and performed the formal analysis. VJ, AMS and SJD contributed with resources. MC wrote the paper with input from VJ, TD, AMS and SJD. MC made the article's figures.

II Effects of a local auxiliary protein on the two-dimensional affinity of a TCR-peptide MHC interaction

VJ planned the project together with PJ. VJ, MC and TD did the experimental investigation and VJ and MC performed the formal analysis. AMS, DH, JP, LMS, JR and SJD contributed with resources. VJ and PJ wrote the paper with input from MC, AMS, JP, JR and SJD. VJ and MC made the article's figures.

III Binding of CD4 to a TCR/pMHC II complex does not increase the affinity of CD4 to pMHC II

MC planned the project together with V.J and PJ. MC conducted the experimental investigation and performed the formal analysis. MC and PJ wrote the manuscript and made the article's figures with input from TD, VJ, AMS and SJD.

Publications not included in this thesis:

Supported lipid bilayers and the study of two-dimensional binding kinetics

Tommy Dam, Manto Chouliara, Victoria Junghans, Peter Jönsson

Frontiers in Molecular Biosciences, 9, 833123, 2022.

Calcium signaling in T Cells is induced by binding to nickel-chelating lipids in supported lipid bilayers

Tommy Dam, Victoria Junghans, Jane Humphrey, Manto Chouliara and Peter Jönsson

Frontiers in Physiology, 11, 613367, 2021.

List of Abbreviations

2D	Two Dimensional
3D	Three Dimensional
AF	Alexa Fluor
APC	Antigen Presenting Cell
BSA	Bovine Serum Albumin
CD	Cluster of Differentiation
D	Diffusion constant
DGS-NTA	1,2-dioleoyl-sn-glycero-3-[(N-(5-amino-1-carboxypentyl)iminodiacetic acid)succinyl] (nickel salt)
FRAP	Fluorescence Recovery After Photobleaching
FRET	Förster Resonance Energy Transfer
GPI	Glycosylphosphatidylinositol
His-Tag	Histidine Tag
Ig	Immunoglobulin
ITAM	Immunoreceptor Tyrosine-based Activation Motifs
ITC	Isothermal Titration Calorimetry
K_d	Dissociation Constant
LAP	Linear Assignment Problem
LcK	Lymphocyte-Specific Protein Tyrosine Kinase
MHC	Major Histocompatibility Complex
MD	Molecular Dynamic
NA	Numerical Aperture
NTA	Nitrilotriacetic Acid

PALM	Photoactivated Localization Microscopy
PSF	Point Spread Function
RBC	Red Blood Cell
rCD2	rat CD2
rCD48	rat CD48
SIM	Structured Illumination Microscopy
SLB	Supported Lipid Bilayer
SPR	Surface Plasmon Resonance
SPT	Single-Particle Tracking
STED	Stimulated Emission Depletion Microscopy
STORM	Stochastic Optical Reconstruction Microscopy
SUV	Small Unilamellar Vesicles
TCR	T-cell Receptor
TIRF	Total Internal Reflection Fluorescence
ZAP-70	Zeta-chain associated protein 70

Abstract

Protein-protein interactions are crucial in numerous cellular functions and biological processes that take place inside our body. It is therefore not surprising that these interactions also govern the response of our body´s defence mechanism, the so-called immune system, towards an infection. Understanding how proteins interact entails studying the binding affinity (strength) and the lifetime (duration) of the protein-protein interaction to better decompose how an immune response is initiated and how we can explore this knowledge to treat diseases. In this thesis, total internal fluorescence microscopy (TIRF) and single-molecule imaging were used to observe and characterize protein-functionalized supported lipid bilayers (SLBs) interacting with immune cells to obtain the binding kinetics of various protein-protein pairs.

In the first part of this thesis, the interaction between the rat CD2 (rCD2) adhesion protein and its ligand rat CD48$_{T92A}$ (rCD48$_{T92A}$), a high-affinity mutant of the wild type rat CD48, was used to establish a new method of obtaining single-cell binding affinities of T cells interacting with SLBs using imidazole titrations. The results showed a relatively small spread in the rCD2-rCD48$_{T92A}$ binding affinity values despite the considerable spread of receptor densities within the cell population. The lifetime of the rCD2/rCD48$_{T92A}$ interaction was also investigated using single-molecule imaging and tracking displaying a similarly small lifetime spread within the cell population. Using both these methods, the single-cell binding affinity and lifetime of the cell population can be investigated and their spread can provide information concealed with population-average techniques.

The second part of the thesis focused on the CD4 co-receptor whose role in initiating an immune response is ambiguous. Even though the CD4 co-receptor increases the sensitivity of T cell signalling manyfold, it binds to its ligand, peptide major histocompatibility complex II (pMHCII), with the lowest binding affinity known to this day. The CD4-MHC II interaction is so weak that adhesion molecules are needed to ensure a successful CD4-MHC II contact formation. For this reason, the influence of an adhesion molecule, rat CD2, on the obtained binding kinetics of the human CD4 co-receptor was initially examined showing that the accumulation of CD4 was influenced when having a high concentration of bound CD2 inside the cell-SLB contacts. Later, the studies focused on the CD4-TCR-MHC II ternary complex where it was demonstrated that the presence of L3-12 TCR strongly supported the CD4-MHC II interaction by increasing the local density of MHC II inside the cell-SLB contacts. However, the presence of TCR did not seem to significantly influence the specific affinity for CD4 to

MHC II. Lastly, CD4 binding studies showed that the co-receptor did not noticeably affect the TCR-MHC II binding at physiological levels of hCD4 in the SLB.

Popular Scientific Summary

The immune system is our body´s defence mechanism whose role is to fight the viruses and bacteria that infect our body. Eliminating these intruders, commonly referred to as pathogens, is vital since they can cause various diseases such as the flu or the common cold. The immune system´s defence is achieved with the help of specialized cells, called immune cells, which act as an immune patrol inside our body that continuously circulate it in search of potential pathogens. There are several immune cells protecting our body but the most prominent ones are the antigen-presenting cells (APCs) and T cells. When an APC detects a pathogen, it engulfs it and later presents a part of the pathogen, called an antigen, on its surface. This process is critical because a subsequent interaction of the APC with a T cell, and more specifically a highly-sensitive association between several specialized protein receptors between the two cells, leads to the initiation of an immune response. With this process, the T cells raise the immune alarm inside our body, informing all the different immune cells that there is a certain pathogen present which needs to be eliminated.

The aim of this thesis was to shed some light into the crucial communication between proteins presented on the surface of T cells and APCs. Studies of protein-protein interactions entail the analysis of the so-called binding kinetics which consist of determining the strength (binding affinity) and the duration (lifetime) of a protein-protein complex. This thesis, therefore, focused on obtaining these two important parameters and on understanding their distribution within the cell population. However, a cell such as a T cell is a very complex system composed of many proteins that, upon successful contact with the APC, are able to communicate and induce very complicated signaling cascades inside the cell. Therefore, with the aim of investigating the T cell-APC binding, supported lipid bilayers (SLBs) are commonly used to replace one of the immune cells with a simplified, artificial model system that facilitates the investigation of individual protein-protein interactions upon cell-SLB binding.

The first project of this thesis focused on developing a novel method of measuring the strength of a protein-protein complex with the aim of obtaining a value for every single cell-SLB interaction, in contrast with pre-existing methodologies which need hundreds of cell-SLB contacts to produce an average value for the binding of the whole cell population. I found that the binding affinity (strength) distribution for a protein-protein binding within the cell population was small indicating the high specificity of this interaction. Furthermore, I studied the distribution of the lifetime (duration) of a protein-protein complex within different cell-

SLB contacts and once more I obtained values with high consistency. The second part of the thesis focused on a specific protein, called CD4 or CD4 co-receptor, whose role is vital in initiating an immune response since it enhances the communication between T cells and APCs. Due to the weak binding of CD4 to its binding partner, called major histocompatibility complex II (MHC II), the presence of adhesion proteins is necessary to facilitate the CD4-MHC II interaction. However, I demonstrated that the concentration of the adhesion proteins strongly affects the binding behaviour of the CD4 co-receptor. By performing binding affinity studies including the CD4 co-receptor and the critical T-cell receptor or TCR, I showed the differences between an adhesion molecule and the TCR upon CD4 binding MHC II. In more detail, I showed that the presence of the TCR strongly supports the CD4-MHC II interaction without significantly influencing the binding affinity of CD4 to MHC II. Because TCR also binds MHC II, I also performed studies showing that the presence of the co-receptor does not affect the TCR-MHC II binding either.

Overall, the findings presented in this thesis could contribute to a better understanding of the mechanisms of protein-protein interactions.

Aim of the Dissertation

Aim of the Dissertation

The aim of this thesis was to study and better understand the binding kinetics of proteins at immune-cell contacts. In particular, my work focused on the CD4 co-receptor, a vital membrane protein that can augment the sensitivity and activation of T cells. However, the exact role of the CD4 co-receptor in T cell activation is particularly ambiguous due to the inherent difficulty in studying such a weakly binding protein. In order to characterize such a weak interaction, a novel binding affinity method was developed to obtain affinities of individual T cells interacting with protein-functionalized SLBs. By using this original approach, it is possible to evaluate the spread of binding affinities within the cell population while reducing the measurement and analysis time significantly. Furthermore, single-molecule imaging and subsequent tracking of distinct proteins diffusing on an SLB were employed in order to estimate the distribution of receptor-ligand binding lifetimes within different formed cell-SLB contacts. For the CD4 studies, the presence of adhesion proteins such as CD2 is vital as a means to support contact formation and promote binding, therefore the first priority was to investigate whether CD4 binding to its ligand MHC II is affected by the presence of auxiliary binding molecules. The last part of the thesis focused on binding studies of the CD4-TCR-MHC II ternary complex. Investigating the influence of CD4 to the TCR-MHC II complex revealed that the presence of the co-receptor does not affect the TCR-MHC II binding affinity. On the other hand, it was shown that the presence of TCR facilitates the CD4-MHC II interaction by recruiting more MHC II inside the cell-SLB contact. However, the affinity of CD4 to TCR-MHC II is of the same order of magnitude as that for binding free pMHC II.

Chapter 1

1. A Short Introduction to the Immune System

Contents

This chapter will provide a brief introduction to our immune system and highlight some of the key cells and proteins that orchestrate this remarkable defence mechanism. The process by which the presence of a pathogen triggers an immune response will be analyzed while emphasizing the complexity of such an important biochemical process.

1.1 The Immune System and T-cell Activation

The immune system is an extraordinarily complex network whose function is to maximize our likelihood of surviving while eliminating any infection such as microbes, viruses, fungi and parasites. In vertebrates, the immune system consists of two overlapping systems: *the innate immune system* and the *adaptive immune system*, distinguished by the specificity in their response toward a pathogen (1). The innate immune response is the first line of defence and consists of several physical and chemical barriers as well as phagocytic cells that target any intruding organism with the general characteristics of a pathogen. On the other hand, the adaptive immune system is antigen-specific, and its hallmark is the capacity for memory permitting it to contribute to a more effective host response against pathogens when they are detected for a second time. T and B cells together constitute the adaptive immune system and while B cells provide humoral immunity by recognizing soluble antigens, T cells recognize antigens as peptides bind to molecules on the surface of specialized immune cells. For the latter case, a pathogen interacting with a phagocyte such as a neutrophil or a dendritic cell will get engulfed and degraded into peptides, which are small amino acid sequences comprised typically of 2-40 amino acids. Through this process, called phagocytosis, the formed peptides are displayed on the surface of the phagocyte coupled with special transmembrane glycoprotein receptors called major histocompatibility complexes (MHCs) (2). Immune cells which are able to display parts of antigens on their surface are called antigen-presenting cells (APCs). It is important to note that the MHC molecules are highly polymorphic allowing the expression of a wide range of presented peptides. The majority of the peptides presented by the MHC complexes on the surface of the APCs are endogenous peptides and only a few pathogenic (agonist) peptides are presented after an infection.

Peptide presentation by an APC is not sufficient to induce an adaptive immune response. Achieving this requires the interaction of the APC with one of the approximately 10^{12} T cells present in the human body (Figure 1.1) (3). T cells are a type of lymphocyte (white blood cell) with each one bearing typically 40,000 identical special receptors, the so-called T cell receptors

(TCRs), which are able to recognize with high selectivity and sensitivity trace levels of different 'foreign' (pathogenic) peptide-MHC complexes among a plethora of 'self'-peptides (produced by the body) (4–6). Each T cell expresses a different TCR on its surface guarantying an immense variety of possible interactions (7). In more detail, the TCR is composed of two polypeptide chains, the α- and β- chains, which are typically coupled with the signaling protein cluster of differentiation 3 (CD3). The later signaling protein has long cytoplasmic domains with tyrosine residues referred to as immunoreceptor tyrosine-based activation motifs (ITAMs) (8). T-cell activation is a result of the interaction between an APC and a T cell, and more specifically, the successful interaction of a TCR with an agonist peptide MHC. This interaction leads to a complex biochemical cascade starting with the phosphorylation of ITAMs by the lymphocyte-specific protein tyrosine kinase (Lck), the recruitment of a signaling protein called zeta-chain associated protein kinase 70 (Zap70) to the TCR-CD3 complex, the activation of the LAT scaffold protein and subsequent calcium signaling to name a few, processes that lead to cytokine production and T cell proliferation marking the initiation of an immune response (9).

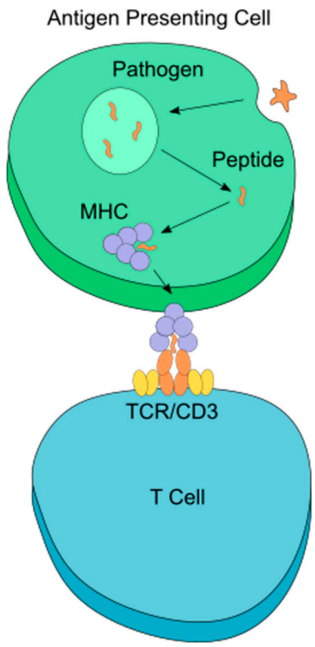

Figure 1.1. Demonstration of the phagocytosis process in which engulfed pathogenic proteins are degraded into peptides and the subsequent interaction of an APC with a T cell.

Despite its significance in initiating an immune response, there are several obstacles concerning the interaction between the TCR and the corresponding MHC. To begin with, TCR and MHC are both small membrane molecules with approximately 7 nm in size while the cell surface is covered by a cushion, hair-like layer of approximately 40 nm in height, the so-called glycocalyx. This layer, formed by glycolipids and glycoproteins (e.g. CD45 and CD43), is negatively charged hence it provides an electrostatic and steric barrier hindering any TCR and MHC engagement (10, 11). Moreover, T cells must be able to recognize a remarkable low amount of agonist peptide MHCs on the surface of APCs among a vast amount of 'self' peptides and even though it has been shown that T cells can be activated in the presence of fewer than 10 agonistic peptide MHC molecules, it is not understood to this day how this can be achieved. (5, 6, 12). Lastly, there are specific proteins that inhibit the T-cell activation which therefore need to be excluded from the formed contact between the T-cell and the APC for a successful immune response. For example, the kinetic-segregation model claims that the first step in TCR triggering is the exclusion of the CD45 glycoprotein from the cell-cell contacts since it contains an intrinsic phosphatase domain able to dephosphorylate tyrosine (13).

On the other hand, there are several membrane proteins including co-stimulatory receptors and adhesion molecules whose function is to facilitate the initial cell-cell contact formation and, in this manner, actively contribute to T cell activation. Due to their significant role in initiating an immune response, these biomolecules will be discussed in more detail in the next sub-chapters. It is noteworthy to mention that a successful antigen detection will result in an extended contact formation between the APC and T cell surfaces. During this process, several surface proteins together with the TCR-MHC complexes accumulate and reorganize into specific domains according to their specific protein binding energies, densities and heights (14–16). This formed contact area, the so-called immunological synapse, covers an area of 50-100 μm^2 in which the TCR-MHC complexes are surrounded by an integrin family of adhesion molecules in a ring-like structure (15, 17). The immunological synapse forms within a few minutes of TCR-MHC engagement and it is considered essential in the stabilization of the T cell-APC interaction which leads to downstream signaling and to a successful T cell activation (15, 18). However, it has been shown that active signaling, indicated by activated kinase recruitment, takes place before the formation of a mature synapse which raises further questions about the exact functions of the immunological synapse in T cell triggering (19, 20). Figure 1.2 illustrates the complexity of cell-cell contact formation between a T cell and an APC

depicting some of the numerous constituents present on a cell membrane such as lipids, proteins and glycosides.

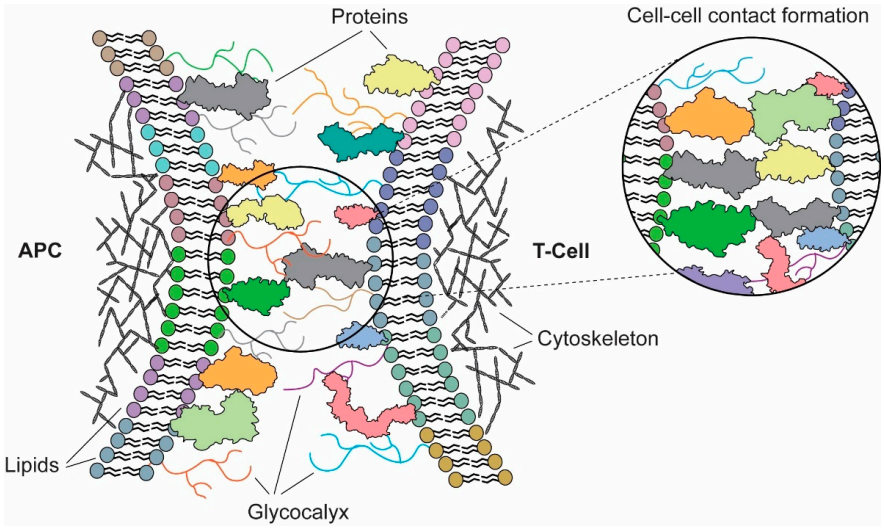

Figure 1.2. Schematic illustration of an APC in contact with a T cell showing the complexity of the cell membrane due to its various lipids, glycosides, and proteins. Membrane protein interactions form the immunological synapse leading to T cell activation. Figure adapted from (21).

1.2 The Role of Co-receptors

The T cells are characterized by the kind of TCR that they express on their surface but also by some specific proteins called co-receptors (22). The term “co-receptor” was employed to emphasize their importance in the signaling process and most T cells express either CD4 or CD8 co-receptors distinguishing the two preeminent classes of T cells, helper T cells and cytotoxic T cells, respectively. Helper T cells recognise MHC class II-bound antigens produced by the process of phagocytosis and, upon activation, they produce cytokines to activate multiple effector mechanisms, especially the antibody production by the B cells. On the other hand, cytotoxic T cells kill infected or cancerous cells preventing any further cell division as a result of recognising MHC class I-bound antigens. Despite their important role in T cell activation, in part due to their association with an activating kinase (23, 24), there are still many questions concerning the function of those two co-receptors in APC-T cell interaction especially since

they both bind their respective ligands weakly (25–27). In particular, the experimental difficulty in elucidating the role of CD4 is owed to its very low binding affinity which is the lowest of any other protein-protein interaction known to this day (27).

1.3 The Role of Adhesion Molecules

There are several adhesion molecules whose presence is considered a dominant factor for a successful T-cell activation. For example, it is established that the CD2-CD58 interaction is considered critical in supporting the initial contact formation between a T cell and an APC (28–31). Different signaling models attempt to describe how the various adhesion molecules assist the cell-cell contact formation but how exactly these binding events take place and their role during the immunological synapse formation remains unclear (32, 33). It is nevertheless generally recognized that the interaction between adhesion molecules is essential in overcoming the repulsion of the glycocalyx and in positioning the two opposing membranes at an optimum intermembrane distance (34). It is also accepted that the adhesion molecules are important in increasing the sensitivity of the TCR for its agonist peptide MHC and hence lower the threshold for activation (15, 33, 35), even though TCR and peptide MHC can bind and signal without the presence of these assisting molecules (14, 36). It is lastly recognized that weak binding interactions strongly depend on the addition of adhesion molecules to ensure contact formation, thus adhesion molecules are vital in studies on immune cell adhesion and communication.

1.4 Summary

Overall, the T cell and APC interaction is crucial for a successful adaptive immune response, however, there has been significant controversy about the molecular mechanism of T cell receptor activation and downstream signaling. Furthermore, the explicit role of the numerous proteins involved in the cell-cell contact formation and their exact contribution to the initiation of an immune response is not fully understood. This long-lasting debate in T-cell activation demonstrates the need for further research in the field of protein-protein interactions and for developing new biophysical models to better understand how an immune response is initiated.

Chapter 2

2. Supported Lipid Bilayers and Microscopy

Contents

In Chapter 2, I will provide a theoretical background of the applied techniques used for the work presented in the following chapters. An emphasis will be given on supported lipid bilayers as a model system to quantify individual protein-protein interactions and on the various microscopy techniques available for image acquisition.

2.1 The Cell Membrane

The cell membrane is a thin semi-permeable biological membrane whose function is to protect the cell from its external environment, to regulate both passive and active transport of essential nutrients across it and to transmit cellular signals (37–39). The view of the cell membrane and its functions has changed substantially over the past decades. It has been almost a century of cell membrane research from Overton´s suggestion that cell membranes are composed of lipids until Singer and Nicholson proposed the fluid mosaic model which is extensively accepted today (40). According to this model, the structure of the plasma membrane can be described as a mosaic of components with a high degree of lateral diffusivity and flexibility on a fluid membrane (40).

In more detail, the cell membrane consists primarily of several building components. Lipids are the most abundant element of a biological membrane consisting of a polar (hydrophilic) head group and one or two apolar (hydrophobic) hydrocarbon chains. From the numerous lipids composing a cell membrane, the most dominant ones are glycerophospholipids (generally referred to as phospholipids), sphingolipids, and sterols. Lipids are particularly interesting as they spontaneously self-organize to supramolecular structures in aqueous solutions due to their amphiphilic nature (41, 42). Therefore, in the aqueous environment of biological systems, these lipids can yield different supramolecular structures. Among those, the lamellar phase is one of the most common in nature: it is composed by a stack of layers, where the hydrophilic heads of the lipids are exposed to the bulk water and the hydrophobic tails interact with the tails of a second layer of lipids, reducing the unfavorable interactions with the water molecules. In such a manner, a lipid bilayer is formed, which can be flat (if it is formed on a surface) or curved (i.e., cells and vesicles).

The second major component of the plasma membranes are the membrane proteins. These biomolecules carry out several important biological cell processes including transport, signal transduction, intracellular joining and cell-cell recognition (43). The membrane proteins can be embedded in and span through the entire cell membrane (integral membrane proteins) or

they can be found on either side of the cell membrane transiently associated with it (peripheral membrane proteins). Many of the cell membrane proteins have heavily glycosylated extracellular domains forming a hair-like layer around the cell, the glycocalyx (Figure 2.1) (44).

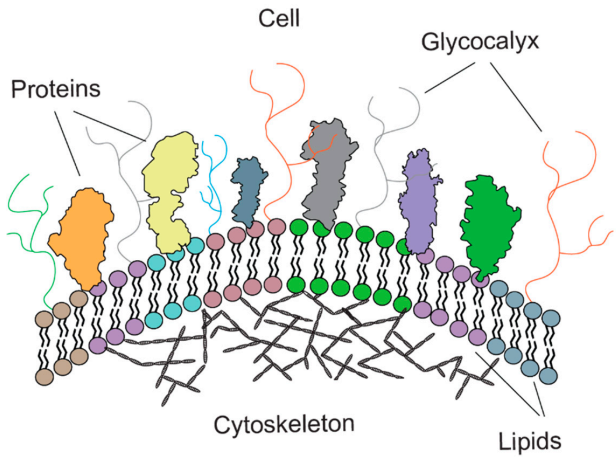

Figure 2.1. Schematic representation of a cell membrane.

Deciphering the complex interaction between lipids and membrane proteins as well as the interaction between the myriad of proteins on opposing membranes constitute two fields of active research. An enhanced understanding of these interactions would substantially expand our knowledge related to cellular processes, such as molecular sorting, intracellular/extracellular vesiculation, and cell triggering and would considerably influence numerous scientific disciplines.

2.2 Model Membranes and Supported Lipid Bilayers

Extensive ongoing research on the cell membrane has been conducted to further comprehend the membrane structure and functions as well as the properties of membrane proteins (45, 46). The properties of cell membranes and the interaction between membrane proteins are of outmost importance in the field of immunology since the communication between cells regulates the outset of an immune response. However, due to the substantial complexity and the dynamic nature of cell membranes, model membranes are often experimentally employed

instead since they allow the investigation of cell components in a simplified and regulated environment. The first model for cell membranes, the so-called free-standing "black lipid membranes", was developed in 1962 by Mueller and Rubin (47). According to this method, the bilayer is formed by "painting" a phospholipid solution across a hole formed in a hydrophobic material between two compartments filled with saline. Despite their ingenuity and their ability to measure the electrical properties of membranes, black lipid membranes are notoriously unstable and the available detection methods are limited (48, 49). The advent of glass-supported lipid bilayers (SLBs) in the early 1980s by McConnell *et al*. paved the way for extensive research of cell membranes properties (48, 50–52). An SLB is a cell membrane mimic in which a bilayer is created on a hydrophilic solid support with an approximately 1 nm thick hydration layer separating the bilayer from the substrate (Figure 2.2) (50, 53). There are several advantages of using SLBs such as their high stability which provides possibilities for long term measurements, their ability to create a natural environment for proteins without suppressing their lateral diffusivity, and their planar geometry which allows the usage of numerous advanced methods for surface and image analysis (54). Nonetheless, the two major disadvantages of using SLBs are that the supported membrane is partially coupled to the underlining substrate and that certain properties due to membrane curvature are lost (48). In addition to being used in studies of cell-cell interfaces, SLBs have also been successfully utilised in various biochemical studies examining phase separation (55) and peptide-lipid interactions (56). The different methods to fabricate SLBs will be presented in the following subsection.

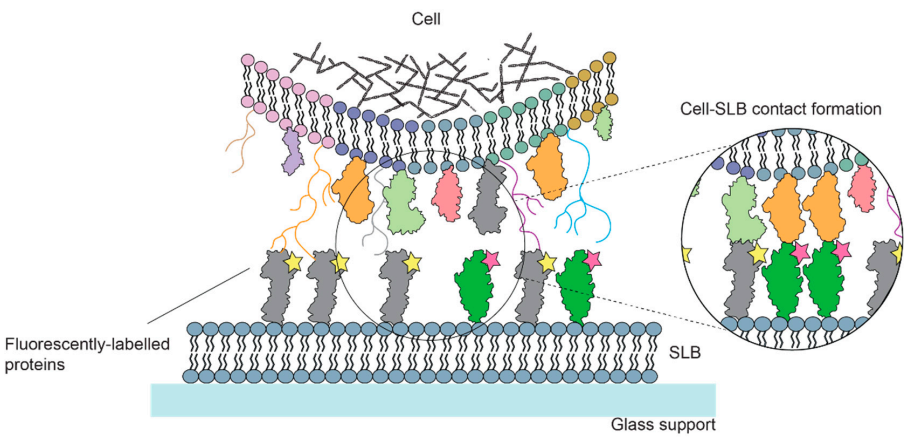

Figure 2.2. Illustration of a cell binding to a model membrane with a controlled composition to mimic the intricate cell-cell interaction.

2.2.1 Fabrication of Supported Lipid Bilayers

A multitude of methods have been developed for forming different types of SLBs (43, 57). The first system consists of a closely packed monolayer of lipid molecules at a liquid-gas interface (Figure 2.3 A) (58). Due to their amphipathic nature, the hydrocarbon chains orient themselves towards the gas phase while the polar headgroups are immersed in the aqueous phase. On the other hand, the Langmuir-Blodgett technique involves the deposition of amphiphilic molecules from the air-water interface to a solid substrate (Figure 2.3 B) (59). The deposition of a second monolayer of lipid molecules onto the first one results in the formation of a lipid bilayer. This technique has the advantage of allowing the customization of the lipid composition of each leaflet however it is time-consuming and requires expensive equipment. The last and most commonly used method involves the adsorption, rupture and fusion of lipid vesicles on a hydrophilic substrate (Figure 2.3 C) (60, 61). Vesicles are usually obtained upon drying lipid films from an organic solvent under vacuum; then, after hydration and mixing via ultrasonication or extrusion, vesicles of a desired lipid composition of various sizes ranging from nm to μm are formed (48). Depending on their diameter, they are categorized as small unilamellar vesicles (10-200 nm), large unilamellar vesicles (200 nm – 1 μm), giant unilamellar vesicles (> 1 μm), and multilamellar vesicles (which are vesicles engulfing one or more vesicles in their inner compartment). Small unilamellar vesicles or SUVs with a typical radius of 25 to 100 nm are utilized to form SLBs since they are more prone to fuse than larger sized vesicles. One common technique to produce SUVs is through ultrasonic sonication in which sound energy is used to disrupt the vesicles causing their continuous rupture and reformation. Upon incubation of SUVs with solid hydrophilic supports such as glass, silica, or mica, the SUVs will adsorb to the substrate surface, rupture, and eventually form bilayer patches before forming a continuous phospholipid bilayer (62).

One essential feature of SLBs is the thin hydration layer between the headgroup layer and the solid surface that ensure the fluidity of the bilayer. Nevertheless, a drawback when using SLBs is that they are not appropriate for incorporating transmembrane proteins due to the limited space between the bottom leaflet of the bilayer and the solid supporting substrate (approximately 1 nm) (63). This interaction leads to undesirable friction forces and hence to

the unavoidable immobilization of the transmembrane proteins (63, 64). However, one possible approach to overcome this unfavourable interaction is to employ polymer-cushioned lipid bilayers such as lipids conjugated to polyethylene glycol, PEG, which sufficiently separate the bilayer from the underlying substrate (Figure 2.3 D) (65, 66).

The Langmuir-Blodgett and the vesicle fusion methods described above result in the formation of a ~5 nm thick continuous lipid bilayer, however, vesicle fusion was preferred for the work following in the next chapters as it is a simple, versatile, and widely accessible technique to produce continuous and robust SLBs.

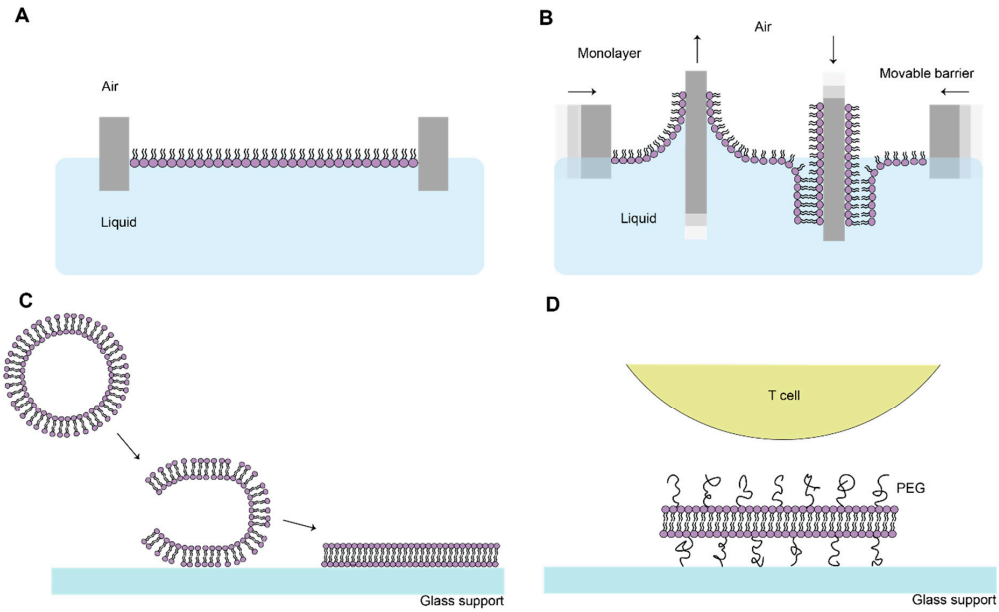

Figure 2.3. Different methods for forming SLBs. (A) The Langmuir film consists of a monolayer of amphiphilic molecules spread at an air-water interface. (B) The Langmuir-Blodgett technique relies on the deposition of the monolayer onto a hydrophilic surface. A subsequent immersion of the solid surface into the liquid results in a continuous and fluid bilayer. (C) Schematic of the adsorption and fusion of lipid vesicles on a hydrophilic glass support resulting in the formation of an SLB. (D) Incorporating lipids with PEG chains attached to their headgroup sufficiently separates the bilayer from the underlying substrate and enables the incorporation of transmembrane proteins. Figure adapted from (21).

2.2.2 Protein-functionalized Supported Lipid Bilayers

SLBs produce an extended two-dimensional area mimicking the cell-membrane surfaces while simultaneously allowing the translation and rotation of purified lipid-associated proteins with diffusion coefficients on the order of 1 $\mu m^2/s$. Generally, approximately 95 % of SLB-anchored proteins are mobile, which makes them suitable for studies of protein adsorption, protein self-assembly, and protein function. The small immobile fraction is attributed to defects in the bilayer which results in proteins being trapped between the bilayer and the glass support (67).

There are numerous accepted methods to link proteins to bilayers, such as *via* nitrilotriacetic acid (NTA)-chelating lipids (68), biotin-streptavidin interactions (69) or a glycosylphosphatidylinositol (GPI) linker (70) (Figure 2.4). All methods result in lateral mobile proteins linked to lipids in an SLB and are used extensively to study inter- or intra-protein interactions. However, biotin-streptavidin-linked proteins introduce a significant extension of around 5nm (the height of streptavidin) to the overall protein size so that they would increase the protein-SLB distance. This height difference could affect the intermolecular interactions and the binding kinetics of the proteins during cell-SLB contact formations which were the focus of this thesis. On the other hand, a disadvantage of using GPI-linked proteins is that the GPI linker itself can cause protein aggregation (71) and that the preparation of GPI-anchored proteins is quite demanding. Therefore, in this thesis, the NTA-chelating approach was preferred in which the proteins of interest are modified with six consecutive histidine molecules (His-tag) at the C-terminus which bind to nickel-chelating head groups on the bilayer. A slight disadvantage of the ionic NTA-Histidine interaction is that, eventually, the proteins detach from the bilayer, especially when multiple protein species are competing for the same binding positions (72). To reduce this effect, polyhistidine-tags with more histidine units coupled with prolonged incubation times of the histidine-tagged proteins with the SLB can be employed (71).

In this work, the used vesicles contained POPC phospholipids and NTA-chelating lipids 1,2-dioleoyl-sn-glycero-3-[(N-(5-amino-1-carboxypentyl)iminodiacetic acid)succinyl] (nickel salt) (DGS-NTA). The vesicles were then sonicated to yield SUVs and were placed inside a silicon well attached to a glass coverslip where a SLB was formed through vesicle rupture. The glass coverslip had been cleaned using piranha solution to render the glass support hydrophilic. After one hour, the unruptured vesicles were washed away and the His-tagged proteins were added to the well. The proteins were incubated for approximately one hour to reduce the

undesirable detachment from the bilayer during the experiment (72). Lastly, by washing away the unbound proteins, the protein functionalized SLBs were prepared for subsequent measurements.

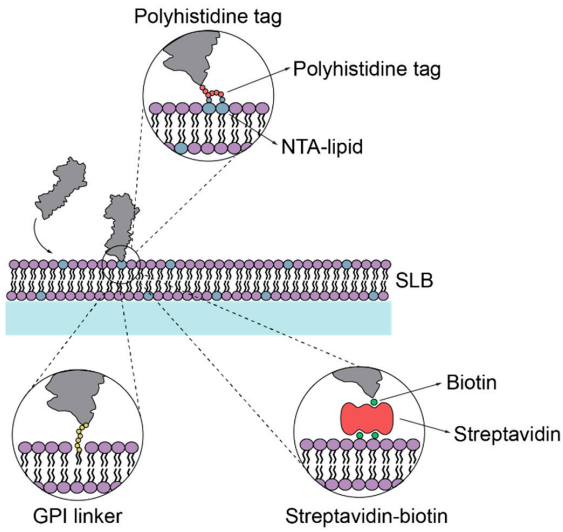

Figure 2.4. Schematic representation of ligand proteins anchored in the SLB using different anchor strategies. Figure adapted from (21).

2.3 Imaging Techniques for Supported Lipid Bilayer Analysis

Several microscopy techniques have been developed in recent decades that have allowed an unprecedented view of protein assemblies bound to SLBs. Fluorescence microscopy is one of the most important techniques used to visualize membrane-bound components as it is a highly sensitive and reliable method. It is an optical technique that depends on the property of fluorescent molecules, commonly called fluorophores, to absorb light at a certain wavelength and re-radiate the light at a longer wavelength. The excitation and emission wavelengths depend on the atoms as well as the structure of the molecule. In more detail, upon absorption of a photon of a suitable wavelength, a valence electron of the molecule is raised to the excited state, but within a time scale of a few nanoseconds, the molecule relaxes to the ground state by emitting a lower energy photon (Figure 2.5 A). The excitation of the electron is followed by its relaxation to the lowest-energy sublevel of the excited state via a combination of vibrational relaxation and dissipation. This leads to a difference in the energy of the electronic transition

between absorption and emission which is called the Stokes's shift (Figure 2.5 B). Nevertheless, fluorescence is not the only possible path by which the electron can return to the ground state. External conversion, which is a non-radiative process due to the collision of molecules, or intersystem crossing, due to different spin multiplicities between the energy levels, can also occur.

The major advantage of using fluorophores is that they can be easily attached to the structures of interest with high specificity and that light from the non-fluorescent material of the sample can be filtered out (73). Nowadays, a plethora of different fluorophores exists with different characteristics. However, an ideal fluorescent molecule should have explicit excitation and emission wavelengths, should not alter the natural behavior of the biomolecule that it is attached to, should have a high fluorescence quantum yield with a steady emission intensity and should be able to emit photons for a long period of time under high illumination intensities (74).

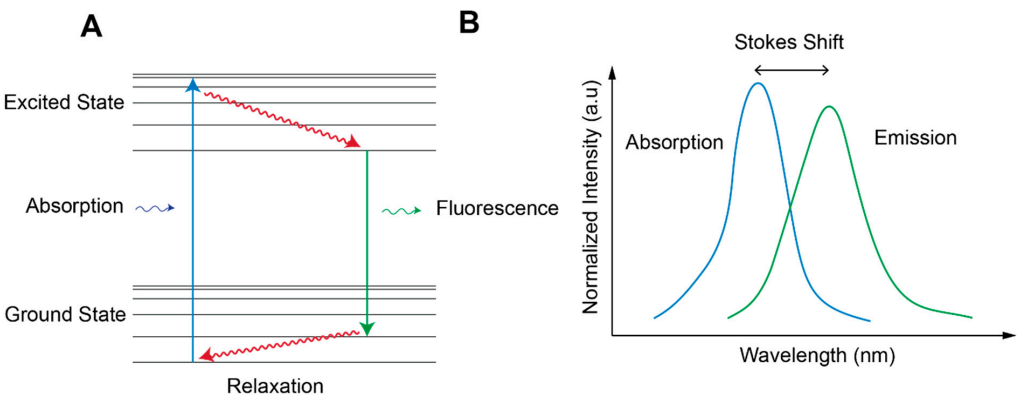

Figure 2.5. **(A)** Jablonski's diagram illustrating the excitation of a valence electron to its excited state followed by subsequent relaxation to the ground state by fluorescence. **(B)** Absorption and emission spectra of a fluorophore depicting the wavelength difference between the positions of band maxima of the two spectra.

However, a considerable limitation of fluorophores is that after a certain characteristic number of excitation and emission cycles, they will irreversibly convert to a dark state thus losing their ability to fluoresce. This photodamage, called photobleaching, is associated with the oxidation of the fluorophore (75). Furthermore, blinking is another tendency of the fluorophores that

should be considered. Blinking is the phenomenon of random switching between the bright and dark states and is usually attributed to intersystem crossing (75).

There are currently numerous prevailing microscopy techniques based on fluorescence illumination to study the dynamical changes in cells, cell membranes and SLBs providing different resolutions, and thus information about the sample. The microscopy methods that were used in this study are explained in the following subsections.

2.3.1 Widefield Epifluorescence Microscopy

Widefield epifluorescence microscopy is an irreplaceable tool used in all the fields of life sciences (76, 77). In an epifluorescence microscope, the objective lens is used as both the illumination condenser and the fluorescent light collector (Figure 2.6). The key element of this optical technique is the dichroic mirror which is used to reflect the shorter excitation wavelength from the light source toward the sample and later transmit the longer emitted wavelength toward the detector. Uniform illumination is achieved by focusing the excitation beam on the back focal plane of the objective. In addition, appropriate filters are used to enhance the selection of relevant excitation and emission wavelengths. The excitation filter removes any light from the excitation source that overlaps with the transmission window of the emission filter while the emission filter dismisses any unwanted excitation light from reaching the detector.

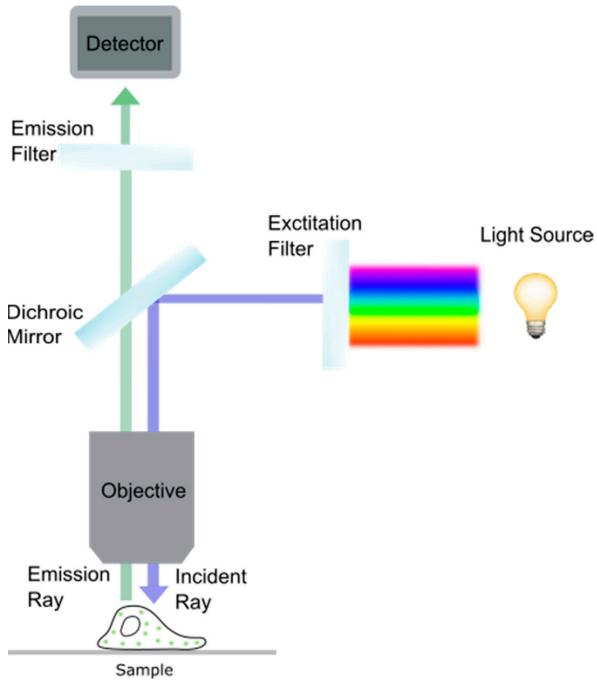

Figure 2.6. Schematic illustration of the epifluorescence microscope set up.

Epifluorescence microscopy offers high sensitivity and selectivity; however, one of the main drawbacks is that in-focus as well as out-of-focus light can reach the detector. This results in strong background fluorescence due to autofluorescence from different cellular components or from fluorescent proteins located in the bulk.

As a matter of fact, a major challenge in optical microscopy is to reduce the fluorescence background as the latter significantly decreases the signal-to-noise ratio thus deteriorating the image quality. Numerous microscopy techniques are able to suppress this background noise by decreasing the excitation volume into a thin film of light (Total Internal Reflection Fluorescence microscopy) (78) or into a small volume of light (Confocal microscopy) (79). The former was used as the main microscopy method to visualize the SLBs and is presented thoroughly in the next subchapter.

2.3.2 Total Internal Reflection Fluorescence Microscopy

Total Internal Reflection Fluorescence Microscopy (TIRF) is a non-invasive and far-field optical imaging technique that is particularly well suited to study the dynamics and the localization of molecules near the plasma membrane or on an SLB. The seminal idea of using total internal reflection to illuminate contacts formed between cells and solid surfaces was first introduced by E.J. Ambrose in 1956 (80). In more detail, the principle of TIRF microscopy is based on Snell's law which describes the path of a propagated beam at the interface of two media that differ in their refractive indices:

$$n_1 sin\theta_1 = n_2 sin\theta_2 \qquad (Eq. 2.1)$$

where n_1 and n_2 are the refractive indices of the two media while θ_1 and θ_2 are the angles relative to the interface normal of incidence and refraction respectively. An excitation beam encountering the interface between a glass coverslip n_1 and the sample media n_2, where $n_2 > n_1$, will get refracted and continue its propagation with $\theta_2 > \theta_1$ (81). By increasing θ_1, θ_2 will eventually reach 90° where the propagated light will travel along the interface (81). This occurs at a critical angle, defined from Snell's law as $\theta_c = \sin^{-1}(n_2/n_1)$ and is approximately 61° for $n_{water}=1.33$ and $n_{glass}=1.52$. At angles of incidence greater than this, total internal reflection of the incident beam occurs at the interface between the sample and the coverslip (Figure 2.7).

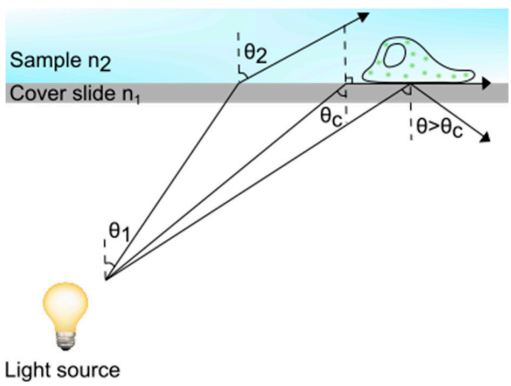

Figure 2.7. Schematic drawing of the crossover from refraction to reflection in TIRF microscopy.

Since the numerical aperture (NA) of the objective is defined as $n \cdot \sin\theta_{max}$, where θ_{max} is the maximum incidence angle, it is evident that the critical angle can be reached only if the NA of the objective is greater than the refractive index of the sample. Because of this, oil immersion objectives have been designed to have a numerical aperture close to 1.5. At total internal reflection conditions, no incident light passes through the sample, however, some of the incident energy does penetrate creating an evanescent field, at the solid-liquid interface (Figure 2.8) (78). The evanescent field decreases exponentially with distance to the interface z as (82):

$$I(z) = I(0)e^{-\frac{z}{d}} \qquad (Eq. 2.2)$$

where I(0) is the intensity of the evanescent field at z=0. Here d is defined as the penetration depth, given by:

$$d = \frac{\lambda}{4\pi\sqrt{n_1^2 sin^2(\theta_1) - n_2^2}} \qquad (Eq. 2.3)$$

where λ is the wavelength of the excitation light in vacuum (82). The penetration depth is typically between 100-200 nm restricting the illumination to a thin volume above the sample coverslip.

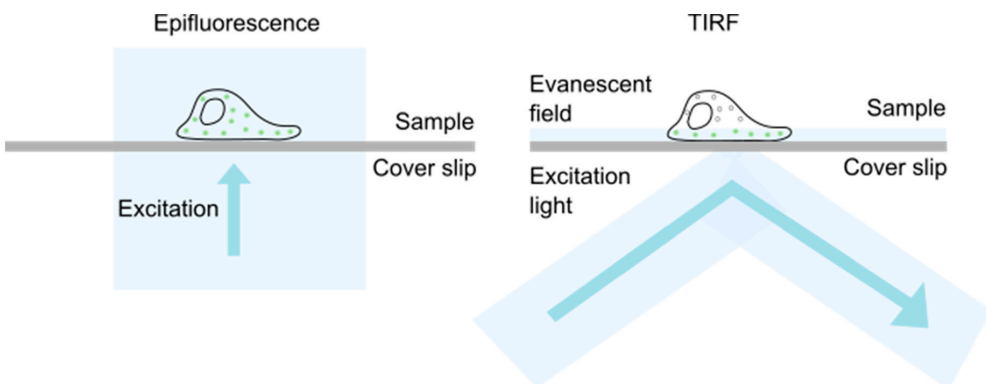

Figure 2.8. Comparison of the optical paths between epifluorescence (left) and TIRF (right) microscopy techniques.

This allows for the selective excitation of fluorophores near the sample surface and the creation of images with a higher signal-to-noise ratio as the background fluorescence is diminished. This selective excitation reduces the phototoxicity throughout the cell as well since a small part of the sample is exposed to the excitation light. Another substantial advantage of TIRF microscopy is that it is compatible with other microscopy methods as the angle of incident light can easily be adjusted from epifluorescence mode to TIRF mode and *vice versa*.

2.3.3 Fluorescence Recovery After Photobleaching

Fluorescence recovery after photobleaching (FRAP) is a prevalent technique in biophysics to obtain information about the mobility and dynamics of proteins and lipids in a membrane structure (83, 84). This pioneering technique emerged from Watt Webb's lab in the mid-1970s and involves the deliberate bleaching of fluorophores on a small area from a high-intensity laser beam (85). Consequently, bleaching of the fluorophores results in a substantial intensity drop and the generation of two subpopulations of molecules: bleached (invisible) and unbleached (visible) (Figure 2.9). Quantifying the extent of any recovery of fluorescence in the bleached region is a metric of molecular mobility and turnover processes. The obtained fluorescent recovery curves provide information about molecular transport parameters such as the mobile fraction and the diffusion coefficient of the proteins in the bilayer (86). In this work, FRAP measurements were performed routinely at the beginning of each experiment to ensure the formation of a fluid bilayer.

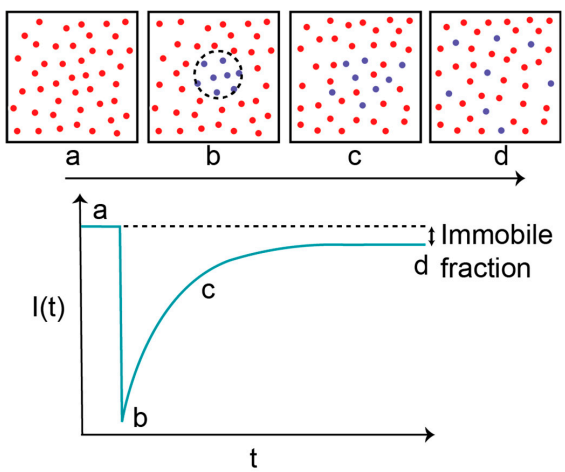

Figure 2.9. Schematic representation of a FRAP experiment on a fluorescently labelled SLB.

2.3.4 Brightfield Microscopy

Brightfield Microscopy is possibly the simplest transmission light microscopy technique that uses variations in the intensity of the transmitted light to generate an image of the specimen. The differences in intensity of light are a result of the sample´s absorbance and scattering caused by the material´s refractive index. The subsequent interference of the attenuated with the unvaried illumination light generates the intensity variation. This technique has low contrast for weakly absorbing samples and low resolution due to out-of-focus light, however, it allows the imaging of whole samples and was thus extensively used to provide information on the position and the viability of the cells interacting with protein-functionalized SLBs.

2.4 Fundamental Limits in Imaging

All the aforementioned microscopy techniques have a spatial resolution that is limited by diffraction. In more detail, the resolution of an optical system describes the minimal distance at which two sources of light are distinguishable from each other. It was in 1873 when Ernst Abbe declared that the resolution of the light microscope is limited by the diffraction properties of light (87). This limitation, commonly known as the Rayleigh criterion, is expressed through the following formulation:

$$\Delta r = \frac{0.61\lambda}{NA} \qquad (Eq.\,2.4)$$

where Δr is the minimum separation distance between two distinguishable point sources, λ is the wavelength of light and NA is the numerical aperture of the objective (88). Hence, if the distance between two sources of lights is smaller than Δr, then they cannot be resolved. The resolution limit is due to the wave nature of light and it can be understood by studying the interaction of light with the microscope objective. When light emitted from a point source passes through a small circular aperture, like an objective lens, it produces a bright circular disc surrounded by much fainter concentric rings of increasing radius from the centre. This circular disc is called an Airy disk, the shape of which is determined by the point spread function (PSF) of the microscope system. Every point source forms a corresponding Airy disk in the image

space therefore the intensity pattern of two-point sources close to each other will be a superposition of the two Airy disks. As the distance between the two sources is decreasing, the superposition of the Airy disks does not allow the imaging system to resolve them. Thus, according to the Rayleigh criterion, Δr is obtained when the first minimum of one of the Airy disk superpositions with the maximum of the other Airy disk. For a conventional light microscope, the horizontal resolution is approximately 220 nm with a 450–700 nm resolution in the axial direction. An important remark is that the resolution in the vertical plane is generally worse than in the horizontal one due to the wider spread of the Airy disk in the former plane.

2.4.1 Super-Resolution Microscopy

There is a series of techniques designed to provide a spatial resolution that surpasses the diffraction limit by temporally or spatially modulating the excitation or activation of light and thus are known as 'super-resolution' microscopy methods. These methods provide insights into the functional localization and interactions of biological particles down to nanoscale precision (89). The most prominent super-resolution microscopy techniques are structured illumination microscopy (SIM) (90), stochastic optical reconstruction microscopy (STORM) (91), stimulated emission depletion microscopy (STED) (92), photoactivated localization microscopy (PALM) (93) and single-molecule imaging (94). Since single-molecule imaging was the method of choice in this thesis, it will be discussed in the following subchapter.

2.4.2 Single-Molecule Detection

Single-molecule imaging and subsequent single-particle tracking (SPT) have been used extensively to study the behavior of lipids and proteins in the plasma membrane since the optical observation of single molecules from Hirschfeld in 1976 (94). The extensive interest in single-molecule studies stems from the fact that they provide data concerning the stochastic nature of single molecule events and their biologically relevant heterogeneity thus revealing multiple fundamental molecular-scale biological processes (95, 96). Single-molecule imaging relies on the successful detection of emitted photons by one or more fluorophores attached to a single biomolecule (97, 98). The fluorescence from low-density emitters is imaged as bright spots, with a width characterising the microscope´s PSF. However, by fitting a 2D Gaussian function to the fluorophore´s PSF it is possible to extract the x- and y- coordinates of the

particles with a spatial resolution that surpasses by a considerable margin the diffraction limit of the microscope (in the order of 10 nm) (99). Subsequent SPT, accessible through a large variety of available tracking algorithms, investigates the movement of individual particles from a time series of microscope images and has played a central role in many of the advances in single-molecule imaging (Figure 2.10) (100–102).

It is important to emphasize that optimization of the signal-to-noise ratio is essential in these optical techniques. Unwanted noise such as shot, readout, dark, and background noises should be suppressed. Furthermore, various image processing algorithms can be applied to separate the fluorescent particles from the background, in particular a combination of smoothing filters and background subtractions (100). Last but foremost, small fluorescent tags with robust photophysical properties and highly sensitive detectors are crucial for successful SPT experiments. In this study, single-molecule imaging and subsequent SPT were used extensively to obtain information about diffusion coefficients and the lifetimes of ligand proteins on an SLB interacting with receptors expressed on the surface of T-cells.

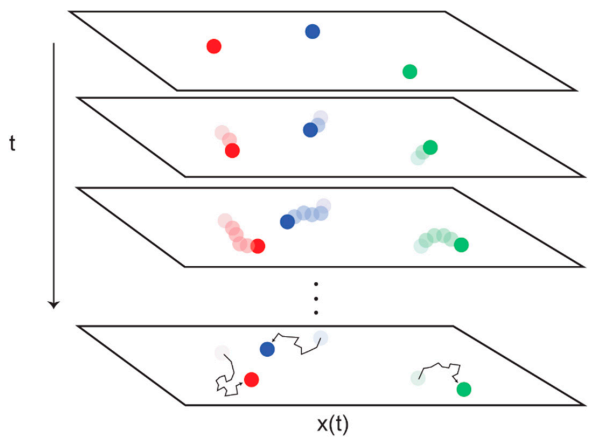

Figure 2.10. Single-molecule fluorescence microscopy is used to track the motion of proteins (red, blue and green circles) on a cell or artificial membrane (white rectangles). The tracked particles diffuse through the membrane (faded circles) and the diffusion over time, *t*, can be reconstructed as trajectories shown in the last rectangular plane.

2.5 Summary

In this chapter, the role of functionalized-SLBs was highlighted as a model system to study the interaction between proteins on contacting cells. SLBs allow for a controlled composition of lipids and proteins with high stability and accessibility by various detection methods. The different microscopy techniques used to study the fluorescently-labelled proteins on the SLBs were later presented discussing their respective advantages and limitations. In the forthcoming work, TIRF microscopy and FRAP measurements were used to observe and characterize protein-functionalized SLBs interacting with immune cells. In addition, functionalizing the SLB with low density fluorescent proteins allowed for SPT which yielded more information regarding the binding kinetics of the examined proteins. Overall, SLBs have made it possible to study the interaction of numerous key protein-protein pairs thus establishing themselves as a vital biophysical and biochemical tool for many years to come.

Chapter 3

3. Single-Cell & Single-Molecule Studies

Contents

In this chapter, I will give an overview of protein-protein interactions focusing on the binding affinity and the lifetime of the studied complex. Later, I will present the most prevailing methods used to obtain the kinetic values that characterize this complex. The focus will then move on to present a novel method of obtaining single-cell binding affinities summarizing the most important findings from **Paper I.** The chapter will finish with results from single-molecule imaging and their relation to the lifetime of the protein-protein complex.

3.1 Receptor-Ligand Binding Kinetics

Protein binding is based on the molecular interaction and subsequent recognition of a protein receptor to its binding partner, called a ligand. The non-covalent binding interaction between a receptor and its ligand can be described by a second-order forward and first-order reverse equation:

$$\mathrm{R} + \mathrm{L} \underset{k_{\mathrm{off}}}{\overset{k_{\mathrm{on}}}{\rightleftharpoons}} \mathrm{RL} \qquad (Eq.\,3.1)$$

where R represents the receptor, L the ligand, and RL the receptor-ligand complex. Since any binding reaction is highly dynamic with a continual transition between binding and unbound states, there are two rate constants to describe this process. The parameter k_{on} is called the association rate constant and describes the rate at which the ligand-receptor complex will be formed as opposed to the dissociation rate constant, k_{off}, which indicates the probability that the complex will dissociate in a unit of time. Over time, the reaction will reach an equilibrium in which the concentrations of R, L and RL are held in steady-state and where the association and dissociation constants are equal:

$$k_{on}[R][L] = k_{off}[RL] \qquad (Eq.\,3.2)$$

where the square brackets denote the equilibrium concentration of the molecular species. From the above equation, the equilibrium-binding association, K_a, and dissociation, K_d, constants can be derived as follows:

$$K_a = \frac{[RL]}{[R][L]} = \frac{k_{on}}{k_{off}} = \frac{1}{K_d} \qquad (Eq. 3.3)$$

The equilibrium dissociation constant is a valuable parameter as it characterizes the binding affinity of a biomolecule to its binding partner and thus essentially, it appreciates the strength of the binding interaction. K_d and binding affinity are inversely related (K_d = 1/affinity) so that the smaller the K_d value, the stronger the affinity of the ligand for its binding partner and vice versa. Besides the binding affinity, another important parameter is the lifetime, τ_{off}, of the protein-protein interaction which describes the average time between the formation and dissociation of the complex. The lifetime of a protein-protein interaction is commonly determined by measuring the kinetic dissociation rate, k_{off}., since the average lifetime of the complex is $1/\langle k_{off} \rangle$ (103). Both binding affinity and lifetime are needed to determine the binding kinetics of a receptor-ligand complex and are therefore of great importance in screening compounds and drug candidates, in studying the regulation of different cellular pathways and in studying the interaction of two biomolecules to name a few. Moreover, determining the binding kinetics of protein-protein interactions is vital in understanding how the immune system works since numerous studies have supported that the TCR response is regulated by the affinity (104, 105), the association (106) and dissociation rates (107, 108) of the TCR-pMHC complex.

Since protein-protein interactions are vital to many aspects of cellular function, it is not surprising that there are numerous experimental techniques that have been developed to investigate different aspects of protein-protein binding (109). In the following subsections, the most frequently used methods to measure the binding affinity and the lifetime of protein-protein interactions will be discussed before presenting the main findings of **Paper I**. A more extensive discussion of the various techniques that have been used to measure binding kinetics of protein-protein complexes, any discrepancies between the obtained data and the different parameters that influence these measurements, such as auxiliary molecules, membrane fluctuations and force, are included in our review (21).

3.2 Three Dimensional Affinities

Three-dimensional (3D) binding affinities are obtained by measuring the interaction between proteins in bulk solution. There are two main methods commonly used to measure 3D binding

affinities: the isothermal titration calorimetry (ITC) (110) and the surface plasmon resonance (SPR) techniques (111). The latter is the most applied method today and hence the following section will focus on the principle of this method.

3.2.1 The Surface Plasmon Resonance Method

In the SPR method, the ligands of interest are immobilized onto a sensor metal surface (usually gold) while the receptors (or analyte) are injected into the flow cell to diffuse freely in an aqueous solution (Figure 3.1). Interaction and subsequent binding of the receptors to ligands result in the accumulation of proteins on the surface and thus in an increase of the refractive index near the surface. After the desired association time, a solution without the analyte is injected followed by a dissociation of the receptors. During this period, a laser is illuminating the ligand functionalized surface at a critical angle able to achieve total internal reflection. Since the critical angle depends on the refractive index near the surface, receptor-ligand interactions lead to a signal increase in a sensorgram from which information regarding the binding kinetics can be derived (112). At the same time, the light causes the electrons in the sensor chip to resonate. The reflected light experiences a characteristic intensity loss in areas where the frequencies of the electrons in the sensor chip and of the incident light become identical. This approach provides information on the k_{on} and k_{off} rates hence the binding affinity and lifetime of the complex can be calculated. The advantages of this method are that it is label-free and capable of measuring real-time receptor-ligand binding kinetics (113). Nevertheless, an important drawback of SPR is that the immobilization of the proteins affects the translational and conformational entropies, therefore the calculated association rate (114). Furthermore, with this method, the effects of ligand diffusion as well as ligand interactions with other cellular proteins cannot be investigated.

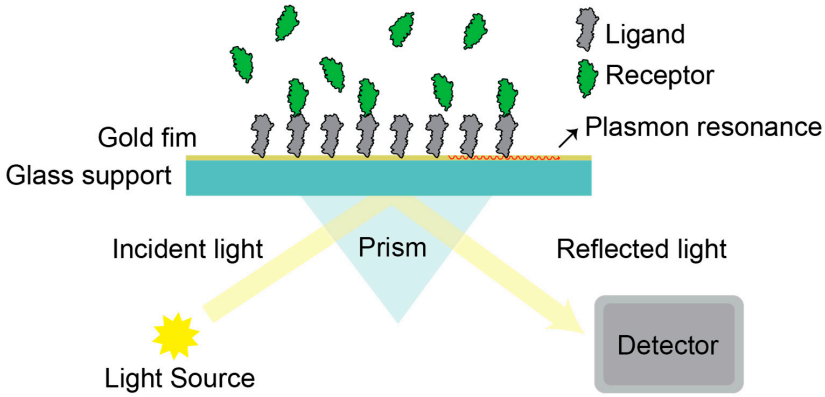

Figure 3.1. Principle of surface plasmon resonance.

For the time being, the lion´s share of the binding kinetics is obtained using 3D measurements. However, these findings do not express various cell and protein dynamics describing the binding of molecules across the cell–cell contacts *in vivo* since several other factors than the protein-protein interaction per se can have a significant impact on the obtained binding affinity (115, 116). Such factors are for example protein density (117, 118) and the use of auxiliary binding molecules (17), the latter being crucial in order to stabilize and initiate the binding of weakly-binding proteins (27). Also applied force on the bond (119) as well as membrane fluctuations (120) can have an important influence on the binding kinetics, although this can differ significantly depending on the under-study system. Lastly, the limited intercellular volume between contacts *in vivo* could significantly accelerate the association rate and augment serial engagement (34, 121). For these reasons, two-dimensional (2D) binding affinities which describe the interaction between proteins diffusing on plasma or artificial membranes are considered important.

3.3 Two Dimensional Affinities

There are two main approaches to measure 2D binding kinetics, the mechanical-based and the fluorescence-based methods. The principle of the most prevailing techniques for both approaches is presented in the next subchapters together with their corresponding advantages and disadvantages.

3.3.1 Mechanical-Based Methods

Numerous mechanical-based methods have been developed to measure 2D K_d values such as the centrifugation method (122), the flow chamber method (123), and the micropipette methods (124–126). Since the micropipette methods are the most applied mechanical-based methods to this day, the following section will focus on the principle of this approach.

3.3.1.1 Micropipette-based Methods

The adhesion frequency assay measures the adhesion probability per contact when a red blood cell (RBC) and a nucleated cell expressing the ligand and receptor of interest, respectively, interact (124, 125). Both cells are aspirated on micropipettes whereby the RBC is carefully brought into contact via micromanipulation resulting in a receptor-ligand interaction for a specified duration of time (Figure 3.2). By retracting the RBC, any attachment site between the two cells will result in an observed deformation of the RBC. This contact-retraction cycle is repeated hundreds of times and so both the lifetime and the effective binding affinity can be obtained (127). Later studies improved the measurement quality while reducing potential RBC-cell interactions by attaching a ligand-coated glass bead to the RBC, a method called thermal fluctuation assay (128). The micropipette methods have provided valuable insights into the initial stages of ligand-receptor bond formation, however, there are some important disadvantages to take into consideration. The effect of the micropipette aspiration on cells and how this can affect the obtainable binding kinetics remains unknown. Furthermore, the micropipette-based methods are limited to comparing the magnitude of the affinities with other interactions measured with the same system since they only provide effective affinities, defined as A_c/K_d, where A_c is the contact area, a parameter that cannot be accurately determined using these methods (129). Lastly, the micropipette approach is typically restricted to studying only one receptor-ligand pair since it is difficult to distinguish the effect of different pair contributions to the obtained adhesion frequency curves.

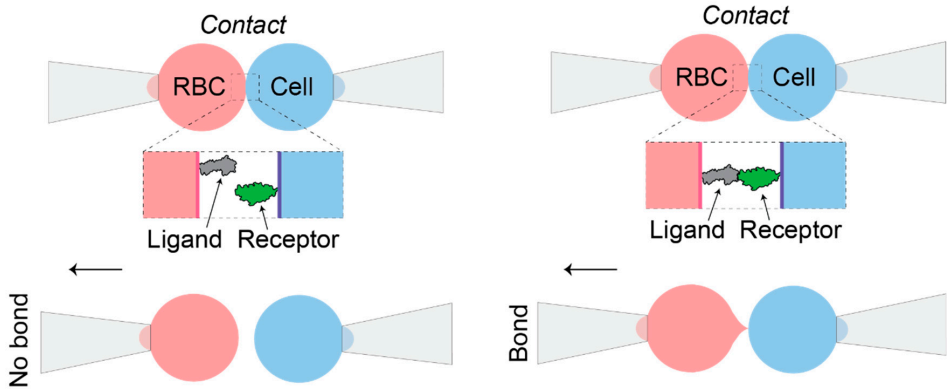

Figure 3.2. Schematic depiction of the micropipette method. The red blood cell (RBC) and the nucleated cell are aspirated onto two separate micropipettes. The RBC is brought repeatedly into contact with the nucleated cell and any shape changes upon receptor-ligand binding is carefully monitored. Figure adapted from (21).

3.3.2 Fluorescence-Based Methods

The earliest recorded ligand-receptor binding assays involved the use of radioligand binding assays, however recent developments in imaging technology combined with safety concerns have paved the way for fluorescent labelling and detection of ligands (130). There are several fluorescence-based methods to obtain 2D binding kinetics such as the Zhu-Golan method (131) and the single-molecule imaging and tracking methods (102). Both approaches were used extensively during my studies in order to obtain the binding affinity and the lifetime of a receptor-ligand complex and will be described in detail below.

3.3.2.1 The Zhu-Golan Method

In the mid-1990s, Dustin et al. performed extensive studies of binding kinetics using ligand-functionalized SLBs interacting with Jurkat T cells to determine the binding affinity of the CD2-CD58 interaction (34), using an analysis proposed by Scatchard in the late 1940s (132). However, the Scatchard method considers the receptor density to be constant, an erroneous assumption for cell-SLB contact formations since the receptors are mobile and can diffuse from outside into the contact area. In 2007, Zhu et. al. studied the CD2-CD58 interaction in order to develop a general methodology to quantitively measure the mechanisms governing cell-cell

adhesion (131). Their analysis, termed the Zhu-Golan analysis, is based on the accumulation of fluorescently-labelled ligands in the contact area of cells interacting with bilayers functionalised with several initial ligand concentrations. The accumulation of the ligands inside the cell-SLB contacts is a consequence of the law of mass action, resulting in an evident fluorescence intensity increase beneath the cell (Figure 3.3 A). By quantifying the change of ligand accumulation in dozens of cell-SLB contacts at various ligand densities, the 2D binding affinity of the protein-protein interaction can be determined. In contrast to the Scatchard method, the Zhu-Golan analysis takes into consideration the lateral mobility of both the ligands and the receptors and their ability to laterally diffuse into the contact area (131). The Zhu-Golan expression is given by the following equation:

$$\frac{B}{F} = \frac{N_t x f}{K_d x\, S_{cell}} - \frac{B\ x\ p}{K_d} \qquad (Eq.\ 3.4)$$

where B and F is the density of bound and free ligands in the contact respectively, $N_t\, x\, f$ is the total number of cell surface mobile receptors, S_{cell} is the cell surface area and p is the ratio of the contact area to S_{cell} (Figure 3.3 B) (131). The mean surface area of the cell is calculated by:

$$S_{cell} = 4\pi r^2 x\ 1.8 \qquad (Eq.\ 3.5)$$

where r is the measured radius of the cell and 1.8 is a correction factor due to the cell´s surface roughness (133). The 2D K_d can be obtained from the negative reciprocal slope of the B/F vs Bxp plot, hereafter called the Zhu-Golan plot (Figure 3.3 C). Furthermore, the intercept of the Zhu-Golan plot with the x-axis corresponds to the total number of mobile receptors on the cell surface:

$$X = \frac{N_{tot} x f}{S_{cell}} \qquad (Eq.\ 3.6)$$

where f can be evaluated by a FRAP measurement on the cell with the receptors tagged with fluorescent antibodies.

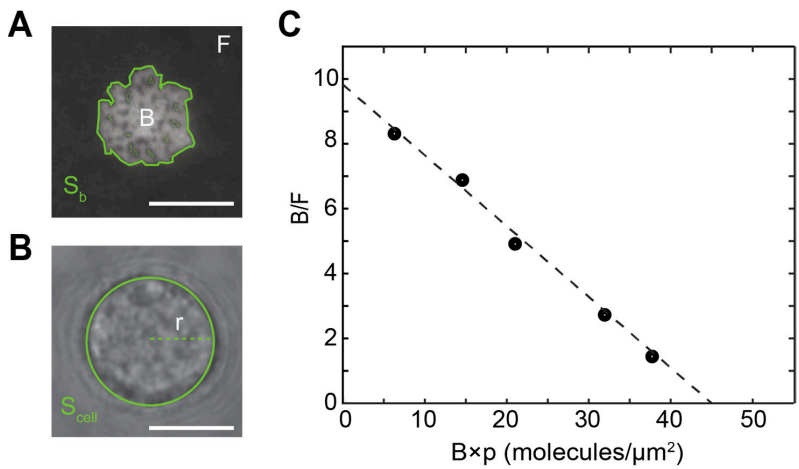

Figure 3.3. **(A)** Fluorescent image of a T-cell interacting with an SLB functionalized with a fluorescently-labelled ligand. **(B)** Calculation of S_{cell} from bright-field images of the cell´s contour. **(C)** Representative Zhu-Golan plot. The negative reciprocal slope provides the 2D K_d of an arbitrary receptor-ligand interaction. The scale bar is 8 μm.

The main advantages of this method are that the contact area can be accurately determined and that different auxiliary proteins can be studied simultaneously granted that they are labelled with different fluorophores. The latter asset is essential in studying weak receptor-ligand pairs such as the CD4-MHC II interaction where the use of adhesion proteins is critical (27). The drawbacks of using the Zhu-Golan approach are that the k_{on} and k_{off} values cannot be directly obtained and complementary methods must be used to obtain them, such as Förster Resonance Energy Transfer (FRET) (134), FRAP (85) or single-molecule detection (135). Moreover, the Zhu-Golan analysis makes the assumption that only the laterally mobile receptors contribute to the binding of the ligands (131). However, this approximation has been shown to yield typically small errors (27). It is also important to note that the free ligand density F is typically lower than the ligand density in the SLB outside of the contact, F^* due to steric effects occurring inside the contact area (14, 117, 133). To compensate for this, the average exclusion of a non-binding protein of similar size inside the cell-SLB contacts can be measured and a

typical “exclusion factor” of 25-50% for proteins of 5-10 nm height has been obtained (27, 117, 131).

3.3.2.2 Single-molecule Imaging and Tracking

This technique relies on the attachment of a fluorescent probe to the ligand of interest and the subsequent detection of the particle´s position as a function of time while it´s diffusing and binding on a cell membrane or an SLB. Thus, this method allows the visualization and characterization of the ligand´s motion. In more detail, the ligand is imaged as an Airy disk with a width characterising the microscope´s PSF. By fitting a two-dimensional Gaussian function to the centre of this Airy disk, the particle (i.e. protein) can be located with a precision well below the light´s wavelength, with a resolution down to 10 nm (99). Once the particles´ positions in each frame are detected, the next step is to link the set of positions between subsequent image frames thus creating a trajectory for each biomolecule. There are several particle-linking algorithms such as the one presented by Serge et al. (136) which only allows connections to nearby detected points or the one introduced by Jagaman et al. (137) which uses the linear assignment problem to initially link the particles between consecutive frames before linking the track segments to close gaps and capture possible merge or split events. The acquisition frequency of SPT is usually between 30-100 Hz and the spatial resolution is between 10-40 nm (138). Therefore, using single-molecule imaging and tracking one can detect the lifetime of protein binding events by identifying the free and bound proteins due to changes in their motion (139) or due to the reduced motion blur when a protein is bound (140).

Nevertheless, there are several complications concerning this method. The first challenge is finding a suitable probe since SPT relies on video acquisition of the particle´s motion and the acquisition time depends on the time it takes for the fluorescent label to bleach. Furthermore, since the rate and number of emitted photons by a single fluorescent label is limited, the use of high-efficiency optics (i.e. high numerical aperture objectives), high-sensitivity detection units (i.e. SCMOS cameras) and bright fluorophores (i.e. extrinsic dyes) are essential (100). Despite a high fluorescence quantum yield, a fluorophore should not be large because it can alter the motion of the ligand (141) and it should not affect any potential interactions of the labelled protein with other proteins or lipids (142). However, the preeminent challenge of single-molecule imaging is to reduce the fluorescence background. This can be achieved by working with low fluorescence optics, with clean buffer solutions, with dyes that can be excited with

long wavelengths but, predominantly, by minimizing the detection volume (e.g., TIRF microscopy). Minimizing the detection volume leads to an improved signal-to-noise ratio and effective particle detection with the use of low laser intensities which in turn leads to increased trajectory lengths. The length of the particle´s trajectory is of utmost importance as it provides the necessary data to detect any variations in the particle´s motion. Through Monte Carlo simulations it has been proven that the number of time points in the trajectory strongly affects the parameters obtained describing the particle´s motion (143, 144). Another important factor in SPT measurements is to have the fluorescent molecule at low densities to avoid possible particle crosslinking when analysing the obtained trajectories. Overall, by using single-molecule imaging and tracking it is possible to extract, from the obtained trajectories, information on the underlying physicochemical mechanisms such as the diffusion coefficient and the lifetime of the protein (138).

3.4 Relationship between 2D and 3D K_d values

For 3D and 2D binding events the K_d *is* expressed in units of molar concentration and of molecules per area, respectively, hindering the direct comparison of the two values. As a consequence, several studies have tried to establish a relationship between the binding equilibrium constants by identifying a characteristic length, h, so that (121, 145):

$$K_d^{2D} = h \cdot K_d^{3D} \qquad (Eq. 3.7)$$

It is considered that the characteristic length corresponds to the maximum distance between a ligand and a receptor for entering the encounter complex, an intermediate state in which the two biomolecules have near-native separations and orientations, with typical values in the order of 1 nm (109, 121). However, several factors can influence the h value, such as the protein density and the flexibility of the molecules (146, 147), therefore, there is a crucial need for more measurements describing the 2D binding kinetics of receptor-ligand complexes.

3.5 Single-Cell Binding Affinity Studies

In general, the cell population is intrinsically heterogeneous with individual cells displaying different physical, chemical, and biological traits. This diversity can arise due to environmental alterations (148), genetic variations (149) or differences in the age of individual cells and their phase in the cell cycle (150). Hence, single-cell measurements are compelling because they provide information about the heterogeneity and time evolution of the cell population as well as about the distribution of individual parameters. A novel approach to measuring single-cell binding affinities of ligand-receptor complexes using fluorescence microscopy is presented in the following sections summarizing the main findings and data displayed in **Paper I.**

3.5.1 The rCD2/CD48$_{T92A}$ Receptor Pair

The here chosen system was Jurkat T-cells transduced with rat CD48$_{T92A}$ (rCD48$_{T92A}$), a high-affinity mutant of the wild type rat CD48, interacting with SLBs functionalized with fluorescently-labelled rat CD2 (rCD2). Both rCD2 and rCD48 are members of the immunoglobulin (Ig) superfamily of proteins and their interaction is considered critical in establishing a contact between the T-cell and APC surfaces (14, 151). This is achieved by positioning the two membranes to an intermembrane distance separation of approximately 15 nm, a distance that is optimal for the TCR-pMHC interaction to occur (151). The rCD2-rCD48$_{T92A}$ interaction has previously been characterized using the Zhu-Golan method yielding a 2D affinity of 6 ± 1 molecules/μm^2 (mean ± SD) (117, 152) an affinity of the same order of magnitude as the 2D affinity of human CD2-CD58 (34, 153). Since the rCD2-rCD48$_{T92A}$ interaction is so well-studied, it was selected in this study as a model system for comparing its behaviour using the classic Zhu-Golan method and the single-cell binding affinity method.

3.5.2 Average vs Single-Cell Binding Affinity Studies

In the original Zhu-Golan approach, several bilayers of increasing ligand densities are used in which the cells are added to interact with the ligand-functionalized SLBs. Therefore, incubating rCD48$_{T92A}$ expressing Jurkat cells with rCD2-functionalized SBLs results in a visible accumulation of fluorescently-labelled rCD2 in the cell-SLB contacts due to receptor-ligand binding (Figure 3.4).

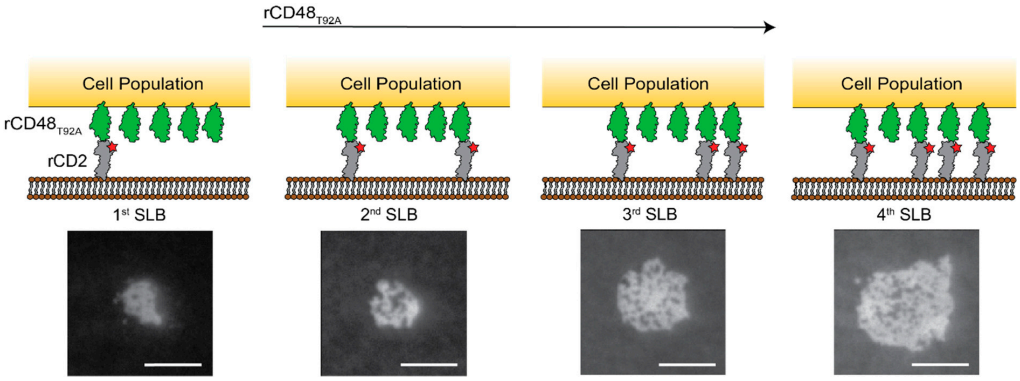

Figure 3.4. Schematic illustration and fluorescence images of rCD48$_{T92A}$ expressing Jurkat T cells binding to SLBs with four different rCD2 densities. The images were captured 40 minutes after the initial contact formation. The scale bar is 8 μm.

As the ligand density on the SLB increases, so does the amount of available rCD2 that can bind rCD48 $_{T92A}$ leading to bigger cell-SLB contact formations (Figure 3.4). In this method, the analysis of dozens of cell-SLB contacts is necessary for each individual ligand density in order to create an accurate Zhu-Golan plot and thus obtain the 2D K_d.

However, obtaining single-cell affinities should entail the study of individual cells' binding behaviour at various ligand densities in contrast to a cell population averaging. Thus, single-cell affinity experiments need to be conducted on the same bilayer. The first attempt to obtain single-cell K_d values involved the use of a bilayer with one initial ligand density to which cells bound and reached a steady-state before adding more ligands. This procedure was repeated for four different ligand concentrations. The two abovementioned methods gave similar average K_d values for the entire population (117), however, the K_d values obtained for individual cells gave a significant spread among the Zhu-Golan curves with several cells even expressing negative K_d values. For this reason, **Paper I** presents an approach of going from high to low ligand concentrations by using imidazole. Imidazole competes with the polyhistidine-tagged ligands for binding to nickel-chelating lipids on the SLB, thus it was able to reduce the protein concentration inside and outside the formed contacts.

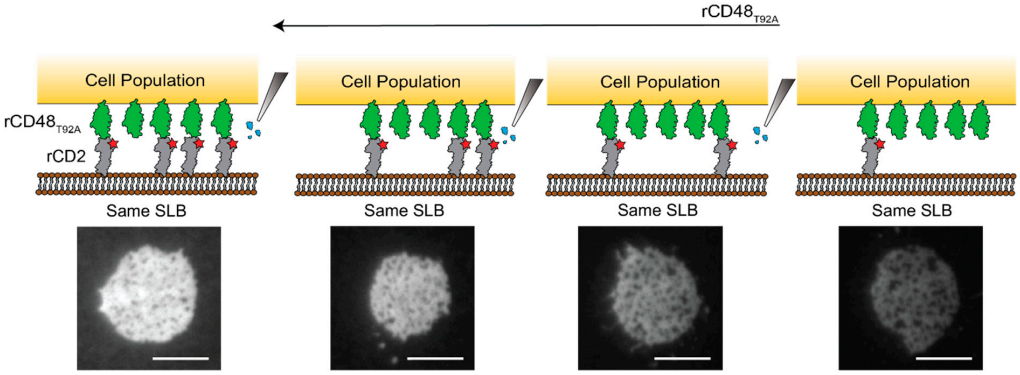

Figure 3.5. Schematic illustration and fluorescence images of rCD48$_{T92A}$ expressing Jurkat T cells binding to an SLB followed by rCD2 titration using imidazole. The images were captured 40 minutes after each ligand titration. The scale bar is 8 μm.

In more detail, an imidazole concentration of 5 mM to 13 mM inside the well for 30 to 60 seconds was sufficient to reduce the free ligand density by half compared to its initial concentration. When the rCD2 concentration was approximately halved, the SLB was washed thoroughly with filtered buffer in order to remove any traces of imidazole. The system was left to reach an equilibrium anew and the whole process was repeated three times resulting in four different ligand concentrations on the SLB (Figure 3.5). The effect of imidazole on the binding affinity of the cells was investigated by comparing the Zhu-Golan plots of the cell population obtained using the classic Zhu-Golan method and the imidazole approach, termed the single-cell binding affinity method.

For the Zhu-Golan method, as the concentration of free rCD2, F, in the various SLBs increased, the relative accumulation of rCD2 in the cell-SLB contacts, B/F, decreased. The 2D K_d of the rCD2-rCD48$_{T92A}$ was obtained by fitting the data to Eq. 3.4 and was estimated to be 4.9 ± 0.4 molecules/μm^2 (mean ± SD), a value which was similar to previously reported values of this system at RT and 37ºC (Figure 3.6 A; green circles) (117, 152). Furthermore, the intersection of the Zhu-Golan plot with the x-axis provided the density of mobile rCD48$_{T92A}$ receptors on the cells. The density of 51 ± 2 mobile rCD48$_{T92A}$ molecules/μm^2 per cell (mean ± SD) was obtained corresponding to a total number of 53,000 receptors per cell (Eq. 3.6) using an average cell surface area of 640 μm^2 and a mobile fraction of 0.62 (117). This value was in agreement with the average number of 47,000 rCD48$_{T92A}$ molecules per cell obtained for this cell line using flow cytometry (152).

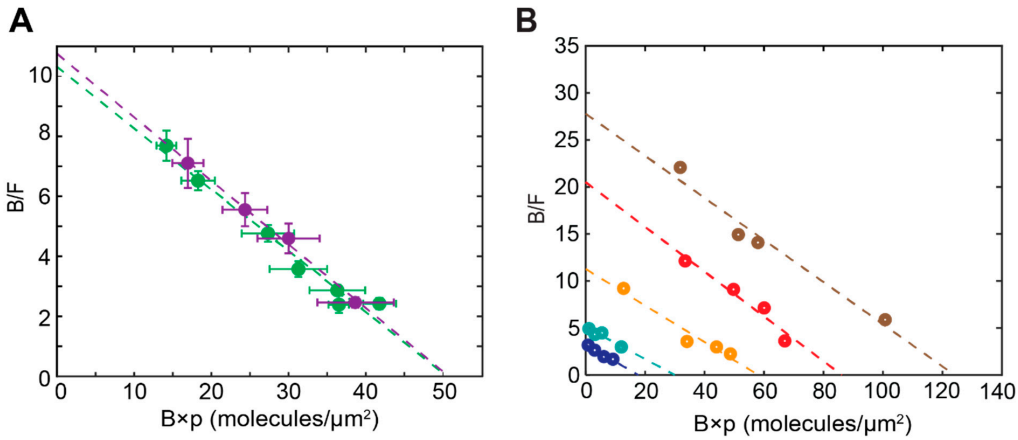

Figure 3.6. **(A)** Zhu-Golan plot for the rCD2-rCD48$_{T92A}$ interaction (mean ± SD). The green data points represent data obtained using the classic Zhu-Golan method and are obtained by analysing 21 different cell-SLB contacts. The purple data points represent data obtained using the single-cell binding affinity method and are obtained by analysing 31 different cell-SLB contacts. **(B)** Zhu-Golan plot for five representative cells with different surface receptor densities. The dashed lines are fitted to Eq. 3.4.

For the single-cell binding affinity method, as the concentration of rCD2 in the SLB decreased, the *B/F* increased. The obtained average 2D K_d for this method was 4.7 ± 0.2 molecules/μm^2 (mean ± SD) with a density of 51 ± 1 mobile rCD48$_{T92A}$ molecules/μm^2, thus an estimated of 53,000 receptors per cell (Figure 3.6 A; purple circles). The evident similarity of the two approaches indicated that the binding affinity of the rCD2-rCD48$_{T92A}$ interaction was not affected by the presence of imidazole under the specific experimental conditions. Most importantly, the principal advantage of the single-cell binding affinity approach is that it provides Zhu-Golan plots for each individual cell from which the corresponding 2D K_d and the receptor density can easily be extracted. Figure 3.6 B shows the characteristic Zhu-Golan plots for five representative cells with different receptor densities.

The dependence of binding affinity and receptor density was later investigated. Figure 3.7 A shows sixty cells that have been grouped into five separate groups based on their distinct mobile receptor densities, as determined from the corresponding x-intersect in their Zhu-Golan plot, and their corresponding K_d values. It was found that even though the receptor density of the

cell population varied by almost an order of magnitude, there was no significant difference in the obtained 2D K_d values. Figure 3.7 B shows a histogram of the individual 2D K_d values obtained from seven different experiments characterizing the binding affinity of sixty individual cells. The distribution was rather narrow following approximately a Gaussian curve with an average value of 4.9 ± 0.9 molecules/μm^2 (mean ± SD). These results indicate that the observed differences in the relative accumulation of rCD2 in the cell-SLB contacts would stem from varying receptor densities on the cells and not from differences in binding affinities. It is important to notice that this narrow spread in single-cell binding affinities has also been detected for other binding pairs using micropipette-based adhesion assays e.g. the binding of OT1 TCR to a panel of pMHCs with increasing potencies (154, 155).

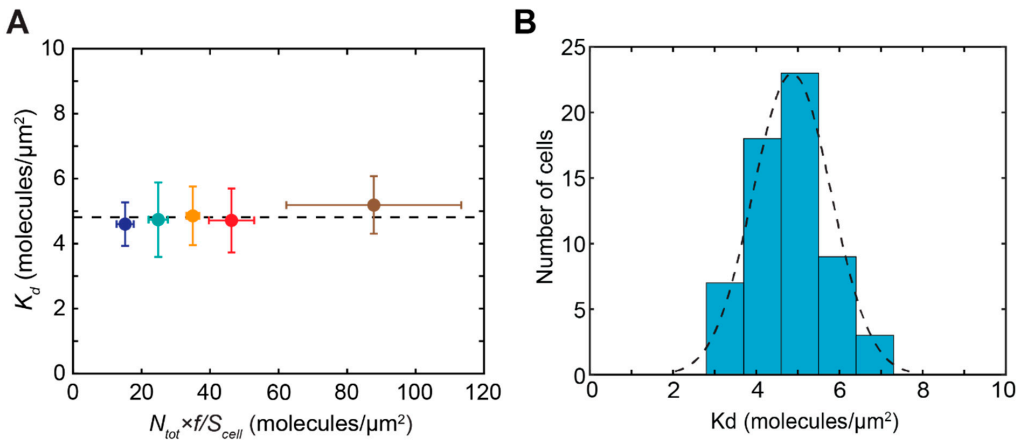

Figure 3.7. **(A)** The dependence of 2D K_d on the cell surface receptor density. The data points represent an average value of 12 cells which are grouped together with respect to the total number of rCD48$_{T92A}$ receptors as determined via the individual Zhu-Golan plots. The dashed line is the average 2D K_d value for all the 60 individual cells. **(B)** Histogram showing the 2D K_d values of 60 individual cells from seven separate experiments. The dashed line is a Gaussian fit to the obtained data with a mean value of 4.9 molecules/μm^2.

3.6 Single-molecule Lifetime Studies

In analogy to single-cell biophysics, single-molecule studies provide access to a wealth of molecular information that is often not obtainable from ensemble experiments. Differences between heterogeneous systems, the ability to distinguish individual molecular trajectories, to

detect transitions between various dynamic behaviours as well as the ability to use single molecules as local probes, are all only available by using single-molecule measurements (95–98). Therefore, there has been an increasing interest in single-molecule imaging since it can provide the full distribution of molecular properties, kinetics, reactions and dynamics (100). For the work presented in the next subchapter, single-molecule imaging and tracking were used to obtain the lifetime of a receptor-ligand complex and to investigate whether the lifetime remained similar for different cell-SLB contact formations.

3.6.1 Single-molecule Imaging & Receptor-Ligand Lifetimes

The notion that proteins embedded in a membrane would be able to undergo translational diffusion at rates defined by the viscosity of the bilayer was already presented by Singer and Nicolson in 1972 (40). In fact, the protein's motion on a membrane is highly dynamic and is determined by the ubiquitous interactions with the surrounding solvent, with other membrane proteins, membrane lipids as well as with various intracellular and extracellular structures (156). Hence, the diffusion of a protein on a membrane is a highly complex process with distinct modes of motion, the most common of which are random diffusion, confinement and directed motion. Random diffusion or Brownian motion occurs when a protein diffuses freely with a rate of diffusion characterized by the biomolecule´s diffusion translational coefficient, *D* (157). On the other hand, confinement occurs when a protein is highly localized to a specific region of the membrane for a certain time period which could be attributed to the presence of lipid rafts, possible interaction with immobile proteins or to cis/trans binding (158). During the confinement mode, the lateral mobility of the protein decreases significantly compared to random diffusion. Finally, directed motion describes proteins whose diffusion exhibits some form of directionality attributed to various biophysical and biochemical factors (158).

Since several transitions between the different types of motion characterize the diffusion of a protein on a cell or a model membrane, the analysis of the molecule´s motion is quite demanding. Optimizing the optical parameters such as laser intensity, exposure time and frame interval is of utmost importance in order to be able to distinguish between the various modes of motion and these parameters should be revised for each ligand-receptor system. In further detail, the laser intensity and the exposure time should be high enough to have a high signal-to-noise ratio and thus clearly distinguish the individual fluorescently-labelled proteins but they should be low enough to allow for a long image acquisition without bleaching the fluorophore.

The optimal exposure time and frame interval depend on the lifetime of the complex since small confinement regions and very short lifetimes require a high time and space resolution which sets a limit on the maximum exposure time that should be used. On the other hand, for prolonged protein-protein lifetimes long frame intervals should be used instead due to undesirable photobleaching effects.

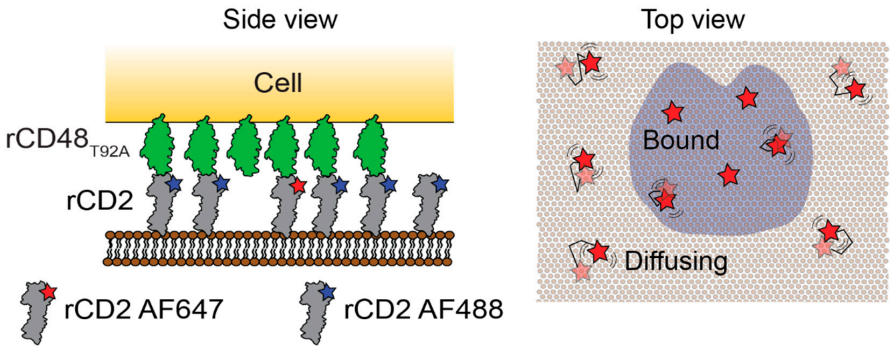

Figure 3.8. Single-molecule fluorescence microscopy is used to track the motion of the rCD2 AF647 proteins (red stars) inside and outside the cell-SLB contact (blue area). Ligands fluorescently labelled with AF488 (blue stars) are used to facilitate contact formation between the cells and the bilayer and determine the exact area of the formed contacts (blue area).

Obtaining the lifetime of a receptor-ligand complex depends on a change in motion in the protein´s trajectory (139) or from reduced motion blur when the protein is bound (159). In the following studies, a tracking algorithm that is based on the linear assignment problem (LAP) presented by Jaqaman et al. (137) was employed to detect changes in the trajectory of fluorescently-labelled proteins diffusing on an SLB. The rCD2/rCD48$_{T92A}$ interaction was selected again (see section 3.5.1) in order to obtain the lifetime of the complex and to investigate whether this binding kinetic parameter remained similar for different cell-SLB contact formations. In more detail, SLBs functionalised with a high concentration of rCD2 fluorescently-labelled with Alexa Fluor 488 (AF488) and single-molecule concentration of rCD2 fluorescently-labelled with Alexa Fluor 647 (AF647) interacted with rCD48$_{T92A}$ expressing Jurkat T cells (Figure 3.8). A concentration of approximately 100-200 molecules/μm^2 of rCD2 AF488 ensured a successful contact formation between rCD48$_{T92A}$ expressing Jurkat T cells and the bilayer (Figure 3.9 A). Single rCD2 AF647 proteins (~ 0.1-

0.2 molecule/μm^2) can be resolved as individual molecules, as identified by single step photobleaching, and can be continuously tracked for multiple frames using TrackMate in Image J (Version 1.49V) (160). Single-particle tracking of rCD2 AF647 proteins inside the contact regions revealed the time intervals over which the proteins distinctly stop their Brownian motion and stay approximately immobile inside the formed contacts, a period that characterizes the lifetime of the rCD2/rCD48$_{T92A}$ complex. The single molecules were chosen to be fluorescently-labelled with AF647 because the background signal was much lower in comparison to using single molecules fluorescently-labelled with AF488 since the AF647 dye does not excite the AF488. The lifetime of the bound complex is estimated by identifying the number of frames in which a rCD2 protein stays nearly immobile within a cell-SLB contact and multiplying it by the frame interval. Since unbinding and photobleaching of the proteins is inevitable, only proteins whose trajectory is visible pre- and post-immobilization are considered for the lifetime calculations. In regions without a cell, the vast majority (~ 97%) of the rCD2 AF647 proteins exhibited an entirely random diffusive motion with a lateral diffusion coefficient, D, of 0.45 ± 0.07 $\mu m^2/s$, a value typical for functionalized supported membranes (Figure 3.9 B) (161, 162). In contrast, the rCD2 AF647 proteins within the cell-SLB contacts exhibit a diffusive motion which was repeatedly interrupted by a period of time where the proteins stayed nearly immobile (Figure 3.9 B). Thus, the average diffusion coefficient of the rCD2 proteins inside the contacts was lower, with a value of 0.19 ± 0.05 $\mu m^2/s$.

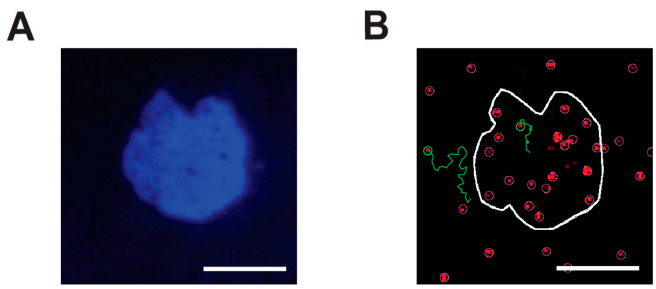

Figure 3.9. **(A)** Contact formations of rCD2 AF488 on a bilayer interacting with rCD48$_{T92A}$ on the surface of a Jurkat T cell. **(B)** Fluorescent image of a rCD2 AF647 protein exhibiting Brownian motion on an SLB outside the cell-SLB contact while another protein is highly localized for a certain period of its trajectory inside the cell-SLB contact (the white line is the contour of the cell-SLB contact). The scale bar is 8 μm.

Single-molecule detection of all the rCD2 proteins inside the contact allowed the characterization of every protein into bound or free for every single frame. Even though the amount of bound and free proteins varied between frames, on average, 71% of the rCD2 were bound at any given instant, which corresponds to a B/F ratio of 3.2. This value is similar to the B/F ratio measured in Figure 3.9 A which was 3.4 ± 0.7 (mean±s.d.).

Figure 3.10 A illustrates the step size distribution of individual rCD2 molecules inside and outside cell-SLB contacts for a 15 ms frame interval. A clear shift towards smaller step sizes is noticed for rCD2 proteins diffusing inside the formed cell-SLB contacts which is indicative of protein binding and/or slowed protein diffusion in the contact. The observed lifetime distribution of ninety rCD2 tracks within ten separate cell-SLB contacts is shown in Figure 3.10 B. An exponential fit of the data gave an average lifetime of 90 ms for this interaction and is of the same order of magnitude as what has previously been estimated for the 3D lifetime for this system (83). However, this lifetime signifies a dissociation constant of approximately 11 s^{-1} which is considerably slower than the corresponding 2D lifetime for hCD2 binding hCD58 using FRAP which was estimated to be 0.074 s^{-1} (83), although the two systems have similar 2D affinities (131). On the other hand, a flow chamber method has reported a lifetime for the hCD2-hCD58 interaction of 7.8 s^{-1} which is similar to the value obtained for the rCD2/rCD48$_{T92A}$ interaction (163). These discrepancies stress once more the differences between the data obtained using various techniques to measure binding kinetics of protein-protein complexes. It is also important to notice that long binding events were obtained during the rCD2/rCD48$_{T92A}$ interaction which were an order of magnitude longer than the average lifetime value (Figure 3.10 B). Studies between AND TCR expressing T cells and SLBs functionalized with IEk/MCC showed similar long-dwelling events and that actually these long binding events were important for T cell activation (164).

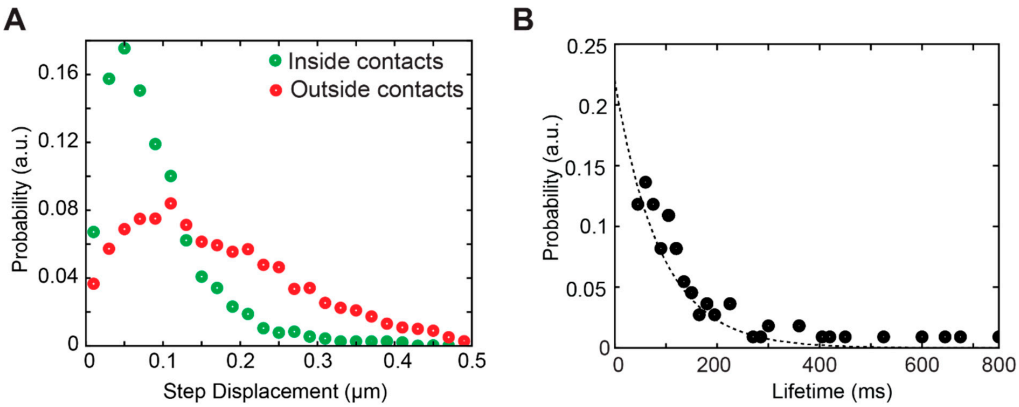

Figure 3.10. **(A)** Step size distribution of rCD2 proteins inside (green) and outside (red) the formed cell-SLB contact areas. **(B)** The overall observed binding lifetime distribution follows an expected exponential decay characterizing molecular binding with an average lifetime of 90 ms.

Lastly, the rCD2/rCD48$_{T92A}$ lifetimes measured in ten different contacts with a varying accumulation of rCD2 AF488 (80 to 150 molecules/μm^2) gave similar results (Figure 3.11) suggesting that the 2D lifetime similarly to the 2D K_d does not vary significantly among the cell population under the specified experimental conditions.

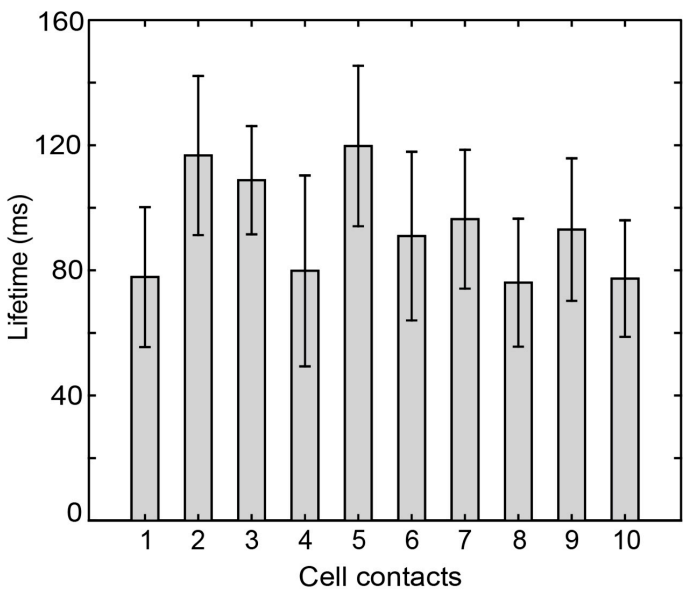

Figure 3.11. Histogram presenting the rCD2/ CD48$_{T92A}$ binding dwell times for ten cell-SLB contacts. The different contacts gave similar 2D lifetimes.

3.7 Summary

In this chapter, the most prominent methods for measuring the binding affinity and the lifetime of a receptor-ligand interaction were initially discussed before presenting a novel approach to obtaining 2D single-cell binding affinities of T cells interacting with SLBs using subsequent imidazole titrations. Using this method, the binding affinity of individual cells can be investigated in contrast to previously used fluorescence-based methods where only the binding affinity of the entire population was monitored. Moreover, the single-cell binding affinity method, by extending the traditional Zhu-Golan approach, can reduce the analysis time significantly since it does not require the image analysis of hundreds of cells-SLB contact formations. Our results showed a relatively small spread in the rCD2-rCD48$_{T92A}$ 2D K_d values even though the receptor density varied by approximately an order of magnitude in the cell population. Lastly, the lifetime of the rCD2/rCD48$_{T92A}$ interaction was investigated using single-molecule imaging and tracking. It was verified that despite the innate stochastic nature of the protein's motion on the bilayer, the lifetime of the complex did not vary significantly among the cell population and was of similar magnitude as that of the corresponding 3D lifetime.

3.8 Discussion & Outlook

The next step is to use the single-cell binding affinity method to investigate the behaviour of other protein-protein interactions involved in the contact formation between a T cell and an APC. It remains to be seen if all protein complexes would produce a similar spread in the obtained 2D K_d values under physiological levels of protein expression. Maybe rCD2´s narrow spread is a consequence of its role as an adhesion molecule, so that it can allow the TCR-pMHC binding for any possible peptide. It is also important to examine how the TCR-pMHC interaction itself would behave. Loading the cells with peptides of various 2D affinities, from agonist to null, and studying the single-cell binding affinities of the population would potentially help us understand the T cells´ capability to distinguish with high specificity the various peptides. It is important to notice however that the relatively narrow spread observed

in the binding affinities of the rCD2/rCD48$_{T92A}$ interaction might be only accurate when there is one type of protein-protein complex present, a quite simplified view of how cell-cell interactions behave *in vivo* where there are numerous receptor-ligand engaging pairs (165–167). It is generally accepted that various mixtures of ligand-receptors pairs can either facilitate or impair cell-cell interaction depending on the properties of the proteins (117, 168). Therefore, an interesting study would include various adhesion pairs with some proteins anchored on the SLB using another linking system than DGS-NTA/his-tag. In this way one can only reduce the DGS-NTA-bound ligand using imidazole and thus examine the influence of the auxiliary proteins in the obtained single-cell K_d values of the under-study receptor-ligand complex. Another possible idea is to exploit the low spread in binding affinities provided by the single-cell binding affinity method to study weak binding protein-protein interactions. In more detail, one can be restricted in analysing cells with the highest number of bound ligands since they provide the strongest signal thus allowing for an accurate affinity measurement of very weakly binding receptor-ligand complexes.

On the other hand, single-molecule imaging and tracking experiments have great potential in estimating the lifetime of the receptor-ligand complex if one can adequately discriminate the protein´s freely diffusing motion against restricted or directed motions. This method can be employed to investigate the 2D lifetime of several receptor-ligand complexes including various TCR-pMHC interactions and determine the relative spread of each protein-protein pair within various cell-SLB contacts. Additionally, single-molecule imaging allows to directly measure the ratio between free and bound molecules at any instant, so that this methodology could be used to determine the relative accumulation in the single-cell Zhu-Golan analysis. This overcomes the need to compensate for the exclusion of free ligands in the contact due to steric effects, which can be between 25-50% and can vary between cells (18, 27, 117). However, it should be highlighted that due to the stochastic nature of the protein´s diffusion on the SLB, it is challenging to unequivocally distinguish between a diminutive Brownian step and a binding behaviour, especially for short-lived receptor-ligand interactions. Integrating experiments and theory with simulations in future studies will be a successful strategy to further understand the kinetics of protein-protein interactions and confirm the data obtained from single-molecule tracking measurements. Overall, it is evident that more 2D binding kinetic studies are needed in order to understand the role of protein-protein interactions in T cell activation and downstream signaling.

Chapter 4

4. The CD4 Co-Receptor

Contents

Chapter 4 will focus on binding kinetic studies involving the CD4 co-receptor. In more detail, the effects of auxiliary proteins on the CD4 binding will be initially presented summarizing the main findings from **Paper II** before focusing on binding kinetic studies involving the CD4-pMHC-TCR complex which is the topic of **Paper III**.

4.1 The CD4/CD8 Co-Receptors

T cells expressing CD4 or CD8 co-receptors are characterized as either helper or cytotoxic T cells. As the name suggests, helper T cells 'help' other immune cells by producing cytokines which activate vital effector defence mechanisms while cytotoxic T cells directly kill infected or cancerous cells. Furthermore, CD4 expressing T cells bind to MHC class II molecules in contrast to CD8 expressing T cells that bind to peptide MHC class I complexes. CD4 and CD8 co-receptors are essential in T cell activation because they augment the effectiveness of the engaged TCR (169). Furthermore, they participate in signal transduction and they are argued to stabilize the T cell-APC interaction (23, 24, 170), even though the latter is debatable for the CD4 co-receptor. There are still many unanswered questions concerning T cell activation and the role of co-receptors in the signaling process therefore the aim of this chapter was to shed some light into their role, and more specifically, into the role of the CD4 co-receptor.

The CD4 receptor is critical in T cell activation and in the proper function of the immune system. CD4, a member of the Ig superfamily, is a 55 kDa type I integral membrane protein with four extracellular domains (D1-D4), a single spanning transmembrane region of 22 amino acids and a short cytoplasmic tail of 40 amino acids noncovalently linked to the Lck (171, 172). CD4´s extensive extracellular segment spans a height of 11 nm and can bind to pMHC class II presenting APCs with the weakest measured interaction to date, with a 2D K_d of 4800 molecules/μm^2 (27). As TCR also bind pMHC class II, T cell and APC interaction leads to the formation of a CD4-pMHC-TCR complex. Crystal structure studies of this ternary complex have proven that it is V-shaped with CD4 bind MHC II at an angle of 65˚relative to the T-cell surface excluding any theories for direct TCR-CD4 interactions (173) (Figure 4.1).

4.2 The Role of the CD4 Co-Receptor

Despite the existing biochemical knowledge of the CD4 co-receptor, the exact role of this biomolecule in antigen recognition and subsequent T cell activation is still highly debated.

Regardless of its very low binding affinity to pMHC II, CD4 is considered to have a crucial role in immune activation as it has been argued that it can simultaneously fulfil several roles; it enhances the T cell sensitivity to antigens by up to a hundred times (169, 174), it is able to convert weak agonists into full agonists (175) and it can recruit the Lck kinase associated with its short cytoplasmic tail into the site of immune recognition to efficiently phosphorylate adjacent TCRs (176, 177). It is also considered that CD4 might stabilize the TCR-APC interaction (174, 178), even though this theory is questioned nowadays (23). Furthermore, it has been established that T cells expressing CD4 can be activated in the presence of even a single agonist pMHC while blocking of the co-receptor renders the T cells unable to detect less than 30 ligands (6). However, CD4 affinity measurements are a demanding task in which auxiliary proteins are often used to ensure successful contact formation (17, 27). Yet, the effect of these auxiliary proteins on the measured K_d values has not been addressed in previous studies (17, 27, 159). The influence of these different types of molecules in the binding kinetics is vital as there are several auxiliary molecules acting in cell-cell contacts *in vivo* (179).

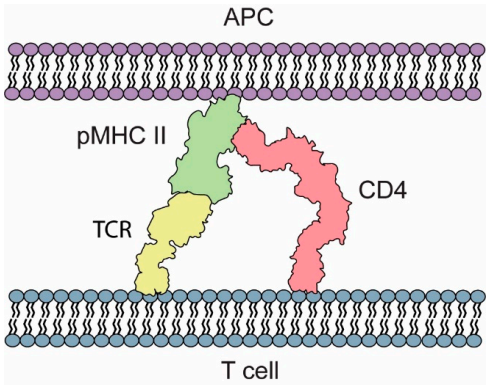

Figure 4.1. Schematic illustration of CD4 binding to peptide MHC II. The crystal structures were obtained from the PDB: for CD4 (1WIO), for TCR (3OF6) and for pMHC II (1AQD).

In the first part of this chapter, the main findings from **Paper II** will be presented which focus on the influence of adhesion molecules on the obtained binding kinetics of a ligand-receptor complex. Emphasis will be given on the data obtained for the CD4 co-receptor and how its binding was influenced by the presence of rCD2 at two different rCD2 concentrations henceforth termed low and high respectively. Later, the effects of TCR-pMHC II on the CD4 binding, and vice versa, will also be presented summarizing the main findings from **Paper III.**

4.3 Effects of Auxiliary Proteins on CD4 Binding

The interaction between rCD2/rCD48$_{T92A}$ (see section 3.5.1) was used as the auxiliary binding pair to study whether the presence of an auxiliary protein could influence the binding kinetics of the CD4 co-receptor. For this purpose, SLBs functionalised with fluorescently-labelled hCD4 and fluorescently-labelled rCD2 were employed. In more detail, SLBs functionalized with hCD4 and different rCD2 densities were studied after incubating them with Jurkat T cells expressing agonist pMHC class II molecules and rCD48$_{T92A}$ receptors. The agonistic MHC II molecule is the human leukocyte antigen DQ8 which presents the α-1 gliadin peptide, called HLA-DQ8-glia-α1 (180). As explained in Chapter 3, rCD2 is an auxiliary molecule that binds rCD48$_{T92A}$ on the surface of Jurkat T cells with a 3D K_d of 11 μM and a 2D K_d of 6 molecules/μm^2 (114, 119). Both HLA-DQ8-glia-α1 MHC and rCD48$_{T92A}$ are not naturally expressed on the surface of T cells, but by using this model system signaling effects that result in cellular alterations such as receptor reorganization and cytoskeletal rearrangements can be avoided since they can potentially influence the obtained binding kinetics (181–183).

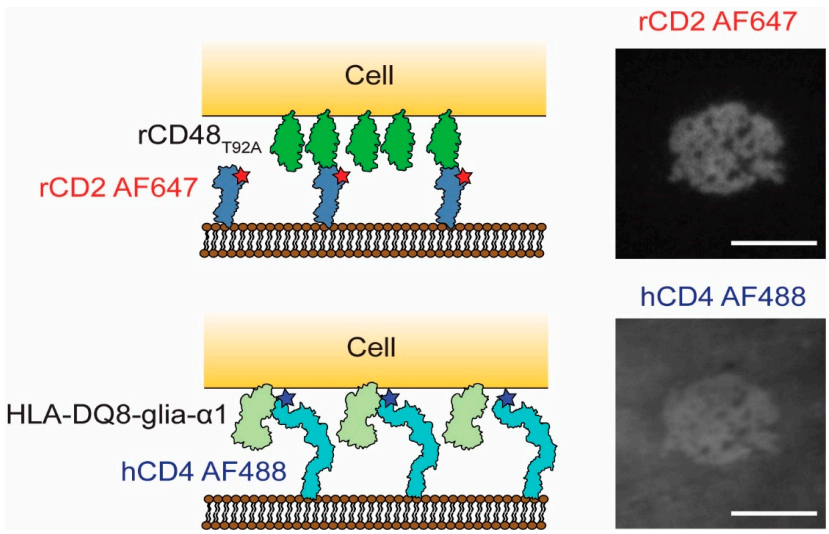

Figure 4.2. Schematic and corresponding representative images of rCD2 and hCD4 accumulation under the same cell-SLB contact at low densities of bound rCD2 (B_{rCD2} < 200 molecules/μm^2). The scale bar is 8 μm.

For free rCD2 densities, F_{rCD2}, of more than 30 molecules/μm^2, nearly all Jurkat T cells were able to bind to SLBs and create homogeneous cell-SLB contact formations. At low ligand densities of bound rCD2 (B_{rCD2} < 200 molecules/μm^2), hCD4 was able to accumulate to a significant extent and distribute homogeneously within most cell contact areas (Figure 4.2). Under these conditions, F_{rCD2} was below 50 molecules/μm^2 which resulted in an average bound rCD2 density, B_{rCD2}, of 117±40 molecules/μm^2 (mean ± SD) in the formed cell-SLB contacts. It is important to note that these low values for F are comparable to the physiological densities of rCD2 (hCD2) and rCD48 (hCD58) on a naïve (inactivated) T cell (50 – 100 molecules/μm^2) (184, 185). At the same time, the free hCD4 density, F_{CD4}, was 926 molecules/μm^2 and the bound hCD4 density, B_{CD4}, was 427 molecules/μm^2.

On the contrary, average free rCD2 densities of ~180 molecules/μm^2 on the SLB resulted in an increase of bound rCD2 in the cell-SLB contacts. More specifically, bound rCD2 densities of above 300 molecules/μm^2 (average B_{rCD2} = 524±160 molecules/μm^2) substantially affected the amount of bound hCD4 proteins inside the cell-SLB contacts and led to a visible exclusion of the co-receptor from most of the formed contacts (Figure 4.3). In this case F_{CD4} and B_{CD4} were 460 molecules/μm^2 and 131 molecules/μm^2, respectively.

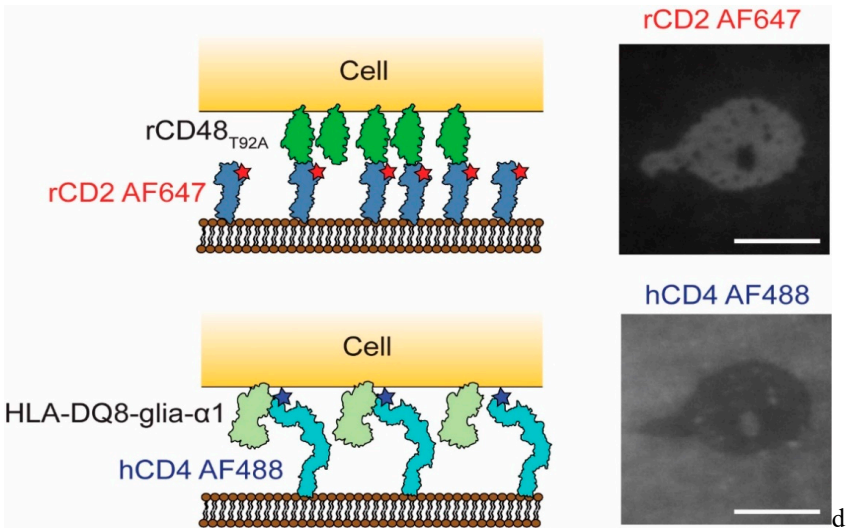

Figure 4.3. Schematic and corresponding representative images of rCD2 and hCD4 exclusion under the same cell-SLB at high densities of bound rCD2 (B > 300 molecules/μm^2). The scale bar is 8 μm.

Figure 4.4 displays the single-cell Zhu-Golan plot of different cell-SLB contacts quantifying the binding behaviour of hCD4 for low (Figure 4.4 A) and high (Figure 4.4 B) densities of bound rCD2. Every single dot in the graph represents an individual cell-SLB contact formation at a certain rCD2 density and the average of all the dots would mark a single Zhu-Golan point (see section 3.3.2.1). The B^* and F^* values are not corrected for the exclusion of free ligands inside the formed cell-SLB contacts hence they correspond to the values of B and F if there was an equal amount of free ligands inside the contact as outside. In greater detail, the plots have two distinct regimes characterizing the CD4´s depletion or accumulation. The first regime, marked on the left of the dashed lines in the single-cell Zhu-Golan plots where the B^*/F^* remains approximately constant, are cells which do not have any visible hCD4 accumulation and therefore represent the exclusion of free hCD4 in the formed cell-SLB contacts. The B^*/F^* values are negative due to the exclusion of free ligands from the cell-SLB contacts making the effective density of ligands inside the contacts very low for weak protein-protein interactions such as CD4 bind pMHC. From the data in Figure 4.4 the exclusion is 25% and 41% at low and high densities of rCD2, respectively. The increased exclusion observed for high bound rCD2 densities would result in a lower effective affinity for hCD4. Two possible explanations for this phenomenon are that the increased rCD2 density excludes free hCD4 and its counter receptor from the cell-SLB contacts due to steric effects or that the presence of rCD2 influences the on- and off- rates of hCD4 due to a possible competition between rCD2 and hCD4 in forming receptor-ligand complexes thus lowering the latter´s affinity. These effects can especially arise when there is a height difference between the auxiliary binding molecules and the studied ligand-receptor pair (168, 186). A height difference between the protein-protein pairs would lead to a higher entropy penalty for bond formation as a result of membrane deformation.

On the other hand, the data points on the right of the dashed lines in the single-cell Zhu-Golan plots where the B^*/F^* increases, indicate cells in which there is hCD4 binding and therefore describe the accumulation of hCD4 in the formed cell-SLB contacts. As it is apparent, different cells exhibit different co-receptor binding which could be attributed to differences in binding kinetics or amount of cell surface receptors, but the average B^*/F^* value of CD4 was 1.8 times lower when having a high concentration of bound rCD2 compared to low concentrations of bound rCD2.

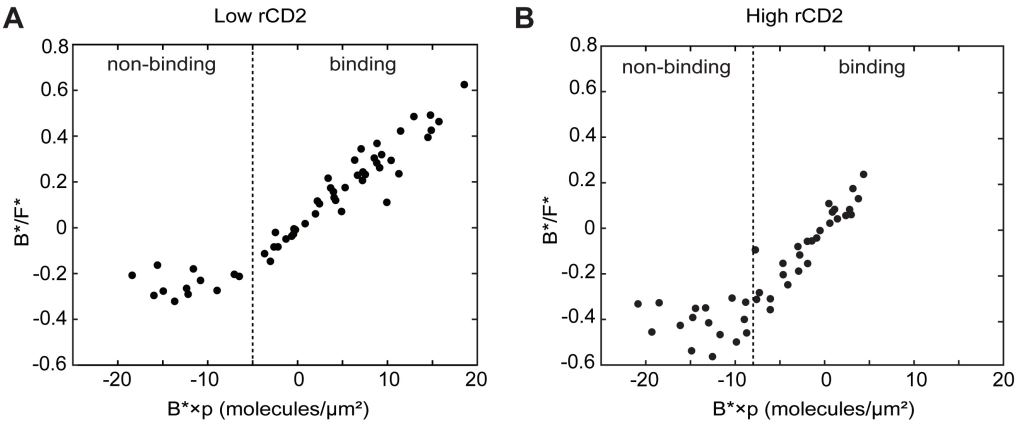

Figure 4.4. Single-cell Zhu-Golan plots in the presence of low **(A)** and high **(B)** bound rCD2 in the cell-SLB contacts. The dashed lines distinguish the areas without (left) and with (right) hCD4 accumulation in the contacts.

Interestingly, a similar behaviour as the one observed for hCD4 was observed when investigating how high and low concentrations of rCD2 binding rCD48$_{T92A}$ affect the binding kinetics of a phenotypical TRBV^{9} TCR (L3-12) binding HLA-DQ8-glia-α1 (117). The 2D K_d for L3-12 TCR binding to HLA-DQ8-glia-α1 was 14 ± 5 molecules/μm^2 (mean ± SD) (117). The bound ligand density and the binding affinity of L3-12 TCR to HLA-DQ8-glia-α1 MHC were marginally influenced by including low rCD2 densities in the system (B_{rCD2} < 200 molecules/μm^2) whereas the effective binding affinity was reduced by a factor of 1.9 (effective K_d = 26 ± 1 molecules/μm^2) at high densities of bound auxiliary molecules (B_{rCD2} > 300 molecules/μm^2) (117). At the same time, the maximum amount of bound L3-12 TCR was reduced by 37% compared to the TCR binding in the absence of rCD2 (117). It is important to notice that the limits for the low and high densities of auxiliary molecules were selected through empirical observation and depend upon the receptor-ligand interaction and each auxiliary molecule. In consequence, a similar decrease in binding affinity by a factor of 1.5 was observed when having the L3-12 TCR as an auxiliary molecule to rCD2/rCD48$_{T92A}$ interaction leading to larger 2D K_d values of 9 ± 1 molecules/μm^2 for the latter complex. However, for this system, the thresholds for low and high densities of bound L3-12 TCR were 700 molecules/μm^2 and 900 molecules/μm^2, respectively. Lastly, it should be noted that the density at which the auxiliary proteins affect the binding affinity might be cell dependent, since no significant

change in the binding of hCD4 to MHC class II molecules on Raji B cells was observed for auxiliary concentrations of human CD2 from 200 to 1200 bound molecules/μm^2 (27).

4.4 Effects of TCR on CD4 Binding

The next step was to investigate whether the presence of TCR would affect CD4 binding in the same way as the rCD2 protein did. Since TCR binds the same ligand as CD4, it is interesting to study whether the TCR-MHC II binding will influence the CD4-MHCII interaction. For this reason, SLBs functionalised with fluorescently-labelled hCD4 and low densities of L3-12 TCR were studied after incubating them with Jurkat T cells expressing HLA-DQ8-glia-α1 MHC (Figure 4.5 A).

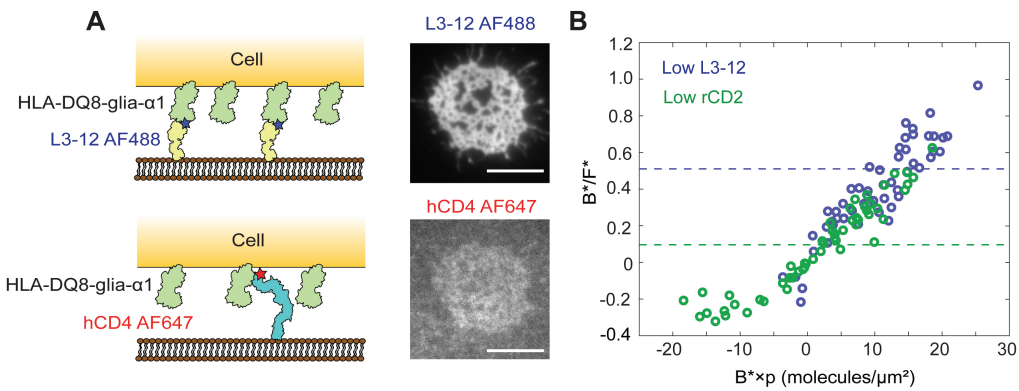

Figure 4.5. **(A)** Schematic and corresponding representative images of L3-12 TCR and hCD4 accumulation beneath a Jurkat T-cell expressing HLA-DQ8-glia-α1 MHC. The scale bar is 8 μm. **(B)** Single-cell Zhu-Golan plot in the presence of low bound L3-12 TCR (blue) and low rCD2 (green) in the cell-SLB contacts. The dashed lines represent the mean values of the two data sets.

For free L3-12 TCR densities of ~ 35 molecules/μm^2, all Jurkat T cells were able to bind to the bilayer and create homogeneous TCR-pMHC II contact formations. It is important to notice that, once more, all Jurkat T cells created TCR contacts with the SLB excluding any possibilities for L3-12 TCR exclusive binding to cells that express high densities of MHC II. Under these conditions, the average bound L3-12 densities, *B*, in the formed cell-SLB contacts was 1759 ± 504 molecules/μm^2 (mean ± SD). At the same time, hCD4 was also able to

accumulate and distribute homogeneously within the observed cell-SLB contacts (F_{CD4} = 140 molecules/μm^2) (Figure 4.5 A). Figure 4.5 B shows the single-cell Zhu-Golan plot of different cell-SLB contacts quantifying the binding behaviour of hCD4 in the presence of low L3-12 densities. The data are compared to the single-cell Zhu-Golan graph obtained for the hCD4 binding in the presence of low densities of rCD2 (see section 4.3). Once more, the B^* and F^* values are not corrected for the exclusion of free ligands inside the formed cell-SLB contacts. According to Figure 4.5 B, the presence of L3-12 TCR did not lead to a noticeable "non-binding" regime where the B^*/F^* remains approximately constant, as was the case with rCD2. The lack of this regime signifies the exclusive CD4 accumulation inside the contacts in the presence of L3-12 TCR. Furthermore, the average B^*/F^* of hCD4 was 0.520±0.319 in the presence of low densities of L3-12 TCR in comparison to 0.091±0.245 in the presence of low densities or rCD2, even though the bound L3-12 TCR was almost fifteen times higher than the bound rCD2 densities. Comparing the L3-12 TCR and rCD2 populations presented in Figure 4.5 B with a two-sample t-test indicated that the data are statistically different with $p<0.001$.

The experiment was later repeated for higher L3-12 TCR densities (F_{TCR} = 89±32 molecules/μm^2) (Figure 4.6 A). Once again, the co-receptor was able to accumulate within all the cell-SLB contacts even at an average bound L3-12 TCR concentration of B_{TCR} = 2616±545 molecules/μm^2 (F_{CD4} = 156 molecules/μm^2) (Figure 4.6 A).

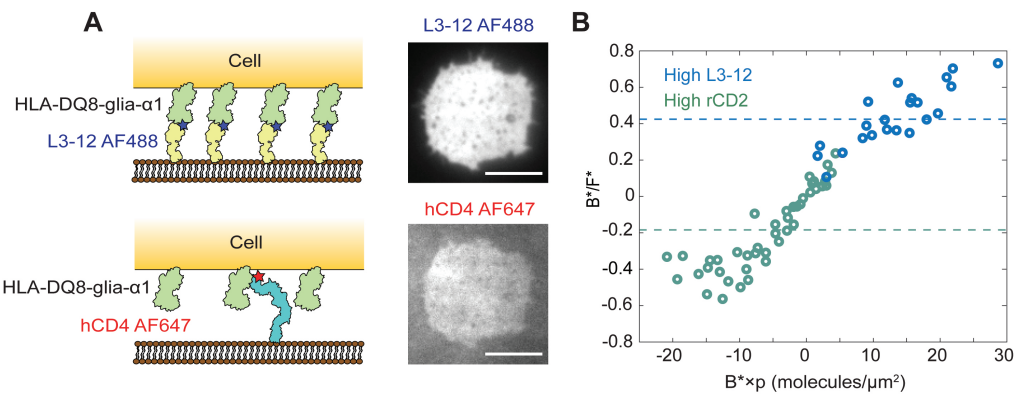

Figure 4.6. **(A)** Schematic and corresponding representative images of L3-12 TCR and hCD4 accumulation beneath a Jurkat T-cell expressing HLA-DQ8-glia-α1 MHC. The scale bar is 8 μm. **(B)** Single-cell Zhu-Golan plot in the presence of high bound L3-12 TCR (blue) and high rCD2 (green) in the cell-SLB contacts. The dashed lines represent the mean values of the two data sets.

Comparing the single-cell Zhu-Golan graph obtained for the hCD4 binding in the presence of high densities of L3-12 TCR and rCD2 highlights the difference between the two proteins. In the presence of high densities of bound rCD2, there was a clear exclusion of hCD4 from inside the formed cell-SLB contacts (Figure 4.6 B green) (see section 4.4) as ~ 40% of the cells were in the non-binding regime. On the other hand, despite the presence of bound L3-12 TCR at high densities, hCD4 was able to accumulate and create homogeneous contacts between all the observed cells that interacted with the bilayer (Figure 4.6 B blue). The average B^*/F^* of hCD4 was 0.432±0.165 in the presence of high densities of L3-12 TCR in comparison to -0.191±0.219 in the presence of high densities of rCD2. A two-sample t-test indicated once more that the abovementioned data are statistically different with $p<0.001$. On the other hand, a two-sample t-test for the B^*/F^* of hCD4 in the presence of high and low L3-12 TCR did not show any statistical difference ($p = 0.245$). Overall, the presence of TCR results to significantly more CD4 binding in the cell-SLB contacts, but the binding is still very weak. These data are in agreement with other biophysical studies that support that co-receptors rarely bind MHC, but their binding is augmented by the presence of TCR (155, 187). The average accumulation of hCD4 beneath the cell-SLB contacts in the presence of L3-12 TCR and rCD2 is presented in Table 4.1.

Table 4.1. Summary of hCD4 accumulation in the presense of L3-12 TCR and rCD2.

Auxiliary molecule	**F Auxiliary molecule**	**B Auxiliary molecule**	**B*/F* of hCD4**
L3-12	33 molecules/μm^2	1759 molecules/μm^2	0.520
L3-12	89 molecules/μm^2	2616 molecules/μm^2	0.432
rCD2	46 molecules/μm^2	117 molecules/μm^2	0.091
rCD2	171 molecules/μm^2	524 molecules/μm^2	-0.191

4.5 Kinetic Binding Theory for the Effects of TCR on CD4 Binding

In the previous sub-chapter, it was shown that TCR augments the binding of CD4 to MHC II. However, it is not clear if the presence of TCR influences the binding affinity of the CD4-pMHC complex or if it just increases the local density of MHC II therefore facilitating CD4-

pMHC interactions. In order to answer this question, we need to compare the dissociation constant for CD4 binding free pMHC II (K_c) with the dissociation constant for CD4 binding TCR-pMHC II (K_{c2}). When having both CD4 and TCR in the SLB binding of the ligands can be both to free pMHC II but also to TCR-pMHC II and to CD4-pMHC II for CD4 and TCR, respectively. Therefore, the Zhu-Golan equation (Eq.3.4) needs to be modified:

$$\frac{B_{\mathrm{CD4}}}{F_{\mathrm{CD4}}} = \frac{N_{\mathrm{tot}} \times f}{S_{\mathrm{cell}} K_{\mathrm{c}}} - \frac{(B_{\mathrm{CD4}} + B_{\mathrm{TCR-pMHC\,II}}) \times p}{K_{\mathrm{c}}} + \frac{B_{\mathrm{TCR-pMHC\,II}}}{K_{\mathrm{c2}}} \qquad (Eq.\,4.1)$$

where B_{CD4} and F_{CD4} is the density of bound and free CD4, respectively and $B_{\mathrm{TCR\text{-}pMHC\,II}}$ is the density of TCR-pMHC II complexes. The first two terms on the right side of Eq. 4.1 describe CD4 binding to pMHC II while the third term describes CD4 binding to TCR-pMHC II. However, due to CD4´s very weak binding to pMHC II, $B_{\mathrm{TCR}} >> B_{\mathrm{CD4}}$ and thus $B_{\mathrm{TCR\text{-}pMHC\,II}} \approx B_{\mathrm{TCR}}$. Therefore, Eq. 4.1 simplifies to:

$$\frac{B_{\mathrm{CD4}}}{F_{\mathrm{CD4}}} \approx \frac{N_{\mathrm{tot}} \times f}{S_{\mathrm{cell}} K_{\mathrm{c}}} - \frac{B_{\mathrm{TCR}} \times p}{K_{\mathrm{c}}} + \frac{B_{\mathrm{TCR}}}{K_{\mathrm{c2}}} \qquad (Eq.\,4.2)$$

The relative change in $B_{\mathrm{TCR}} \times p$ between SLBs with different TCR densities is generally much larger than the relative change in B_{TCR} and plotting $B_{\mathrm{CD4}}/F_{\mathrm{CD4}}$ vs $B_{\mathrm{TCR}} \times p$ will therefore approximately give a line with negative reciprocal slope K_c.

This is presented in Figure 4.7 for F_{CD4}=210 ± 100 molecules/μm^2 (Figure 4.7 A) and F_{CD4}=550 ± 65 molecules/μm^2 (Figure 4.7 B). A linear fit to the data gave a K_c of 2000 molecules/μm^2 and 1250 molecules/μm^2 for F_{CD4}=210 ± 100 molecules/μm^2 and F_{CD4}=550 ± 65 molecules/μm^2, respectively. By omitting the last data point in the two fits due to possible cell lamellipodia formation that could influence the obtained binding affinities (117), the two K_c values are now 2300 molecules/μm^2 and 1800 molecules/μm^2, for Figure 4.7A and 4.8B, respectively. Hence, an average K_c of 2000 molecules/μm^2 was obtained for CD4 binding free pMHC II. This 2D binding affinity value is smaller than the value measured by Jönsson et al. in a previous study between Raji B cells interacting with SLBs containing CD4 and human CD2 to align the contacts (27). However, this discrepancy could be due to the difference in cell lines and in pMHC II types expressed. For the rCD2 data presented in section 4.3, using an

average $(B/F)_{CD4} = 0.46$ and $(B/F)_{CD4} = 0.37$ for "low" and "high" rCD2 and a $N_{tot} \times f/S_{cell} = 580$ molecules/μm^2 (27), the 2D binding affinity of CD4 to pMHC II is 1260 and 1570 molecules/μm^2, for "low" and "high", respectively. Once again, the differences in affinity can be attributed to measurement uncertainty but is of the same order of magnitude as the value obtained from Figure 4.7. Hence, TCR does not seem to significantly influence the affinity of CD4 towards free pMHC II.

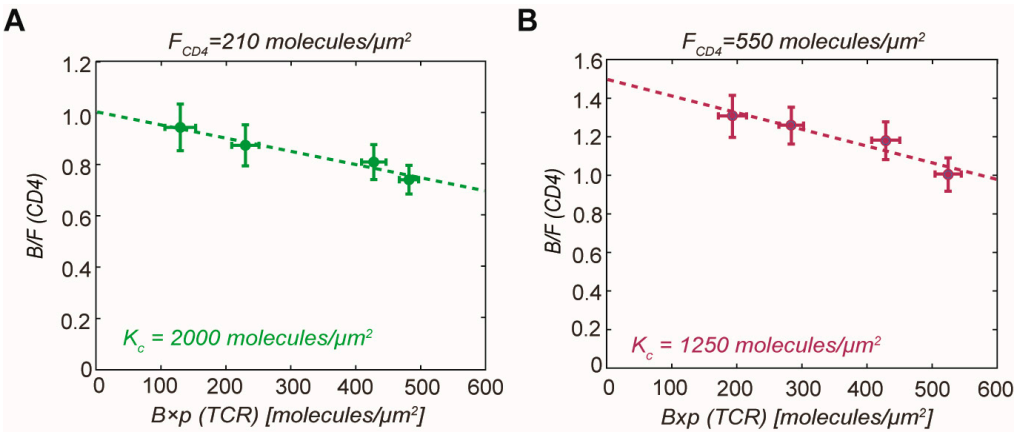

Figure 4.7. **(A)** Zhu-Golan plot of B/F of hCD4 vs $B \times p$ for the L3-12 TCR binding HLA-DQ8-glia-α1 for F_{CD4}=210 ± 100 molecules/μm^2 which resulted in a K_c of 2000 molecules/μm^2. **(B)** Zhu-Golan plot of B/F of hCD4 vs $B \times p$ for the L3-12 TCR binding HLA-DQ8-glia-α1 for F_{CD4}=550 ± 65 molecules/μm^2 which resulted in a K_c of 1250 molecules/μm^2. The data points represent mean ± SEM from 10-20 different cell-SLB contacts.

Inserting the values presented in Figure 4.7 into Eq.4.2 where $N_{tot}*f/S_{cell} = 707$ molecules/μm^2 and K_c is 2000 molecules/μm^2, the K_{c2} can be obtained. Using the first point in Figure 4.7, with the lowest amount of bound TCR, a K_{c2} value of 2080 molecules/μm^2 was obtained when having $F_{CD4} = 210$ molecules/μm^2 and a K_{c2} value of 3170 molecules/μm^2 was obtained when having $F_{CD4} = 550$ molecules/μm^2. The spread in the corresponding K_c values is attributed to measurement uncertainties. However, both K_c and K_{c2} are on the same magnitude which indicates that CD4 binding free MHC II is not very different than CD4 binding TCR-MHC II.

On the other hand, for TCR binding pMHC II in the presence of CD4 the Zhu-Golan equation (Eq.3.4) needs to be modified once more:

$$\frac{B_{\mathrm{TCR}}}{F_{\mathrm{TCR}}} = \frac{N_{\mathrm{tot}} \times f}{S_{\mathrm{cell}} K} - \frac{(B_{\mathrm{TCR}} + B_{\mathrm{CD4-pMHC\ II}}) \times p}{K} + \frac{B_{\mathrm{CD4-pMHC\ II}}}{K_2} \qquad (Eq.\ 4.3)$$

where B_{TCR} and F_{TCR} is the density of bound and free TCR, respectively, K is the 2D K_{d} for TCR binding free pMHC II, $B_{\mathrm{CD4\text{-}pMHC\ II}}$ is the density of CD4-pMHC II complexes and K_2 is the 2D K_{d} for TCR binding CD4-pMHC II. The first two terms on the right side of Eq. 4.3 describe TCR binding free pMHC II and the third term describes TCR binding CD4-pMHC II. Generally, $B_{\mathrm{TCR}} >> B_{\mathrm{CD4}}$ and therefore CD4 will only have a minor influence in the density of TCR binding free pMHC II. Nevertheless, since $p << 1$, CD4 can still produce a noticeable effect on the binding of TCR to CD4-pMHC II. The amount of $B_{\mathrm{CD4\text{-}pMHC\ II}}$ can be calculated from the following expression:

$$B_{\mathrm{CD4-pMHC\ II}} \approx \frac{N_{\mathrm{tot}} \times f}{S_{\mathrm{cell}} K_{\mathrm{c}}} - \frac{B_{\mathrm{TCR}} \times p}{K_{\mathrm{c}}} \qquad (Eq.\ 4.4)$$

4.6 Effects of CD4 on the TCR-MHC II Interaction

The effect of CD4 on the TCR-MHC II binding was investigated next. For this reason, Jurkat T cells expressing HLA-DQ8-glia-α1 MHC were initially incubated with SLBs functionalised only with different densities of fluorescently-labelled L3-12 TCR (Figure 4.8 A). As expected, the relative accumulation of L3-12 TCR in the cell-SLB contacts, B/F, decreased as the concentration of free L3-12 TCR increased on the SLB. Fitting the data in Figure 4.8 B to a line according to Eq. 3.4 (see section 3.3.2.1) gave a 2D K_{d} of 13 molecules/μm^2 for the L3-12 TCR bind HLA-DQ8-glia-α1, a value similar to previously obtained 2D K_{d} of this interaction measured at 37 ºC (14 molecules/μm^2) (117). Moreover, the total amount of mobile HLA-DQ8-glia-α1 receptors on the cells´ surface was 550 000 receptors per cell which was obtained from the x-intersect in the Zhu–Golan plot using S_{cell} = 700 μm^2 and assuming f = 0.9. These results explain the high bound L3-12 densities observed in the previous sub-chapter for low free densities of TCR on the SLB.

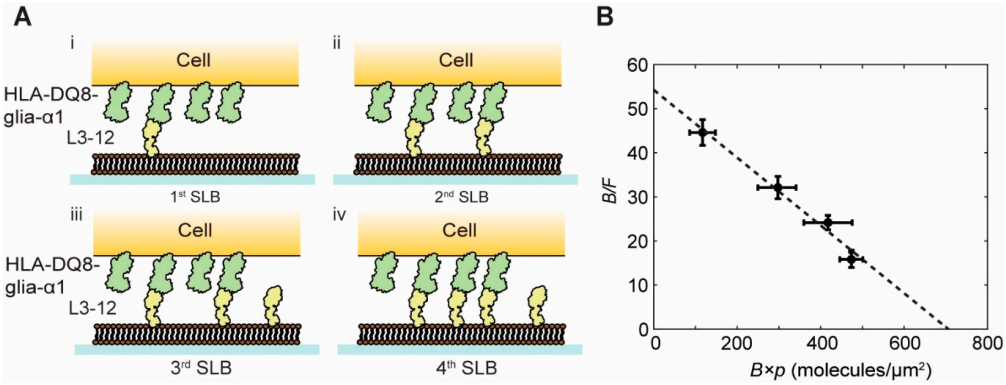

Figure 4.8. **(A)** Schematic illustration showing Jurkat T cells expressing HLA-DQ8-glia-α1 binding to SLBs with increasing L3-12 TCR densities (1st to 4th SLB). **(B)** Zhu-Golan plot of B/F vs $B\times p$ for the L3-12 TCR binding HLA-DQ8-glia-α1, which resulted in a K_d of 13 molecules/μm^2 for L3-12 TCR binding HLA-DQ8-glia-α1.

In order to investigate if the presence of CD4 influences TCR-MHC II binding, the K_d value of 13 molecules/μm^2 which was obtained when having only L3-12 TCR on the SLB was compared to the one obtained when having two different concentrations of hCD4 on the SLBs (Figure 4.9 A). Having hCD4 at free average densities of 210 molecules/μm^2 (Figure 4.9 B green) and 550 molecules/μm^2 (Figure 4.9 B purple) did not significantly affect the 2D K_d of the L3-12 TCR binding HLA-DQ8-glia-α1 interaction as it was 13 molecules/μm^2 and 12 molecules/μm^2, respectively. Comparing the two 2D K_d values in the presence of hCD4 with a two-sample t-test indicated that the data are not statistically different with p=0.933.

From Eq. 4.4 using K_c = 2000 molecules/μm^2 and $N_{tot}\times f/S_{cell}$ = 707 molecules/μm^2, the density of bound CD4-pMHC II complexes was determined as 61 molecules/μm^2 and 139 molecules/μm^2 for the first data point in Figure 4.7A and 47B, respectively. Inserted in Eq. 4.3 with $N_{tot}\times f/S_{cell}$ = 707 molecules/μm^2 and K = 13 molecules/μm^2 gives a 2D K_d for L3-12 TCR binding CD4-pMHC II of K_2 = 12 molecules/μm^2. The values are close to the K = 13 molecules/μm^2 obtained without CD4, signifying again that the TCR binds with similar affinity to CD4-pMHC II as to free pMHC II. Therefore, even though CD4 binding to pMHC influences the sensitivity of the T cell (169, 174), it is possible that CD4 does not affect the strength of agonistic TCR-pMHC interactions (188, 189). These results are in agreement with previous studies that showed a negligible effect of CD4 on the binding kinetics of the TCR-pMHC II complex (190, 191).

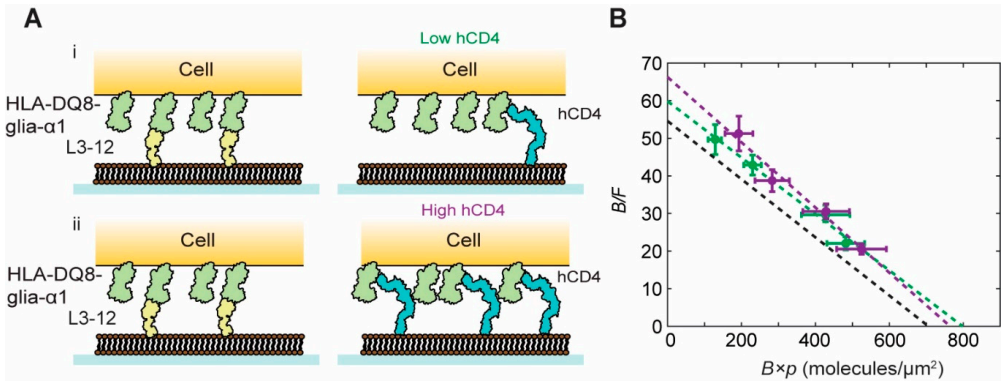

Figure 4.9. **(A)** Schematic illustration showing Jurkat T cells expressing HLA-DQ8-glia-α1 binding to SLBs in the presence of F_{CD4} = 210 molecules/μm^2 or F_{CD4} = 550 molecules/μm^2. **(B)** Zhu-Golan plots of B/F vs $B\times p$ for the L3-12 TCR binding HLA-DQ8-glia-α1 in the presence of F_{CD4} = 210 molecules/μm^2 (green) and F_{CD4} = 550 molecules/μm^2 (purple) hCD4 concentrations. The black dashed line is the Zhu-Golan plot for the L3-12 TCR binding HLA-DQ8-glia-α1 without hCD4. The obtained 2D K_d values were 13 molecules/μm^2 (green) and 12 molecules/μm^2 (purple) for low and high hCD4 concentrations, respectively while the 2D K_d value without the co-receptor was 13 molecules/μm^2.

4.7 Single-Cell Binding Affinities of the CD4 Co-receptor

Lastly, the single-cell binding affinity method that was presented in Chapter 3 (see section 3.5.2) was used to obtain single-cell K_d values for the CD4 co-receptor. Since having only hCD4 on the SLBs did not result in any observable cell-SLB contacts, rCD2 and L3-12 TCR were used once more to ensure successful contact formation between the co-receptor and the cells. For the first set of experiments, SLBs functionalized with fluorescently-labelled rCD2 and hCD4 were used which interacted with Jurkat T cells expressing HLA-DQ8-glia-α1 MHC and rCD48$_{T92A}$. For low densities of bound rCD2 (B_{rCD2} < 200 molecules/μm^2), the co-receptor was able to accumulate and distribute homogeneously within the cell-SLB contacts (see section 4.3). After allowing the system to reach an equilibrium, imidazole was used to reduce the concentration of hCD4 in steps. The hCD4 and rCD2 proteins were genetically modified at the C-terminus with a single histidine tag (6xH) and a double histidine tag (12xH), respectively (27, 183). It was thus speculated that CD4 would detach quicker under imidazole treatment.

However, an imidazole concentration of 5 mM to 13 mM inside the well for 30 to 60 seconds resulted in reducing both ligands and various changes in the imidazole concentration or incubation period did not change this outcome. Reducing the rCD2 concentration as well resulted in positive Zhu-Golan plots for the hCD4 and therefore the 2D K_d could not be obtained (data not shown). It is not yet understood how reducing the concentration of rCD2 affects the CD4 binding. Also, by reducing the concentration of the auxiliary ligand, eventually the CD4 contacts disappeared since CD4 binding MHC II is so weak that it cannot maintain contact formations. A solution to this problem could be to anchor the rCD2 proteins on the SLB without DGS-NTA, for example using a GPI-linker (70) or biotin-streptavidin linked proteins (69), which would mean that only the his-tagged CD4 would be titrated with imidazole.

The experiments were later repeated by replacing the rCD2 with the L3-12 TCR (Figure 4.10 A). This time the imidazole did not significantly influence the L3-12 TCR density on the SLB which remained approximately 90 molecules/μm^2 and only the hCD4 densities decreased (~1700 molecules/μm^2 to 1200 molecules/μm^2). Both L3-12 TCR and rCD2 had equally many histidine tags (12xH) but the TCR has one histidine tag (6xH) on the C-terminus of each of the α- and β- chains, so it is possible that it has a bigger area to bind stronger to the SLB than the rCD2 and therefore it was less influenced by imidazole. Figure 4.10 B shows the fluorescence images for L3-12 TCR and hCD4 of a cell-SLB contact before (i) and after (ii) an imidazole titration. A second imidazole step reduced the CD4 concentration further and the CD4 contacts disappeared. Therefore, a single-cell Zhu-Golan plot was obtained for only two hCD4 densities (Figure 4.10 C). The average K_d value for CD4 binding pMHC II was 3200 ± 1400 molecules/μm^2 (n = 12) which is comparable to previous results (27). It would be interesting to anchor the L3-12 TCR proteins on the SLB without DGS-NTA and compare the obtained single-cell K_d value of CD4 in the presence of rCD2 and L3-12 TCR.

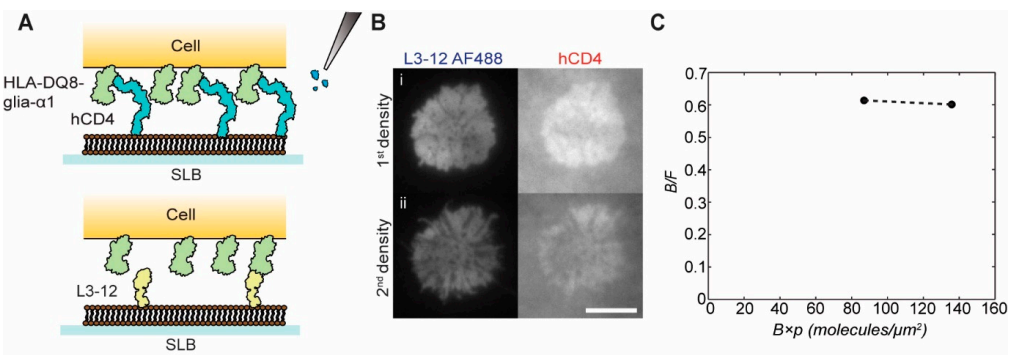

Figure 4.10. **(A)** Schematic illustration showing Jurkat T cells expressing HLA-DQ8-glia-α1 binding to SLBs functionalized with L3-12 TCR and CD4. **(B)** Fluorescence images of a cell-SLB contact at two hCD4 densities in the presence of stable L3-12 TCR concentration. The images were captured 40 min after the cells adhered on the SLB (1st density) and 40 min after an imidazole titration (2nd density). The scale bar is 8 μm, and the scale is the same for all images. **(C)** Zhu-Golan plot of B/F vs $B \times p$ for the hCD4 binding HLA-DQ8-glia-α1 in the presence of L3-12 TCR presented in **(B)**. The obtained 2D single-cell K_d value is 3333 molecules/μm^2.

4.8 Summary

The first part of this chapter focused on the influence of rCD2 as an adhesion molecule on the obtained binding kinetics of the CD4 co-receptor. The obtained data showed that the average accumulation of CD4 was 1.8 times lower when having a high concentration of bound rCD2 compared to low concentrations of bound rCD2 inside the cell-SLB contacts highlighting the impact of auxiliary proteins on the measured binding kinetics. The second part of the chapter focused on the CD4-pMHC-TCR ternary complex. It was demonstrated that the presence of L3-12 TCR strongly supported the CD4-pMHC interaction, but it did not seem to significantly affect the binding of CD4 to pMHC. Moreover it was found that CD4 did not noticeably affect TCR-MHC II binding at two distinct CD4 concentrations.

4.9 Discussion & Outlook

Adhesion molecules, such as CD2, assist the cell-cell contact formation (13, 14) and in doing so promote the binding of lower affinity proteins such as CD4 (27). This was also noticed in the aforementioned studies since the presence of rCD2 in the SLB was essential for forming CD4-MHC II contacts. However, the data presented in this chapter show that, at certain densities, the presence of an auxiliary molecule can give rise to protein exclusion which would result in a lower efffective affinity for the studied ligand-receptor interaction. It is therefore possible that there is an optimal concentration range within which adhesion molecules promote contact formation without affecting the affinities of other interactions. Since these results indicate that there is not a single parameter defining the 2D binding affinity of protein-protein interactions, it is of utmost importance to better understand how different parameters affect the

obtained binding values for future binding kinetic studies. In particular, more studies are needed in order to determine how the presence of various auxiliary binding molecules of different lengths and affinities affect the under-study receptor-ligand binding. These studies would help understand if and how auxiliary binding molecules influence the protein affinity *in vivo* where numerous ligand–receptor pairs are acting in unison (179).

On the other hand, it was interesting to observe the distinction between CD4′s binding behaviour in the presence of TCR compared to CD2. At greater length, our data showed that the presence of TCR strongly facilitates CD4 binding which is in agreement with previous biophysical studies (155, 187, 191). This is achieved by increasing the local density of MHC II inside the cell-SLB contact and not by significantly affecting the binding affinity of CD4 to MHC II since the affinity of CD4 to TCR-pMHC II is of the same order of magnitude as that to free pMHC II. At the same time having physiological levels of CD4 in the SLB (~200 molecules/μm^2) did not noticeably affect TCR-MHC II binding in agreement with previous studies that showed a negligible effect of CD4 on the binding kinetics of the TCR-MHC complex (190, 191). These results could possibly suggest that an initial TCR-MHC II interaction is followed by a CD4-MHC II interaction. It is likely that the co-receptor′s main role is to recruit Lck to the TCR complex and thus phosphorylate it or to recruit Lck to a pre-phosphorylated TCR-CD3 complex to augment a pre-existing activation. The latter hypothesis is termed the two-step co-receptor recruitment model and was proposed by Xu and Littman in 1993 (192). Several studies have provided experimental evidence supporting the two-step cooperative binding model while studying the CD8-TCR-pMHC interaction (188, 193). This model would also agree with theoretical models that showed that the recruitment of Lck by the CD4 to a pre-phosphorylated TCR resulted in an up to 40-fold increase in the rate of receptor phosphorylation compared to when the Lck was recruited to an unphosphorylated TCR (27). Lastly, the two-step co-receptor recruitment model also agrees with studies showing that the co-receptors are not essential for triggering (194) or that they have a surprisingly small Lck occupancy as it was reported recently (195, 196). It would be interesting to perform the experiments presented in this chapter while having the full-length transmembrane proteins into the model membrane and investigate whether the presence of Lck in CD4′s cytoplasmatic tail would affect the obtained data. It is also a pursuit for future studies to determine if CD4 recruitment follows an initial TCR-MHC interaction as well as to determine the lifetime of each protein in the ternary complex. Coupling binding kinetic studies of the CD4-TCR-MHC

II interaction to T-cell triggering could also provide a crucial insight into the role of this ternary complex in T-cell activation and downstream signaling.

Chapter 5

5. Conclusions

Contents

5.1 Summary & Outlook

The main aim of this thesis was to better understand the binding kinetics of proteins at immune-cell contacts. On that account, a new approach for obtaining 2D single-cell binding affinities of T cells interacting with SLBs was presented and the obtained results for the rCD2-rCD48$_{T92A}$ interaction showed a small spread in the 2D K_d values even though the receptor density varied significantly within the cell population. Moreover, by using single-molecule imaging and tracking, the lifetime of the rCD2-rCD48$_{T92A}$ interaction was estimated which displayed a similar narrow spread between the various cell-SLB contacts. The next projects focused on the CD4 co-receptor, a vital protein for proper immune function whose remarkably low binding affinity renders it a challenging biomolecule for binding studies. The effects of rCD2 on the CD4 binding were studied in the presence of two distinct concentrations of the auxiliary protein. It was observed that the density of an auxiliary protein can substantially affect the binding behavior and therefore the binding affinity of the under-study interaction. Later, the CD4-pMHC-TCR ternary complex was investigated where it was shown that CD4 binding is enhanced in the presence of any TCR density. However, this is achieved by increasing the local density of MHC II inside the cell-SLB contact and not by significantly affecting the binding affinity of CD4 to MHC II. Lastly, it was demonstrated that the presence of CD4 at physiological levels did not noticeably affect the TCR-MHC II binding affinity.

Despite the existing knowledge and the expanding number of available techniques to measure the binding kinetics of receptor-ligand complexes, there is still considerable room for improvement in future studies. In more detail, future work will involve the use of more complex compositions of lipids coupled with the incorporation and observation of complex membrane protein assemblies. In particular, the development and study of membranes with a different composition on the two bilayer leaflets to better mimic the cell environment is already attracting considerable attention (197). Including the glycocalyx as well as several auxiliary binding proteins in the studied systems will augment the accuracy of the obtained data and moderate the observed differences between *in vitro* and *in vivo*. Furthermore, super-resolution imaging methods such as STED, STORM, PALM, and SIM will be used more extensively to image the membranes at length scales relevant to macromolecular biological assemblies (198). Their optimization as well as the emergence of new fluorophores with enhanced brightness and photostability will continue. Super-resolution techniques can especially be used to study the function of cilia and microvilli in the movement and sensory functions of the cells, an area that

remains elusive with other microscopy techniques. On the other hand, novel theoretical models describing non-equilibrium processes on the membranes will be better established to help couple the experimental observations with the theory (199). At the same time, the current models should be reformed to include the effects of membrane deformation and the actin cytoskeleton in protein diffusion and rearrangement with higher accuracy (199). Integrating experiments and theory with simulations in future studies is also another successful strategy to further understand the kinetics of protein-protein interactions. In particular, computational methods based on molecular dynamic (MD) simulations have proven valuable in understanding how conformational changes affect the lifetime of a receptor-ligand complex (200) and are currently emerging as an extremely valuable tool in studying the binding kinetics (201, 202). Finally, the use of machine learning techniques in identifying overestimated or underestimated values inside the immense amount of data produced by simulations is very auspicious and considerable efforts are already taking place in this direction (203, 204). It is evident that the continuous development of novel biophysical tools and techniques as well as the utilization of interdisciplinary science approaches in the field of protein-protein interactions will continue to expand the limits of our knowledge in crucial cellular processes.

6. References

References

1. Medzhitov, R. 2007. Recognition of microorganisms and activation of the immune response. *Nature*. 449:819–826.
2. Rosales, C., and E. Uribe-Querol. 2017. Phagocytosis: A Fundamental Process in Immunity. *Biomed Res. Int.*
3. Arstila, T.P., A. Casrouge, V. Baron, J. Even, J. Kanellopoulos, and P. Kourilsky. 1999. A direct estimate of the human αβ T cell receptor diversity. *Science (80-.).* 286:958–961.
4. Kageyama, S., T.J. Tsomides, Y. Sykulev, and H.N. Eisen. 1995. Variations in the number of peptide-MHC class I complexes required to activate cytotoxic T cell responses. *J. Immunol.*
5. Huang, J., M. Brameshuber, X. Zeng, J. Xie, Q. jing Li, Y. hsiu Chien, S. Valitutti, and M.M. Davis. 2013. A Single peptide-major histocompatibility complex ligand triggers digital cytokine secretion in CD4+ T Cells. *Immunity*.
6. Irvine, D.J., M.A. Purbhoo, M. Krogsgaard, and M.M. Davis. 2002. Direct observation of ligand recognition by T cells. *Nature*.
7. Murphy, K., and C. Weaver. 2017. Janeway's Immunobiology. 9th ed. New York: .
8. De Aós, I., M.H. Metzger, M. Exley, C.E. Dahl, S. Misra, D. Zheng, L. Varticovski, C. Terhorst, and J. Sancho. 1997. Tyrosine phosphorylation of the CD3-ε subunit of the T cell antigen receptor mediates enhanced association with phosphatidylinositol 3-kinase in Jurkat T cells. *J. Biol. Chem.* 272:25310–25318.
9. Courtney, A.H., W.L. Lo, and A. Weiss. 2018. TCR Signaling: Mechanisms of Initiation and Propagation. *Trends Biochem. Sci.*
10. Manjunath, N., M. Correa, M. Ardman, and B. Ardman. 1995. Negative regulation of T-cell adhesion and activation by CD43. *Nature*. 377:535–538.
11. Pettmann, J., A.M. Santos, O. Dushek, and S.J. Davis. 2018. Membrane Ultrastructure and T Cell Activation. *Front. Immunol.* 9:1–9.
12. Purbhoo, M.A., D.J. Irvine, J.B. Huppa, and M.M. Davis. 2004. T cell killing does not require the formation of a stable mature immunological synapse. *Nat. Immunol.*
13. Davis, S.J., and P.A. van der Merwe. 2006. The kinetic-segregation model: TCR triggering and beyond. *Nat. Immunol.* 7:803–809.
14. James, J.R., and R.D. Vale. 2012. Biophysical mechanism of T-cell receptor triggering in a reconstituted system. *Nature*. 487:64–69.
15. Dustin, M.L. 2014. The Immunological Synapse. *Cancer Immunol. Res.* 2:1023–1033.
16. Schmid, E.M., M.H. Bakalar, K. Choudhuri, J. Weichsel, H.S. Ann, P.L. Geissler, M.L. Dustin, and D.A. Fletcher. 2016. Size-dependent protein segregation at membrane interfaces. *Nat. Phys.* 12:704–711.
17. Grakoui, A. 1999. The Immunological Synapse: A Molecular Machine Controlling T Cell Activation. *Science (80-.).* 285:221–227.

18. Bromley, S.K., A. Iaboni, S.J. Davis, A. Whitty, J.M. Green, A.S. Shaw, A. Weiss, and M.L. Dustin. 2001. The immunological synapse and CD28-CD80 interactions. *Nat. Immunol.* 2:1159–1166.

19. R. Varma, G. Campi, T. Yokosuka, T. Saito, and M.L.D. 2006. T Cell Receptor-Proximal Signals Are Sustained in Peripheral Microclusters and Terminated in the Central Supramolecular Activation Cluster. *Immunity*. 25:117–127.

20. Yokosuka, T., K. Sakata-Sogawa, W. Kobayashi, M. Hiroshima, A. Hashimoto-Tane, M. Tokunaga, M.L. Dustin, and T. Saito. 2005. Newly generated T cell receptor microclusters initiate and sustain T cell activation by recruitment of Zap70 and SLP-76. *Nat. Immunol.* 6:1253–1262.

21. Dam, T., M. Chouliara, V. Junghans, and P. Jönsson. 2022. Supported Lipid Bilayers and the Study of Two-Dimensional Binding Kinetics. *Front. Mol. Biosci.* 9:1–15.

22. Murphy, K., and C. Weaver. 2017. Janeway ' S 9 Th Edition. .

23. Artyomov, M.N., M. Lis, S. Devadas, M.M. Davis, and A.K. Chakraborty. 2010. CD4 and CD8 binding to MHC molecules primarily acts to enhance Lck delivery. *Proc. Natl. Acad. Sci. U. S. A.*

24. Bosselut, R., L. Feigenbaum, S.O. Sharrow, and A. Singer. 2001. Strength of signaling by CD4 and CD8 coreceptor tails determines the number but not the lineage direction of positively selected thymocytes. *Immunity*.

25. Van Laethem, F., S.D. Sarafova, J.H. Park, X. Tai, L. Pobezinsky, T.I.I. Guinter, S. Adoro, A. Adams, S.O. Sharrow, L. Feigenbaum, and A. Singer. 2007. Deletion of CD4 and CD8 Coreceptors Permits Generation of αβT Cells that Recognize Antigens Independently of the MHC. *Immunity*. 27:735–750.

26. Wyer, J.R., B.E. Willcox, G. George F, U.C. Gerth, S.J. Davis, J.I. Bell, P.A. Van Der Merwe, and B.K. Jakobsen. 1999. T cell receptor and coreceptor CD8αα bind peptide-MHC independently and with distinct kinetics. *Immunity*. 10:219–225.

27. Jönsson, P., J.H. Southcombe, A.M. Santos, J. Huo, R.A. Fernandes, J. McColl, M. Lever, E.J. Evans, A. Hudson, V.T. Chang, T. Hanke, A. Godkin, P.D. Dunne, M.H. Horrocks, M. Palayret, G.R. Screaton, J. Petersen, J. Rossjohn, L. Fugger, O. Dushek, X.-N. Xu, S.J. Davis, and D. Klenerman. 2016. Remarkably low affinity of CD4/peptide-major histocompatibility complex class II protein interactions. *Proc. Natl. Acad. Sci.* 113:5682–5687.

28. Katakai, T., K. Habiro, and T. Kinashi. 2013. Dendritic Cells Regulate High-Speed Interstitial T Cell Migration in the Lymph Node via LFA-1/ICAM-1. *J. Immunol.* 191:1188–1199.

29. Springer, T.A. 1995. Traffic signals on endothelium for lymphocyte recirculation and leukocyte emigration. *Annu. Rev. Physiol.* 57:827–72.

30. van der Merwe, P.A., A.N. Barclay, D.W. Mason, E.A. Davies, S.J. Davis, B.P. Morgan, M. Tone, A.K.C. Krishnam, and C. Ianelli. 1994. Human Cell-Adhesion Molecule CD2 Binds CD58 (LFA-3) with a Very Low Affinity and an Extremely Fast Dissociation Rate but Does Not Bind CD48 or CD59. *Biochemistry*.

31. Zhu, D.-M., M.L. Dustin, C.W. Cairo, H.S. Thatte, and D.E. Golan. 2006. Mechanisms of Cellular Avidity Regulation in CD2–CD58-Mediated T Cell Adhesion. *ACS Chem. Biol.* 1:649–658.

32. Davis, S.J., and P.A. van der Merwe. 1996. The structure and ligand interactions of CD2: implications for T-cell function. *Immunol. Today*. 17:177–187.

33. Shaw, A.S., and M.L. Dustin. 1997. Making the T Cell Receptor Go the Distance: A Topological View of T Cell Activation. *Immunity*. 6:361–369.

34. Dustin, M.L., L.M. Ferguson, P. Chan, T.A. Springer, and D.E. Golan. 1996. Visualization of CD2 Interaction with LFA-3 and Determination of the Two-Dimensional Dissociation Constant for Adhesion Receptors in a Contact Area. 132:465–474.

35. Dustin, M.L., S.K. Bromley, M.M. Davis, and C. Zhu. 2001. Identification of Self Through Two-Dimensional Chemistry and Synapses. *Annu. Rev. Cell Dev. Biol.* 17:133–157.

36. Bachmann, M.F., K. Mckall-faienza, R. Schmits, D. Bouchard, J. Beach, D.E. Speiser, T.W. Mak, and P.S. Ohashi. 1997. Distinct Roles for LFA-1 and CD28 during Activation of Naive T Cells : Adhesion versus Costimulation. 7:549–557.

37. Lombard, J. 2014. Once upon a time the cell membranes: 175 years of cell boundary research. *Biol. Direct*.

38. Verkade, P., and K. Simons. 1997. Lipid microdomains and membrane trafficking in mammalian cells. In: Histochemistry and Cell Biology. .

39. Helms, J.B., and C. Zurzolo. 2004. Lipids as targeting signals: Lipid rafts and intracellular trafficking. *Traffic*.

40. Singer, S.J., and G.L. Nicolson. 1972. The fluid mosaic model of the structure of cell membranes. *Science (80-.).*

41. Israelachvili, J. 2011. Intermolecular and Surface Forces. Elsevier.

42. Watson, H. 2015. Biological membranes. *Essays Biochem.*

43. Khan, M.S., N.S. Dosoky, and J.D. Williams. 2013. Engineering lipid bilayer membranes for protein studies. *Int. J. Mol. Sci.*

44. Möckl, L. 2020. The Emerging Role of the Mammalian Glycocalyx in Functional Membrane Organization and Immune System Regulation. *Front. Cell Dev. Biol.* 8:1–14.

45. Tanaka, M., and E. Sackmann. 2005. Polymer-supported membranes as models of the cell surface. *Nature*.

46. Sinner, E.K., and W. Knoll. 2001. Functional tethered membranes. *Curr. Opin. Chem. Biol.*

47. Mueller, P., D.O. Rudin, H. Ti Tien, and W.C. Wescott. 1962. Reconstitution of cell membrane structure in vitro and its transformation into an excitable system. *Nature*.

48. Castellana, E.T., and P.S. Cremer. 2006. Solid supported lipid bilayers: From biophysical studies to sensor design. *Surf. Sci. Rep.* 61:429–444.

49. Winterhalter, M. 2000. Black lipid membranes. *Curr. Opin. Colloid Interface Sci.*

50. Tamm, L.K., and H.M. McConnell. 1985. Supported phospholipid bilayers. *Biophys. J.*

51. McConnell, H.M., T.H. Watts, R.M. Weis, and A.A. Brian. 1986. Supported planar membranes in studies of cell-cell recognition in the immune system. *BBA - Rev. Biomembr.*

52. Sackmann, E. 1996. Supported membranes: Scientific and practical applications. *Science (80-.).*

53. Kim, J., G. Kim, and P.S. Cremer. 2001. Investigations of water structure at the solid/liquid interface in the presence of supported lipid bilayers by vibrational sum frequency spectroscopy. *Langmuir*.

54. Afanasenkau, D., and A. Offenhäusser. 2012. Positively charged supported lipid bilayers as a biomimetic platform for neuronal cell culture. *Langmuir*.

55. Alessandrini, A., and P. Facci. 2014. Phase transitions in supported lipid bilayers studied by AFM. *Soft Matter*. 10:7145–7164.

56. Killian, J.A., and T.K. Nyholm. 2006. Peptides in lipid bilayers: the power of simple models. *Curr. Opin. Struct. Biol.* 16:473–479.

57. Richter, R.P., R. Bérat, and A.R. Brisson. 2006. Formation of solid-supported lipid bilayers: An integrated view. *Langmuir*. 22:3497–3505.

58. MacDonald, R.C., and S.A. Simon. 1987. Lipid monolayer states and their relationships to bilayers. *Proc. Natl. Acad. Sci. U. S. A.*

59. Daniel, M.F., and G.W. Smith. 1983. Langmuir-Blodgett films. *Phys. Educ.*

60. Kalb, E., S. Frey, and L.K. Tamm. 1992. Formation of supported planar bilayers by fusion of vesicles to supported phospholipid monolayers. *BBA - Biomembr.*

61. Nollert, P., H. Kiefer, and F. Jähnig. 1995. Lipid vesicle adsorption versus formation of planar bilayers on solid surfaces. *Biophys. J.*

62. Hardy, G.J., R. Nayak, and S. Zauscher. 2013. Model cell membranes: Techniques to form complex biomimetic supported lipid bilayers via vesicle fusion. *Curr. Opin. Colloid Interface Sci.* 18:448–458.

63. Salafsky, J., J.T. Groves, and S.G. Boxer. 1996. Architecture and function of membrane proteins in planar supported bilayers: A study with photosynthetic reaction centers. *Biochemistry*.

64. Kalb, E., and L.K. Tamm. 1992. Incorporation of cytochrome b5 into supported phospholipid bilayers by vesicle fusion to supported monolayers. *Thin Solid Films*.

65. Goennenwein, S., M. Tanaka, B. Hu, L. Moroder, and E. Sackmann. 2003. Functional incorporation of integrins into solid supported membranes on ultrathin films of cellulose: Impact on adhesion. *Biophys. J.*

66. Munro, J.C., and C.W. Frank. 2004. In situ formation and characterization of poly(ethylene glycol)-supported lipid bilayers on gold surfaces. *Langmuir*.

67. Groves, J.T., and M.L. Dustin. 2003. Supported planar bilayers in studies on immune cell adhesion and communication. *J. Immunol. Methods*. 278:19–32.

68. Schmitt, L., C. Dietrich, and R. Tampé. 1994. Synthesis and Characterization of Chelator-Lipids for Reversible Immobilization of Engineered Proteins at Self-Assembled Lipid Interfaces. *J. Am. Chem. Soc.*

69. Liu, Z., H. Qin, C. Xiao, C. Wen, S. Wang, and S. Sui. 1995. Specific binding of avidin to biotin containing lipid lamella surfaces studied with monolayers and liposomes. *Eur. Biophys. J.* 24:31–38.

70. Paulick, M.G., and C.R. Bertozzi. 2008. The glycosylphosphatidylinositol anchor: A complex membrane-anchoring structure for proteins. *Biochemistry*. 47:6991–7000.

71. Dustin, M.L., and J.T. Groves. 2012. Receptor Signaling Clusters in the Immune Synapse. *Annu. Rev. Biophys.* 41:543–556.

72. Nye, J.A., and J.T. Groves. 2008. Kinetic control of histidine-tagged protein surface density on supported lipid bilayers. *Langmuir*. 24:4145–4149.

73. Giepmans, B.N.G., S.R. Adams, M.H. Ellisman, and R.Y. Tsien. 2006. The fluorescent toolbox for assessing protein location and function. *Science (80-.).*

74. Peterman, E.J.G. 2018. Single Molecule Analysis Methods and Protocols. .

75. Gensch, T., M. Böhmer, and P.F. Aramendía. 2005. Single molecule blinking and photobleaching separated by wide-field fluorescence microscopy. *J. Phys. Chem. A*.

76. Ploem, J.S. 1967. The use of a vertical illuminator with interchangeable dichroic mirrors for fluorescence microscopy with incidental light. *Z. Wiss. Mikrosk.*

77. Masters, B.R. 2010. The Development of Fluorescence Microscopy. In: Encyclopedia of Life Sciences. .

78. Axelrod, D., T.P. Burghardt, and N.L. Thompson. 1984. Total internal reflection fluorescence. *Annu. Rev. Biophys. Bioeng.*

79. Pawley, J.B. 2006. Handbook of biological confocal microscopy: Third edition. *Handb. Biol. Confocal Microsc. Third Ed.* 1–985.

80. E. J. AMBROSE. 1956. A Surface Contact Microscope for the study of Cell Movements. *Nature*. 11:1956.

81. Mattheyses, A.L., S.M. Simon, and J.Z. Rappoport. 2010. Imaging with total internal reflection fluorescence microscopy for the cell biologist. *J. Cell Sci.* 123:3621–3628.

82. Axelrod, D. 2001. Total internal reflection fluorescence microscopy in cell biology. *Traffic*.

83. Tolentino, T.P., J. Wu, V.I. Zarnitsyna, Y. Fang, M.L. Dustin, and C. Zhu. 2008. Measuring Diffusion and Binding Kinetics by Contact Area FRAP. *Biophys. J.* 95:920–930.

84. Klonis, N., M. Rug, I. Harper, M. Wickham, A. Cowman, and L. Tilley. 2002. Fluorescence photobleaching analysis for the study of cellular dynamics. *Eur. Biophys. J.* 31:36–51.

85. Axelrod, D., D.E. Koppel, J. Schlessinger, E. Elson, and W.W. Webb. 1976. Mobility measurement by analysis of fluorescence photobleaching recovery kinetics. *Biophys. J.*

86. Jönsson, P., M.P. Jonsson, J.O. Tegenfeldt, and F. Höök. 2008. A Method Improving the Accuracy of Fluorescence Recovery after Photobleaching Analysis. *Biophys. J.* 95:5334–5348.

87. Abbe, E. 1873. Beiträge zur Theorie des Mikroskops und der mikroskopischen Wahrnehmung. *Arch. für Mikroskopische Anat.*

88. Rayleigh. 1896. On the theory of optical images, with special reference to the microscope. *Philos. Mag. Ser. 5*. 42:167–195.

89. Chiu, S.W., and M.C. Leake. 2011. Functioning nanomachines seen in real-time in living bacteria using single-molecule and super-resolution fluorescence imaging. *Int. J. Mol. Sci.*

90. Gustafsson, M.G.L. 2000. Surpassing the lateral resolution limit by a factor of two using structured illumination microscopy. *J. Microsc.* 198:82–87.

91. Heintzmann, R., and T. Huser. 2017. Super-Resolution Structured Illumination Microscopy. *Chem. Rev.* 117:13890–13908.

92. Hell, S.W., and J. Wichmann. 1994. Breaking the diffraction resolution limit by stimulated emission: stimulated-emission-depletion fluorescence microscopy. *Opt. Lett.*

93. Betzig, E., G.H. Patterson, R. Sougrat, O.W. Lindwasser, S. Olenych, J.S. Bonifacino, M.W. Davidson, J. Lippincott-Schwartz, and H.F. Hess. 2006. Imaging intracellular fluorescent proteins at nanometer resolution. *Science (80-.).* 313:1642–1645.

94. Hirschfeld, T. 1976. Optical microscopic observation of single small molecules. *Appl. Opt.* 15:2965.

95. Kural, C., H. Kim, S. Syed, G. Goshima, V.I. Gelfand, and P.R. Selvin. 2005. Cell Biology: Kinesin and dynein move a peroxisome in vivo: A tug-of-war or coordinated movement? *Science (80-.).* 308:1469–1472.

96. Kisley, L., J. Chen, A.P. Mansur, B. Shuang, K. Kourentzi, M.V. Poongavanam, W.H. Chen, S. Dhamane, R.C. Willson, and C.F. Landes. 2014. Unified superresolution experiments and stochastic theory provide mechanistic insight into protein ion-exchange adsorptive separations. *Proc. Natl. Acad. Sci. U. S. A.* 111:2075–2080.

97. Moerner, W.E., and D.P. Fromm. 2003. Methods of single-molecule fluorescence spectroscopy and microscopy. *Rev. Sci. Instrum.* 74:3597–3619.

98. Yildiz, A., J.N. Forkey, S.A. McKinney, T. Ha, Y.E. Goldman, and P.R. Selvin. 2003. Myosin V walks hand-over-hand: Single fluorophore imaging with 1.5-nm localization. *Science (80-.).* 300:2061–2065.

99. Thompson, R.E., D.R. Larson, and W.W. Webb. 2002. Precise nanometer localization analysis for individual fluorescent probes. *Biophys. J.* 82:2775–2783.

100. Shen, H., L.J. Tauzin, R. Baiyasi, W. Wang, N. Moringo, B. Shuang, and C.F. Landes. 2017. Single Particle Tracking: From Theory to Biophysical Applications. *Chem. Rev.* 117:7331–7376.

101. Saxton, M.J., and K. Jacobson. 1997. Single-particle tracking: Applications to membrane dynamics. *Annu. Rev. Biophys. Biomol. Struct.* 26:373–399.

102. Manzo, C., and M.F. Garcia-Parajo. 2015. A review of progress in single particle tracking: From methods to biophysical insights. *Reports Prog. Phys.*

103. Corzo, J. 2006. Time, the forgotten dimension of ligand binding teaching. *Biochem. Mol. Biol. Educ.* 34:413–416.

104. Tian, S., R. Maile, E.J. Collins, and J.A. Frelinger. 2007. CD8 + T Cell Activation Is Governed by TCR-Peptide/MHC Affinity, Not Dissociation Rate . *J. Immunol.*

105. Alam, S.M., P.J. Travers, J.L. Wung, W. Nasholds, S. Redpath, S.C. Jameson, and N.R.J. Gascoigne. 1996. T cell-receptor affinity and thymocyte positive selection. *Nature*.

106. Aleksic, M., O. Dushek, H. Zhang, E. Shenderov, J.L. Chen, V. Cerundolo, D. Coombs, and P.A. van der Merwe. 2010. Dependence of T Cell Antigen Recognition on T Cell Receptor-Peptide MHC Confinement Time. *Immunity*.

107. Matsui, K., J.J. Boniface, P. Steffner, P.A. Reay, and M.M. Davis. 1994. Kinetics of T-cell receptor binding to peptide/I-E(k) complexes: Correlation of the dissociation rate with T-cell responsiveness. *Proc. Natl. Acad. Sci. U. S. A.*

108. Kersh, G.J., E.N. Kersh, D.H. Fremont, and P.M. Allen. 1998. High- and low-potency ligands with similar affinities for the TCR: The importance of kinetic in TCR signaling. *Immunity*.

109. Schreiber, G., G. Haran, and H.X. Zhou. 2009. Fundamental aspects of protein - Protein association kinetics. *Chem. Rev.*

110. Ladbury, J.E., and B.Z. Chowdhry. 1996. Sensing the heat: The application of isothermal titration calorimetry to thermodynamic studies of biomolecular interactions. *Chem. Biol.*

111. Merwe, P.A. Van Der. 2010. Surface plasmon resonance GENERAL PRINCIPLES OF BIACORE EXPERIMENTS. *Physics (College. Park. Md).*

112. Arima, Y., M. Toda, and H. Iwata. 2011. Surface plasmon resonance in monitoring of complement activation on biomaterials. *Adv. Drug Deliv. Rev.* 63:988–999.

113. Patching, S.G. 2014. Biochimica et Biophysica Acta Surface plasmon resonance spectroscopy for characterisation of membrane protein – ligand interactions and its potential for drug discovery. *BBA - Biomembr.* 1838:43–55.

114. Kastritis, P.L., and A.M.J.J. Bonvin. 2013. On the binding affinity of macromolecular interactions: daring to ask why proteins interact. *J. R. Soc. Interface*. 10:20120835.

115. Steinkühler, J., B. Rózycki, C. Alvey, R. Lipowsky, T.R. Weikl, R. Dimova, and D.E. Discher. 2019. Membrane fluctuations and acidosis regulate cooperative binding of 'marker of self' protein CD47 with the macrophage checkpoint receptor SIRPα. *J. Cell Sci.* 132:1–8.

116. Fenz, S.F., T. Bihr, D. Schmidt, R. Merkel, U. Seifert, K. Sengupta, and A.S. Smith. 2017. Membrane fluctuations mediate lateral interaction between cadherin bonds. *Nat. Phys.* 13:906–913.

117. Junghans, V., M. Chouliara, A.M. Santos, D. Hatherley, J. Petersen, T. Dam, L.M. Svensson, J. Rossjohn, S.J. Davis, and P. Jönsson. 2020. Effects of a local auxiliary protein on the two-dimensional affinity of a TCR-peptide MHC interaction. *J. Cell Sci.* 133:jcs245985.

118. Reister-Gottfried, E., K. Sengupta, B. Lorz, E. Sackmann, U. Seifert, and A.S. Smith. 2008. Dynamics of specific vesicle-substrate adhesion: From local events to global dynamics. *Phys. Rev. Lett.* 101:1–4.

119. Bongrand, P. 1999. Ligand-receptor interactions. *Reports Prog. Phys.*

120. Hu, J., R. Lipowsky, and T.R. Weikl. 2013. Binding constants of membrane-anchored receptors and ligands depend strongly on the nanoscale roughness of membranes. *Proc. Natl. Acad. Sci.*

121. Bell, G.I. 1978. Models for the Specific Adhesion of Cells to Cells. 200:618–627.

122. Piper, J.W., R.A. Swerlick, and C. Zhu. 1998. Determining Force Dependence of Two-Dimensional Receptor-Ligand Binding Affinity by Centrifugation. *Biophys. J.* 74:492–513.

123. Kaplanski, G., C. Farnarier, O. Tissot, A. Pierres, A.M. Benoliel, M.C. Alessi, S. Kaplanski, and P. Bongrand. 1993. Granulocyte-endothelium initial adhesion. Analysis of transient binding events mediated by E-selectin in a laminar shear flow. *Biophys. J.* 64:1922–1933.

124. E. Evans,*' D. Berk, * and A. Leung. 1991. Detachment of agglutinin-bonded red blood cells 1 . Forces to rupture molecular-point attachments. 59.

125. Evans, E., K. Ritchie, and R. Merkel. 1995. Sensitive Force Technique to Probe Molecular Adhesion and Structural Linkages at Biological Interfaces. 68:2580–2587.

126. Dustin, M.L. 2009. Supported bilayers at the vanguard of immune cell activation studies. *J. Struct. Biol.* 168:152–160.

127. Chesla, S.E., P. Selvaraj, and C. Zhu. 1998. Measuring Two-Dimensional Receptor-Ligand Binding Kinetics by Micropipette. *Biophys. J.* 75:1553–1572.

128. Chen, W., V.I. Zarnitsyna, K.K. Sarangapani, J. Huang, and C. Zhu. 2008. Measuring Receptor–Ligand Binding Kinetics on Cell Surfaces: From Adhesion Frequency to Thermal Fluctuation Methods. *Cell. Mol. Bioeng.* 1:276–288.

129. Huang, J., V.I. Zarnitsyna, B. Liu, L.J. Edwards, N. Jiang, B.D. Evavold, and C. Zhu. 2010. The kinetics of two-dimensional TCR and pMHC interactions determine T-cell responsiveness. *Nature*. 464:932–936.

130. De Jong, L.A.A., D.R.A. Uges, J.P. Franke, and R. Bischoff. 2005. Receptor-ligand binding assays: Technologies and applications. *J. Chromatogr. B Anal. Technol. Biomed. Life Sci.*

131. Zhu, D.-M., M.L. Dustin, C.W. Cairo, and D.E. Golan. 2007. Analysis of Two-Dimensional Dissociation Constant of Laterally Mobile Cell Adhesion Molecules. *Biophys. J.* 92:1022–1034.

132. Scatchard, G. 1949. THE ATTRACTIONS OF PROTEINS FOR SMALL MOLECULES AND IONS. *Ann. N. Y. Acad. Sci.*

133. Mege, J.-L., C. Capo, A.-M. Benoliel, C. Foa, R. Galindo, and P. Bongrand. 1986. Quantification of cell surface roughness; a method for studying cell mechanical and adhesive properties. *J. Theor. Biol.* 119:147–160.

134. Whitaker, N., U.K. Bageshwar, and S.M. Musser. 2012. Kinetics of precursor interactions with the bacterial Tat translocase detected by real-time FRET. *J. Biol. Chem.* 287:11252–11260.

135. Shashkova, S., and M.C. Leake. 2017. Single-molecule fluorescence microscopy review: Shedding new light on old problems. *Biosci. Rep.*

136. Sergé, A., N. Bertaux, H. Rigneault, and D. Marguet. 2008. Dynamic multiple-target tracing to probe spatiotemporal cartography of cell membranes. *Nat. Methods*. 5:687–694.

137. Jaqaman, K., D. Loerke, M. Mettlen, H. Kuwata, S. Grinstein, S.L. Schmid, and G. Danuser. 2008. Robust single-particle tracking in live-cell time-lapse sequences. *Nat. Methods*. 5:695–702.

138. Alcor, D., G. Gouzer, and A. Triller. 2009. Single-particle tracking methods for the study of membrane receptors dynamics. *Eur. J. Neurosci.* 30:987–997.

139. Axmann, M., J.B. Huppa, M.M. Davis, and G.J. Schütz. 2012. Determination of interaction kinetics between the T cell receptor and peptide-loaded MHC class II via single-molecule diffusion measurements. *Biophys. J.* 103:17–19.

140. O'Donoghue, G.P., R.M. Pielak, A.A. Smoligovets, J.J. Lin, and J.T. Groves. 2013. Direct single molecule measurement of TCR triggering by agonist pMHC in living primary T cells. *Elife*. 2:1–16.

141. Lee, G.M., F. Zhang, A. Ishihara, C.L. McNeil, and K.A. Jacobson. 1993. Unconfined lateral diffusion and an estimate of pericellular matrix viscosity revealed by measuring the mobility of gold-tagged lipids. *J. Cell Biol.* 120:25–36.

142. Che, A., and R.J. Cherry. 1995. Loss of rotational mobility of band 3 proteins in human erythrocyte membranes induced by antibodies to glycophorin A. *Biophys. J.* 68:1881–1887.

143. Saxton, M.J. 1997. Single-particle tracking: The distribution of diffusion coefficients. *Biophys. J.* 72:1744–1753.

144. Saxton, M.J. 2008. Single-particle tracking : connecting the dots. 5:671–672.

145. Bell, G.I., M. Dembo, and P. Bongrand. 1984. Cell adhesion. Competition between nonspecific repulsion and specific bonding. *Biophys. J.* 45:1051–1064.

146. Pierres, A., A.M. Benoliel, and P. Bongrand. 1998. Studying Receptor-Mediated Cell Adhesion at the Single Molecule Level. *Cell Commun. Adhes.* 5:375–395.

147. Wu, Y., J. Vendome, L. Shapiro, A. Ben-Shaul, and B. Honig. 2011. Transforming binding affinities from three dimensions to two with application to cadherin clustering. *Nature*. 475:510–513.

148. Harriman, O.L.J., and M.C. Leake. 2011. Single molecule experimentation in biological physics: Exploring the living component of soft condensed matter one molecule at a time. *J. Phys. Condens. Matter*.

149. Elowitz, M.B., A.J. Levine, E.D. Siggia, and P.S. Swain. 2002. Stochastic gene expression in a single cell. *Science (80-.).*

150. Sott, K., E. Eriksson, E. Petelenz, and M. Goksör. 2008. Optical systems for single cell analyses. *Expert Opin. Drug Discov.*

151. Dustin, M.L., D.E. Golan, D.-M. Zhu, J.M. Miller, W. Meier, E.A. Davies, and P.A. van der Merwe. 1997. Low Affinity Interaction of Human or Rat T Cell Adhesion Molecule CD2 with Its Ligand Aligns Adhering Membranes to Achieve High Physiological Affinity. *J. Biol. Chem.* 272:30889–30898.

152. Dam, T., V. Junghans, J. Humphrey, M. Chouliara, and P. Jönsson. 2021. Calcium Signaling in T Cells Is Induced by Binding to Nickel-Chelating Lipids in Supported Lipid Bilayers. *Front. Physiol.* 11.

153. Tolentino, T.P., J. Wu, V.I. Zarnitsyna, Y. Fang, and M.L. Dustin. 2008. Measuring Diffusion and Binding Kinetics by Contact Area FRAP. 95:920–930.

154. Huang, J., V.I. Zarnitsyna, B. Liu, L.J. Edwards, N. Jiang, B.D. Evavold, and C. Zhu. 2010. The kinetics of two-dimensional TCR and pMHC interactions determine T-cell responsiveness. *Nature*. 464:932–936.

155. Huang, J., L.J. Edwards, B.D. Evavold, and C. Zhu. 2007. Kinetics of MHC-CD8 Interaction at the T Cell Membrane. *J. Immunol.* 179:7653–7662.

156. Alenghat, F.J., and D.E. Golan. 2013. Membrane Protein Dynamics and Functional Implications in Mammalian Cells. . pp. 89–120.

157. P. G. SAFFMAN AND M. DELBROCK. 1975. Brownian Motion in biological membranes. *Proc. Nat. Acad. Sci*. 72:3111-3113,.

158. Kapanidis, A.N., S. Uphoff, and M. Stracy. 2018. Understanding Protein Mobility in Bacteria by Tracking Single Molecules. *J. Mol. Biol.* 430:4443–4455.

159. Donoghue, G.P.O., R.M. Pielak, A.A. Smoligovets, J.J. Lin, J.T. Groves, U. States, P.B. Division, and L. Berkeley. 2013. Direct single molecule measurement of TCR triggering by agonist pMHC in living primary T cells. 1–16.

160. Tinevez, J.Y., N. Perry, J. Schindelin, G.M. Hoopes, G.D. Reynolds, E. Laplantine, S.Y. Bednarek, S.L. Shorte, and K.W. Eliceiri. 2017. TrackMate: An open and extensible platform for single-particle tracking. *Methods*.

161. O'Donoghue, G.P., R.M. Pielak, A.A. Smoligovets, J.J. Lin, and J.T. Groves. 2013. Direct single molecule measurement of TCR triggering by agonist pMHC in living primary T cells. *Elife*. 2013:1–16.

162. Lin, W.-C., C.-H. Yu, S. Triffo, and J.T. Groves. 2010. Supported Membrane Formation, Characterization, Functionalization, and Patterning for Application in Biological Science and Technology. *Curr. Protoc. Chem. Biol.*

163. Pierres, A., A.M. Benoliel, P. Bongrand, and P.A. van der Merwe. 1996. Determination of the lifetime and force dependence of interactions of single bonds between surface-attached CD2 and CD48 adhesion molecules. *Proc. Natl. Acad. Sci.* 93:15114–15118.

164. Jenny J. Y. Lin*, Shalini T. Low-Nam*, Katherine N. Alfieri†, D.B.M., and J.T.G. Nicole C. Fay‡. 2019. Mapping the stochastic sequence of individual ligand-receptor binding events to cellular activation : T cells act on the rare events. *Sci. Signal.* 1–14.

165. Doyle, C., and J.L. Strominger. 1987. Interaction between CD4 and class II MHC molecules mediates cell adhesion. *Nature*. 330:256–259.

166. Luescher, I.F., E. Vivier, A. Layer, J. Mahiou, F. Godeau, B. Malissen, and P. Romero. 1995. CD8 modulation of T-cell antigen receptor–ligand interactions on living cytotoxic T lymphocytes. *Nature*. 373:353–356.

167. Matsui, K., J. Boniface, P. Reay, H. Schild, B. Fazekas de St Groth, and M. Davis. 1991. Low affinity interaction of peptide-MHC complexes with T cell receptors. *Science (80-.).* 254:1788–1791.

168. Milstein, O., S.-Y. Tseng, T. Starr, J. Llodra, A. Nans, M. Liu, M.K. Wild, P.A. van der Merwe, D.L. Stokes, Y. Reisner, and M.L. Dustin. 2008. Nanoscale Increases in CD2-CD48-mediated Intermembrane Spacing Decrease Adhesion and Reorganize the Immunological Synapse. *J. Biol. Chem.* 283:34414–34422.

169. Janeway, C.A. 1992. The T cell receptor as a multicomponent signalling machine: CD4/CD8 coreceptors and CD45 in T cell activation. *Annu. Rev. Immunol.*

170. Koretzky, G.A. 2010. Multiple Roles of CD4 and CD8 in T Cell Activation. *J. Immunol.*

171. Ryu, S.-E., P.D. Kwong, A. Truneh, T.G. Porter, J. Arthos, M. Rosenberg, X. Dai, N. Xuong, R. Axel, R.W. Sweet, and W.A. Hendrickson. 1990. Crystal structure of an HIV-binding recombinant fragment of human CD4. *Nature*. 348:419–426.

172. Maddon, P.J., D.R. Littman, M. Godfrey, D.E. Maddon, L. Chess, and R. Axel. 1985. The isolation and nucleotide sequence of a cDNA encoding the T cell surface protein T4: a new member of the immunoglobulin gene family. *Cell*.

173. Wang, J.H., R. Meijers, Y. Xiong, J.H. Liu, T. Sakihama, R. Zhang, A. Joachimiak, and E.L. Reinherz. 2001. Crystal structure of the human CD4 N-terminal two-domain fragment complexed to a class II MHC molecule. *Proc. Natl. Acad. Sci. U. S. A.*

174. Miceli, M.C., P. Von Hoegen, and J.R. Parnes. 1991. Adhesion versus coreceptor function of CD4 and CD8: Role of the cytoplasmic tail in coreceptor activity. *Proc. Natl. Acad. Sci. U. S. A.*

175. Hampl, J., Y.H. Chien, and M.M. Davis. 1997. CD4 augments the response of a T cell to agonist but not to antagonist ligands. *Immunity*.

176. Xiong, Y., P. Kern, H.C. Chang, and E.L. Reinherz. 2001. T Cell Receptor Binding to a pMHCII Ligand Is Kinetically Distinct from and Independent of CD4. *J. Biol. Chem.*

177. Krogsgaard, M., and M.M. Davis. 2005. How T cells ‘ see ’ antigen. 6:239–245.

178. Gay, D., P. Maddon, R. Sekaly, M.A. Talle, M. Godfrey, E. Long, G. Goldstein, L. Chess, R. Axel, J. Kappler, and P. Marrack. 1988. Functional interaction between human T-cell protein CD4 and the major histocompatibility complex HLA-DR antigen. *Nature*.

179. Huppa, J.B., and M.M. Davis. 2013. The Interdisciplinary Science of T-cell Recognition. In: Advances in Immunology. . pp. 1–50.

180. Broughton, S.E., J. Petersen, A. Theodossis, S.W. Scally, K.L. Loh, A. Thompson, J. van Bergen, Y. Kooy-Winkelaar, K.N. Henderson, T. Beddoe, J.A. Tye-Din, S.I. Mannering, A.W. Purcell, J. McCluskey, R.P. Anderson, F. Koning, H.H. Reid, and J. Rossjohn. 2012. Biased T Cell Receptor Usage Directed against Human Leukocyte Antigen DQ8-Restricted Gliadin Peptides Is Associated with Celiac Disease. *Immunity*. 37:611–621.

181. Limozin, L., M. Bridge, P. Bongrand, O. Dushek, P.A. van der Merwe, and P. Robert. 2019. TCR–pMHC kinetics under force in a cell-free system show no intrinsic catch bond, but a minimal encounter duration before binding. *Proc. Natl. Acad. Sci. U. S. A.* 116:16943–16948.

182. Zhu, D.M., M.L. Dustin, C.W. Cairo, H.S. Thatte, and D.E. Golan. 2006. Mechanisms of Cellular Avidity Regulation in CD2-CD58-Mediated T Cell Adhesion. *ACS Chem. Biol.*

183. Chang, V.T., R.A. Fernandes, K.A. Ganzinger, S.F. Lee, C. Siebold, J. McColl, P. Jönsson, M. Palayret, K. Harlos, C.H. Coles, E.Y. Jones, Y. Lui, E. Huang, R.J.C. Gilbert, D. Klenerman, A.R. Aricescu, and S.J. Davis. 2016. Initiation of T cell signaling by CD45 segregation at “close contacts.” *Nat. Immunol.* 17:574–582.

184. Bergwelt-baildon, M.S. Von, R.H. Vonderheide, B. Maecker, N. Hirano, K.S. Anderson, M.O. Butler, Z. Xia, W.Y. Zeng, K.W. Wucherpfennig, L.M. Nadler, and J.L. Schultze. 2002. Human primary and memory cytotoxic T lymphocyte responses are efficiently induced by means of CD40-activated B cells as antigen-presenting cells : potential for clinical application. 99:3319–3325.

185. Demetriou, P., E. Abu-Shah, S. McCuaig, V. Mayya, S. Valvo, K. Korobchevskaya, M. Friedrich, E. Mann, L.Y.W. Lee, T. Starkey, M.A. Kutuzov, J. Afrose, A. Siokis, M. Meyer-Hermann, D. Depoil, and M.L. Dustin. 2019. CD2 expression acts as a quantitative checkpoint for immunological synapse structure and T-cell activation. *bioRxiv*.

186. Weikl, T.R., J. Hu, B. Kav, and B. Różycki. 2019. Binding and segregation of proteins in membrane adhesion: theory, modeling, and simulations. *Adv. Biomembr. Lipid Self-Assembly*. 30:159–194.

187. van der Merwe, P.A., and S.P. Cordoba. 2011. Late Arrival: Recruiting Coreceptors to the T Cell Receptor Complex. *Immunity*. 34:1–3.

188. Jiang, N., J. Huang, L.J. Edwards, B. Liu, Y. Zhang, C.D. Beal, B.D. Evavold, and C. Zhu. 2011. Two-Stage Cooperative T Cell Receptor-Peptide Major Histocompatibility Complex-CD8 Trimolecular Interactions Amplify Antigen Discrimination. *Immunity*. 34:13–23.

189. Glassman, C.R., H.L. Parrish, M.S. Lee, and M.S. Kuhns. 2018. Reciprocal TCR-CD3 and CD4 engagement of a nucleating pMHCII stabilizes a functional receptor macrocomplex. 22:1263–1275.

190. Huppa, J.B., M. Axmann, M.A. Mörtelmaier, B.F. Lillemeier, E.W. Newell, M. Brameshuber, L.O. Klein, G.J. Schütz, and M.M. Davis. 2010. TCR–peptide–MHC interactions in situ show accelerated kinetics and increased affinity. *Nature*. 463:963–967.

191. Hong, J., S.P. Persaud, S. Horvath, P.M. Allen, B.D. Evavold, and C. Zhu. 2015. Force-Regulated In Situ TCR–Peptide-Bound MHC Class II Kinetics Determine Functions of CD4 + T Cells. *J. Immunol.* 195:3557–3564.

192. Xu, H., and D.R. Littman. 1993. A kinase-independent function of Lck in potentiating antigen-specific T cell activation. *Cell*. 74:633–643.

193. Liu, B., S. Zhong, K. Malecek, L.A. Johnson, S.A. Rosenberg, C. Zhu, and M. Krogsgaard. 2014. 2D TCR-pMHC-CD8 kinetics determines T-cell responses in a self-antigen-specific TCR system. *Eur. J. Immunol.* 44:239–250.

194. Schilham, M.W., W.-P. Fung-Leung, A. Rahemtulla, T. Kuendig, L. Zhang, J. Potter, R.G. Miller, H. Hengartner, and T.W. Mak. 1993. Alloreactive cytotoxic T cells can develop and function in mice lacking both CD4 and CD8. *Eur. J. Immunol.* 23:1299–1304.

195. Parrish, H.L., N.R. Deshpande, J. Vasic, and M.S. Kuhns. 2016. Functional evidence for TCR-intrinsic specificity for MHCII. *Proc. Natl. Acad. Sci. U. S. A.* 113:3000–3005.

196. Horkova, V., A. Drobek, D. Mueller, C. Gubser, V. Niederlova, L. Wyss, C.G. King, D. Zehn, and O. Stepanek. 2020. Dynamics of the Coreceptor-LCK Interactions during T Cell Development Shape the Self-Reactivity of Peripheral CD4 and CD8 T Cells. *Cell Rep.* 30:1504-1514.e7.

197. Chiantia, S., P. Schwille, A.S. Klymchenko, and E. London. 2011. Asymmetric GUVs Prepared by M b CD-Mediated Lipid Exchange : An FCS Study. *Biophysj*. 100:L1–L3.

198. Stone, M.B., S.A. Shelby, and S.L. Veatch. 2017. Super-resolution microscopy: shedding light on the cellular plasma membrane. *Chem Rev*. 117:7457–7477.

199. Alimohamadi, H., and P. Rangamani. 2018. Modeling membrane-protein interactions. 24–27.

200. Seow, V., J. Lim, A.J. Cotterell, M. Yau, W. Xu, R. Lohman, W.M. Kok, M.J. Stoermer, M.J. Sweet, R.C. Reid, J.Y. Suen, and D.P. Fairlie. 2016. Receptor residence time trumps drug-likeness and oral bioavailability in determining efficacy of complement C5a antagonists. *Nat. Publ. Gr.* 1–12.

201. Tiwary, P., V. Limongelli, M. Salvalaglio, and M. Parrinello. 2015. Kinetics of protein – ligand unbinding : Predicting pathways , rates , and rate-limiting steps. .

202. Mollica, L., S. Decherchi, S.R. Zia, R. Gaspari, and A. Cavalli. Kinetics of protein-ligand unbinding via smoothed potential molecular dynamics simulations. *Nat. Publ. Gr.*

203. Tieleman, D.P., S.J. Marrink, V. Corradi, P.C.T. Souza, H.I. Ingo, M.S.P. Sansom, and A. Tn. 2019. Computational Modeling of Realistic Cell Membranes. .

204. Zhang, L., J. Han, H. Wang, R. Car, and E. Weinan. 2018. DeePCG : Constructing coarse-grained models via deep neural networks. 034101:1–9.

Scientific Publications

Printed by Media-Tryck, Lund 2022 NORDIC SWAN ECOLABEL 3041 0903

ISBN: 978-91-7422-876-2

Physical Chemistry
Faculty of Science
Lund University